Cardiovascular roles of TRPV1 and TRPA1 channels: Polymodal receptors at the intersection of energy, temperature, and immune homeostasis

Doctoral (PhD) thesis

Leonardo Kelava

Department of Thermophysiology, Institute for Translational Medicine

Medical School, University of Pécs, Pécs, Hungary

Doctoral School Leader: Erika Pintér MD, PhD, DSc

Program Leader: Péter Hegyi MD, PhD, DSc

Supervisor: András Garami MD, PhD

Doctoral Council and Habilitation Committee of Medical and Pharmaceutical Sciences of the University of Pécs

PÉCS, 2024

Contents

Abbreviations

BAT - brown adipose tissue

CBS - cystathionine β-synthase

COX – cyclooxygenase

CSE - cystathionine ϒ-lyase

EC - endothelial cell

EDH - endothelial-derived hyperpolarization

eNOS - endothelial nitric oxide synthase

GPCR – G protein-coupled receptors

HDL - high-density lipoprotein

IK - intermediate conductance calcium-activated potassium channels

IL - interleukin

K_{ir} - inward-rectifier K^+ channel

LDL - low-density lipoprotein

MEGJ - myo-endothelial gap junction

NO - nitric oxide

POA - preoptic area of the hypothalamus

SK - small conductance calcium-activated potassium channels

TNF - tumor necrosis factor

TRPA1 - transient receptor potential ankyrin-1

TRPV1 - transient receptor potential vanilloid-1

VSMC - vascular smooth muscle cell

1. Introduction

Thermal regulation in mammals is a complex process, involving the management of energy and water resources to maintain optimal core temperature. It also prioritizes core temperature over the temperature of skin and limbs, also called shell temperature, to protect vital body organs. The process of thermoregulation can be delineated into three functional domains: thermal sensing, feedback and feedforward processes, and activation of thermal effectors to maintain core temperature in the normal range [76]. In mammals, it is suggested that the balance point is composed of several separate controllers and can be further affected by specific circumstances. For example, in inflammation, both hypothermia and fever may occur during the thermoregulatory response. Similarly, in states where the body is programmed to conserve energy, such as sleep, hibernation, and torpor, one can observe a gradual drop in core temperature [100]. Within all three functional domains, there is still a lot of research to be done and in the past two decades, a lot of efforts in elucidating the mechanisms of thermoregulation were focused on transient receptor potential (TRP) receptors [10].

Thermoregulatory systems differ between mammalian species, and each species has a system tailored to their needs. This is an important consideration in translational research, where the two most common model animals are mice and rats, both significantly smaller than humans. The much higher surface-to-volume ratio makes it more challenging to maintain body temperature in rodents. Thus, mice and rats have higher metabolic rates than humans, higher relative amounts of brown adipose tissue (BAT), and higher fluctuations in the core body temperature, which differences should be considered [37]. One component of the thermoregulatory system is peripheral blood flow, an important thermal effector. The experiments on isolated arteries show similarities between the species, but can also capture the differences between vascular beds within each species. The authors of a recent review concluded that such experiments are of high translational value [71].

1.1 Components of Thermoregulatory System

In mammals, core body temperature is strictly regulated in a narrow range and this process is controlled primarily through the neuronal system. Thermoregulatory nuclei are thought to be in the preoptic area of the hypothalamus (POA), where the information from thermal sensors is conveyed, processed, and the appropriate thermoeffector responses are triggered.

The thermal sensors can be divided into heat and cold sensors which are asymmetrically distributed throughout the body; heat sensors are more abundant in the core, where heat is produced and thus the focal point is to restrain heat production, while cold sensors are more abundant in the periphery, where heat loss has to be quickly perceived and reacted in order to prevent cooling of the core [99].

Signals from central and peripheral thermal sensors are relayed to the median preoptic nucleus of the POA *via* the trigeminal dorsal horn and lateral parabrachial nucleus. From there, they project to the medial preoptic hypothalamus, where the signals from warm and cold sensors pass through to the output of inhibitory neurons that project to *raphae nuclei*, from where other inhibitory, GABAergic neurons emerge. The temperature is actively maintained in the thermoneutral zone and there is commonly a basal output to thermal effectors. Thus, the neurons from the rostral *raphae pallidus* and adjacent rostral ventrolateral medulla inhibit the sympathetic output to blood vessels, which modulates the vasoconstrictor tone. Heat increases this activity, leading to higher inhibition and vasodilation. In the case of the cold, the tonic inhibition of the sympathetic system from *raphae pallidus* is released, allowing for higher expression of sympathetic activity and consequential vasoconstriction [58].

Each heat gain and heat loss effector has its separate threshold, at which it is activated. These thresholds depend on the energetic costs of specific thermal effectors, as the most economic ones are activated first. Thus, in order of recruitment, thermal effectors for defense against the cold are behavioral control, followed by vasoconstriction, piloerection, BAT thermogenesis, and shivering, while the heat defenses in order of recruitment are behavioral regulation, vasodilation, sweating, panting, and pronation [76].

1.2 Vascular Thermoregulation

The priority of vasomotor control of core temperature reflects the fact that it is an economic mechanism of thermoregulation; in cold, it needs less energy than BAT activation or shivering, and in warmth, it consumes less water and energy than sweating or panting. An increase in vessel diameter, vasodilation, increases the blood flow, enabling an exchange of heat between body and environment, typically leading to loss of heat, as the core temperature is usually higher than the ambient. A decrease in vessel diameter, vasoconstriction, promotes the preservation of core temperature, as the heat exchange between the body core and ambient is shut down [76].

The contractile responses of the vessels are under the control of the sympathetic branch of the autonomic nervous system, which activates vascular smooth muscle cells (VSMCs) through adrenergic receptors. Specifically, the increased sympathetic activation stimulates alpha-1 adrenergic receptors on vascular smooth muscle cells. It was also shown that in response to cold, adrenergic α2c receptors are specifically translocated to the cell membrane of VSMCs, thereby enabling and maintaining vasoconstriction [22].

Dilation can be passive, happening just through inhibition of sympathetic activation of VSMCs, or active, which happens through as of yet poorly defined mechanisms but is shown to be independent of inhibition of vasoconstrictor tone. Acetylcholine is revealed to be an effector in active dilation, working with so far unidentified cotransmitter that accounts for the majority of vasodilation. There is still ongoing debate whether the presence of nitric oxide (NO) has just a permissive role or is needed for active vasodilation [46]. Upon activating muscarinic receptors on endothelial cells (ECs), acetylcholine produces hyperpolarization in VSMCs *via* different mechanisms.

ECs may produce chemical substances, such as NO or prostaglandins, that traverse intercellular space to activate soluble guanyl-cyclase or G-protein coupled receptors (GPCRs) associated with adenyl cyclase, respectively [84]. However, after inhibiting eNOS and COX, two major sources of NO and prostaglandins, respectively, there is still residual vasodilation, termed endothelial-derived hyperpolarization (EDH). There have been several suggested mechanisms of EDH, which may all be cooperating. ECs are connected with each other and with VSMCs *via* gap junctions, where the

connection between the cytoplasm of ECs and VSMCs is termed myo-endothelial gap junction (MEGJ). Hyperpolarization of ECs might travel radially through the MEGJ to VSMCs, producing their hyperpolarization and subsequent relaxation. Alternatively, K^+ ions from ECs might be released in the extracellular space, activating the inward-rectifier K^+ channel (K_{ir}) and Na^+/K^+-ATPase in VSMCs, which would lead to hyperpolarization. In many experiments, it was shown that calcium-activated potassium channels of small conductance (SK) and intermediate conductance (IK) are essential for the hyperpolarization of ECs and subsequent EDH [15].

The vasomotor tone is dynamically regulated. Measurements of blood flow in rats show that even in the thermoneutral zone, the tail artery periodically constricts [12, 78]. At low temperatures, the tail artery is constricted for longer periods and similarly, vasodilation is maintained during exposure to a hot environment. However, after the initial vasoconstriction to cold, the phenomenon of cold-activated vasodilation also occurs, as the organism seeks to find a new balance between heat conservation and blood flow to protect the tissue from cold-induced injuries [6].

1.3 Thermoregulation and Inflammation

Inflammation is a systemic response to infection by microbial infections, but it can also be aseptic, for example in case of excess cellular damage. It is energetically expensive and thus it is necessary to find a fine balance between the energy demands of the thermoregulatory and immune systems. The usual result of this integration is fever, but in severe cases and where energy resources are scarce, hypothermia may occur. It is suggested that both have adaptive value in specific circumstances [79]. A recent meta-analysis has suggested that hypothermia is associated with worse outcomes in sepsis [80]. A prolonged increase in body temperature caused by fever may also have a detrimental impact on energy demands, exhausting the organism and leading to negative outcomes, but it can also be beneficial, helping the organism to fight off an infection. In agreement with that, different investigations yielded opposite results and it should be stressed that each research was limited to small cohorts with specific medical condition, so the effect of fever duration on the final outcome remains an open question [51].

Inflammatory signals are communicated between cells through two major classes of molecules: prostaglandins and cytokines. Cytokines are mostly produced by

immune cells, and the pyrogenic cytokines interleukin (IL)-1, -6, and tumor necrosis factor (TNF) induce the production of prostaglandins in pyrogen-processing peripheral organs and the central nervous system. Prostaglandins can then affect the thresholds of various thermal effectors [68]. Lack of prostaglandin receptor EP3 makes mice unable to produce febrile response [103]. A recent research in rats identified the specific subset of EP3-expressing neurons in the POA, whose inhibition produces hyperthermia mimicking fever through increased sympathetic tone that activates BAT and vasoconstriction. It was suggested that increased BAT activity at a lower threshold is an important contributor to fever [67]. More recently, another group found that upstream of that pathway, lies the lateral parabrachial nucleus (LPBN). LPBN contains both PGE_2-producing cells as well as EP3 neurons responsive to PGE_2 that control the mounting of febrile response in rats through increased skin vasoconstriction and BAT activation [107]. However, another group obtained different results in mice and suggested that peripheral vasoconstriction is responsible for fever, with negligible BAT contribution, since the knockout of uncoupling protein-1 did not affect the febrile response [29].

1.4 TRP Receptors

TRP proteins are a family of cation channels, comprising 27 proteins in humans, classified into six groups: TRPV, TRPC, TRPM, TRPP, TRPML, TRPA, and TRPN. They are often polymodal, and able to respond to chemical and/or physical stimuli, and although they are non-selective cation channels, most of them show a preference for some cations, as determined by their pore structure [52]. A subgroup of 11 TRP receptors was recognized to be sensitive to temperature change and they are classified as thermoTRP receptors. This temperature sensitivity is shown through the Q10 value; an increase in conductivity after a 10°C change in temperature. The conductivity of ion channels naturally increases with an increase in temperature, as the diffusion rates are directly proportional to temperature, but this change is typically small, ~2 fold to ~3 fold. In thermoTRPs, the Q10 value is well over ~5 [23].

TRP vanilloid-1 (V1) was the first discovered TRP receptor, isolated and characterized in 1997 [19], thankfully due to its conspicuous property of reacting to capsaicin, a pungent ingredient in chili. In the noxious temperature range, from 40°C to

50°C, its Q10 value was 23.5. As such, it was also the first identified member of thermoTRP receptors [18, 19]. TRP ankyrin-1 (A1) is another polymodal cation channel that can be activated by chemicals and changes in temperature. Unlike TRPV1, human TRPA1 is activated by noxious cold at temperatures below 17°C [48]. TRPA1 shows great plasticity in evolution and it was shown that in different animal species it responds to different temperature ranges to accommodate for the ecological niche of the species in question [54, 56]. In several species, it was shown to be activated by noxious heat as well. This fuels the debate about whether TRPA1 detects heat change or its activation depends on its surrounding molecules, which are primary temperature sensors. In support of the latter theory, TRPA1 has a large number of ankyrin repeats, that are thought to be able to bind many different proteins. Furthermore, it was suggested that only with the double knockout, removing both TRPA1 and TRP melastatin-8 genes, the cold response is completely abolished, with either receptor being able to partially compensate for the lack of the other [106]. Similarly, in pain sensation, it was shown that extracellular miRNA can activate nociceptors only when both TRPA1 and toll-like receptor 7 are present [72], and NO-induced pain sensation at the periphery is completely abolished only in double TRPV1/TRPA1 knockout mice [62]. However, a recent experiment with human TRPA1 in reconstituted lipid bilayers has suggested that its ability to sense both high and low temperatures is an internal property that can be disrupted by the deletion of channel segments and can be affected by the redox state at one region [63].

Both receptors, TRPA1 and TRPV1, are activated by a variety of chemical agonists. TRPV1 can be activated by endogenous compounds such as anandamide and oxytocin, as well as by exogenous compounds, including capsaicin and resiniferatoxin. In the case of palmitoyletanolamide, different authors suggested either activation or interaction that facilitates its activation [10]. Chemical stimuli that activate TRPA1 include a variety of electrophilic compounds, such as allicin from garlic, alil isothiocyanate (AITC), hydrogen sulfide (H_2S), polysulfides, and various reactive oxygen/nitrogen species and products of oxidative stress, such as hydrogen peroxide or oxidized lipids like 4-hydroxy nonenal [97, 98].

TRPA1 and TRPV1 both share other similarities; they have similar expression profiles, particularly in the neurons of dorsal root ganglia and nodose ganglia, where they colocalize to a high extent. Both were investigated as potential targets for the

treatment of pain, as they are present in thin, unmyelinated C fibers and partly myelinated A_δ fibers that receive and conduct pain stimuli [91]. TRPA1 is also expressed in keratinocytes, bladder, and vascular system [31], where it was found in both endothelial and VSMCs in small arteries. However, so far, the only arteries where TRPA1 was detected in endothelial cells through immuno-hybridization are the cerebral, pial, and dural arteries [27]. Being activated by changes in temperatures, TRPV1 and TRPA1 were suggested to be involved in thermal regulation.

The importance of TRPV1 in thermoregulation was shown in clinical trials with TRPV1 antagonists, which caused hyperthermia. However, despite the fact that TRPV1 can be activated by a change in temperature, it is suggested that this activation is not the one that drives these TRPV1-dependent thermoregulatory responses. Steiner et al. showed that the starting temperature at which TRPV1 is blocked does not affect the magnitude of hyperthermia, thus suggesting the driving stimuli of TRPV1 activation do not depend on temperature. The temperatures in the experiment were below the threshold of TRPV1 activation, the highest being 28°C, further implying that at these temperatures, TRPV1 inhibits hyperthermia through tonic activation by some unknown agonist [90]. It was proposed that this tonic agonist might be pH. A recent meta-analysis suggested that TRPV1 has several modes of activation: agonist-mediated, pH-mediated, and temperature-mediated and that only the antagonists targeting pH-mediated activation affect body temperature in rodents, while the blockade of both the proton and heat activation modes contributes to the hyperthermia in humans [35].

The above responses are logical in the context of TRPV1 protecting from hyperthermia. However, this picture is complicated by several TRPV1 antagonists which were determined to cause hypothermia instead [34]. Furthermore, capsaicin, as a chief TRPV1 agonist, has dual effects on thermoregulation. While, on one hand, it induces sweating, protecting from heat, it also activates thermogenesis through BAT activation. So, TRPV1 can participate in both thermoeffector branches, and this further suggests that its thermosensory properties are not linked to its thermoeffector roles, at least not at the temperatures below noxious heat threshold [77].

The thermoregulatory roles of TRPA1 are even more challenging to study, as they show great variability in thermal sensing between the species. While the majority of the research identified its cold-sensing properties, several groups recognized it could

be activated by both cold and heat in humans and mice. At evolutionary older phylogenetic branches, such as reptiles, fish, and insects, TRPA1 is prevalently identified as a heat sensor, although its cold sensing properties were also shown in several species [110].

TRPV1 and TRPA1 thermoeffector roles could be manifested through their regulation of vasomotor responses since both receptors are widely expressed in the cardiovascular system. TRPA1 activation causes vasodilation in mesenteric arteries [45], skin arteries, and cerebral arteries [94]. It was shown that when mouse feet are immersed in cold water, activation of TRPA1 is essential for cold-induced vasoconstriction and furthermore, TRPA1 was also needed for restoration of blood flow *i.e.* cold-induced vasodilation [6]. In the past decade, a gasotransmitter that was suggested to activate TRPA1 was H_2S. A paper by Pozsgai demonstrated that H_2S causes vasodilation in ear arteries of wild-type mice, but not in the TRPA1 knockout ($^{-/-}$) mice [73]. Likewise, our previous paper showed that intracerebroventricular infusion of H_2S causes pronounced hypothermia and a decrease of blood flow in mice and these responses were less pronounced in TRPA1$^{-/-}$ mice. However, similar responses were not observed upon intraperitoneal injection, suggesting only central H_2S has these effects [70].

1.5 Hydrogen Sulfide

H_2S is a gas that was long known only for its toxic properties. Only in the 1990s, it was realized that it is also naturally produced in the body through different metabolic pathways and it has plausible biological roles, the first identified being the role in neuromodulation [2]. As of now, three different pathways of H_2S production have been recognized: through cystathionine β-synthase (CBS), cystathionine ϒ-lyase (CSE), and cysteine aminotransferase coupled with mercaptopyruvate sulfur transferase. It has been suggested that H_2S may also be released through non-enzymatic reactions [82].

The investigation of the biological functions of H_2S faces numerous technical challenges. Many experiments relied on knockouts of the enzymes that produce it, but these are involved in a wide range of processes that are affected by sulfur metabolism. For example, the availability of methionine affects protein synthesis, and the availability of cysteine, a chief substrate for H_2S production, affects redox systems, as cysteine is

one of the 3 amino acids in glutathione, the most prevalent antioxidant that cells use. Methods of H_2S detection have also been criticized for lack of specificity, as it has been speculated that they can't differentiate between H_2S and other sulfur pools, such as acid-labile sulfur or dithiothreitol-labile sulfur, so many authors implied that the measured concentrations are overestimated [74]. Different kinds of salts have been used as H_2S donors, but it was suggested that they release H_2S too rapidly, instantly increasing its concentration to physiologically irrelevant levels. Recently, new classes of slow-H_2S-release molecules have been developed, such as GYY4137. GYY4137 was suggested to be a better mimic of physiologic H_2S but was also criticized for lack of precision, as CO may also be released upon the degradation of dichloromethane [59]. It should also be noted that H_2S is a volatile molecule, so it rapidly evaporates from open systems, such are Petri dishes, wire myographs, and other types of *in vitro* experiments [25].

H_2S has a prominent role in thermal regulation and energetics, as it was shown that it induces „suspended animation" in mice [13] and similar effects in rats, lowering heart rate and body temperature [5, 32]. Further, H_2S has modulatory effects on mitochondrial respiration; at low concentrations, H_2S acts like an electron donor to the electron transport chain, supporting energy production, while at high concentrations, H_2S inhibits respiration through blockage of electron transport to Complex IV [104]. Finally, H_2S is a product of several chemical reactions catalyzed by two enzymes, CBS and CSE, within the transulfuration pathway, a biochemical pathway responsible for the conversion of methionine to cysteine [4]. It should be noted that the reactions that produce H_2S are side reactions, using products of methionine degradation, such as homocysteine and cysteine, which drive further methionine catabolism. Reduction of methionine might lead to global inhibition of protein synthesis, as methionine is needed for initiation of translation, so it would perhaps be no surprise that H_2S evolved a function within the energy conservation framework. Indeed, it was found that in eukaryotic cells, H_2S enhances the phosphorylation of the eIF2α elongation factor, inhibiting global protein synthesis [108]. Furthermore, in a state of inhibited protein synthesis in *Caenorhabditis elegans*, the ATF4 transcription factor induces enzymes that produce H_2S, and this in turn is suggested to be a mechanism that increases longevity in this species [89]. These papers show that H_2S is involved in energy conservation processes at the cellular level.

Such processes might be used in severe inflammation, where an organism needs to preserve energy to fight the infection. As such, H_2S was suggested to play a role in septic shock. Several animal models of sepsis through cecal ligation and puncture demonstrated that the addition of H_2S-releasing compounds, such as NaHS, aggravates the effects of systemic inflammation [4, 111]. Likewise, it was shown that H_2S production in mice is increased following CLP [112]. A clinical trial in humans also demonstrated that plasma H_2S levels were increased in septic vs. non-septic patients and increased H_2S concentration correlated with worse outcomes[53].

2. Hypothesis and Aims of the Study

My PhD research is divided into different parts all aiming to explore the roles of TRP receptors and H_2S in the vascular system that might affect the distribution of energy either through metabolic changes or heat dissipation/preservation. TRPV1 and TRPA1 receptors, as the two most prominent representatives of the family were the primary subjects of interest. In addition, we wanted to assess the interactions of H_2S with TRPA1 and whether these interactions change at the temperatures at which TRPA1 is activated. This knowledge would contribute to our understanding of how these molecules interact at the crossroads between inflammation, energy balance, and thermoregulation. In specifics, my work consisted of the following parts:

1. Low-density lipoprotein (LDL) is a major risk factor and predictor for atherosclerosis, a cardiovascular disease that annually contributes to 15 million deaths worldwide, and which is suggested to be caused by sub-clinical inflammation of vascular tissue, diabetes mellitus, and obesity, among others [17]. An interaction between TRPV1 signaling and lipid metabolism could be suspected based on previous studies [1, 64], therefore we conducted a meta-analysis to evaluate how does the oral supplementation of capsaicinoids (TRPV1 agonists) affects the lipid profile in human blood serum.

2. Wire myography is a commonly used method to evaluate the pharmacological effects of drugs on vasomotor responses. The vessels are placed in the chambers of the wire myograph device, where they can be maintained at different temperatures. However, by default only heating of the chambers up to 45°C can be achieved, disabling the device from being used at extreme body temperatures, such as temperatures above

45°C, or temperatures below room temperature, such as the activating temperature of TRPA1. Both these temperatures can occur at the surfaces contacting the external environment, such as the skin and the digestive tube. We aimed to design special heat-exchange plates to be produced by using 3D printing technology. These could fit under the chambers of wire myograph DMT 610 to enable better control over the temperature of each experiment.

3. The DMT wire myograph instruction manual states that all experiments should be conducted at the designated and constant temperature, to which the device must be calibrated before the experiments. This is to prevent the introduction of measurement errors due to drift, which is likely introduced because the resistors within the Wheatstone bridge, the electric circuit for balancing electric currents and measuring the force generated by vessels, are affected by temperature [36]. Since this would disable us to measure the real-time effect of temperature change on vessels, a series of experiments were performed to see how the temperature change affects the system when there are no vessels mounted.

4. The heat-exchange system was then tested in experiments with rat carotid and tail arteries, to evaluate the reproducibility of temperatures and to measure how are the pharmacological effects of commonly used substances in wire myography, such as phenylephrine (PE), sodium nitroprussid (SNP), and potassium chloride (KCl), affected by the temperature change.

5. The above-designed system was used to explore the effects of H_2S at normal and low temperatures in the tail artery and carotid artery from rats and mice. We further evaluated the effects of H_2S in tail artery from $TRPA1^{+/+}$ and $TRPA1^{-/-}$ mice to see whether these effects are mediated by TRPA1.

3. Methods

3.1. Meta-analysis

The PICO format for the meta-analysis was framed as follows: (P)atients were the general human population, (I)ntervention was oral supplementation of capsinoids, (C)omparator was placebo control and (O)utcomes were serum lipids at the end of the trial: total cholesterol, LDL, high-density lipoprotein (HDL), and triglycerides, as well as parameters of glucose metabolism, such as fasting plasma glucose and insulin. The search was performed in three databases, Pubmed, EMBASE, and Cochrane CENTRAL with the following key: capsa* OR capsi* OR TRPV1 OR vanilloid) AND (LDL OR HDL OR lipoprotein OR triglyceride OR cholester* OR "lipid".

Study eligibility was independently evaluated by two authors and data was extracted from the selected studies. Studies were required to include the following: controlled human trial design; a group with TRPV1 agonist administration; a placebo control group; and serum cholesterol level among the outcome measures. The following data were extracted from the eligible studies: author names, publication year, age, sex, body mass index, and number of participants, as well as, different outcome measures, *viz*., serum levels of total cholesterol, HDL, LDL, and triglycerides.

The statistical analysis was performed according to the standard methods of meta-analysis by using the Stata/IC 16.0 software (StataCorp LLC, College Station, TX, USA). Subjects were grouped as either administered with a TRPV1 agonist (*i.e*., intervention group) or not (*i.e.*, controls). Standardized mean difference (SMD) with 95% confidence intervals (CIs) between intervention and control groups was used as a primary measure of the effect size on serum lipid level response at the end of the substance administration. For standardization, the means were divided by their corresponding standard deviation (SD) values, which was required because the different lipid level-measuring methods and TRPV1 agonist dose ranges could result in different variances among the study groups, and, therefore, influence the results. SMD values were calculated by using the random effect model by DerSimonian and Laird [26], and then compared by using standard meta-analysis tools, such as "forest plot". Statistical heterogeneity was determined by the I^2 statistical test ($p < 0.1$ indicating significant heterogeneity). As an attempt to reduce heterogeneity, subgroups administered with

capsaicin only and with capsaicin in a mixture with other substances were analyzed separately.

3.2 Design and Manufacture of the Heat-exchange Device

DMT 610 is a device that captures the vasomotor responses of small vessels in isometric conditions. In short, two wires are protruded through the lumen of the vessel, keeping it in place and at a constant diameter. One wire is connected to the force transducer, which measures the force that the vessel creates upon constriction, while the other wire is connected to the micrometer, which enables the measurement of the distance between two wires and thus the diameter of the vessel. The device has 4 chambers, each containing one short vessel segment. The chambers may be heated to up to 45°C, but there is no option for cooling, limiting its usage to measuring vasomotor responses only at or above room temperature. In collaboration with the 3D printing team from PTE's 3D Printing and Visualization Center, we have conceptualized and manufactured a heat exchange device that enables us to measure vasomotor responses at higher and lower temperatures than the original capacity of the device.

3.2.1 3D Printing and Mechanical Testing

To fabricate a watertight system, SLA additive manufacturing technology was applied. For 3D printing, a Formlabs Form 2 SLA desktop printer was used (Form-labs Inc., Somerville, MA, USA), and the selected material was the transparent Clear Resin V4 (Formlabs Inc., Somerville, MA, USA). To fabricate the test specimens for mechanical testing and thermal conductivity, the printer has been set to the parameters shown in Table 1. The parameters were chosen based on the material data sheet of the resin and based on our previous experience with the fabrication of microfluidic systems.

Table 1. Printing and post-processing parameters of SLA 3D printing [49].

		SLA Printing technology			Post-processing		
Material	Color	Laser beam focus width (μm)	Touchpoint size (mm)	Raft type	Layer thickness (μm)	Washing time in Isopropyl alcohol (min)	Time in 60°C infrared chamber (min)
Clear resin	Clear	85	0.7	Full	100	10	15

3.2.2. 3-Point Flexural Test

The 3-point bending tests were carried out by a Zwick/Roell Z100THW universal material tester (sn: 731741/2018; ZwickRoell, Ulm, Germany). The tests were conducted according to ISO 178:2010 with the fabricated specimen. According to the standard, the size of the specimen was 4 mm × 10 mm × 80 mm. The preload was 0.1 MPa and the speed was set at 2 mm/min during the entire test. The support distance was 64 mm and the maximum deformation was 4.7%. The tests were performed 5 times.

3.2.3. Tensile Test

The tensile tests were carried out with the same Zwick/Roell Z100THW tester, supplemented with an extensometer. The tests were conducted according to ISO 527-1:2019 with the fabricated specimen. The type of specimen was A1 from ISO 527-2:2012 and the preload was 0.1 MPa. The speed was set at 1 mm/min during the determination of Young's modulus, while it was 50 mm/min during the test. The number of test specimens was 5.

3.2.4. Charpy Test

The Charpy impact tests were performed by a Zwick/Roell Hit50P instrument with a 5 J pendulum (ZwickRoell, Ulm, Germany) according to the 179-1:2010 standard: the size of the specimen was 4 mm × 10 mm × 80 mm; the hit impacted the edge; and the tests were repeated 5 times.

3.2.5. Shore D Hardness

The Shore D hardness tester was a Zwick/Roell 3131/320154 device (ZwickRoell, Ulm, Germany). The tests were performed according to the 868:2003 standard. The instrument was on a stand and the specimen thickness was 5 mm. All measurements were carried out 5 times.

3.2.6. Thermal Conductivity

Thermal conductivity measurements were performed on 3 test samples. To perform the measurement, an apparatus was built with the following elements (see also Figure 1):

- Arduino Uno (Arduino, Somerville, MA, USA) with 2 thermistors;
- Rohde@Schwarz HMC8012 Digital Multimeter (Rohde & Schwarz, München, Germany);
- Ender 3 3D printer controller (Creality, Shenzhen, China) for control of the heated bed;
- 24 V, 160 W heated bed (Creality, Shenzhen, China);
- 8-cm thick Energosystem ES-EPS-80-8 polystyrene (Thermotrading Ltd., Cegléd, Hungary) for insulation of the measured system from the environment;
- Thermal grease (model: 51634; Qoltec, Gliwice, Poland) for thermal conductive adhesion.

The heating plate was surrounded by polystyrene foam (λ = 0.039 W/mK) as insulation, except for a 7 cm x 7 cm wide opening, through which the test specimens were placed inside. The size of the 3D-printed test specimen was 5 mm x 70 mm x 70 mm. For the calibration of the device, a glass plate was used, which had the same size as the sample (λ_{ref} = 1 W/mK). Thermal sensors were positioned on the test specimen's top and bottom, and then the sample was placed on the heating bed. Measurements were recorded by the Arduino Uno with a frequency of 0.2/sec. The heat flow was determined by the electric energy consumption of the heating bed. The multimeter was serially

connected to the heating bed and the Ender 3 printer controller. Power consumption as a function of time was recorded on a personal computer (Figure 1).

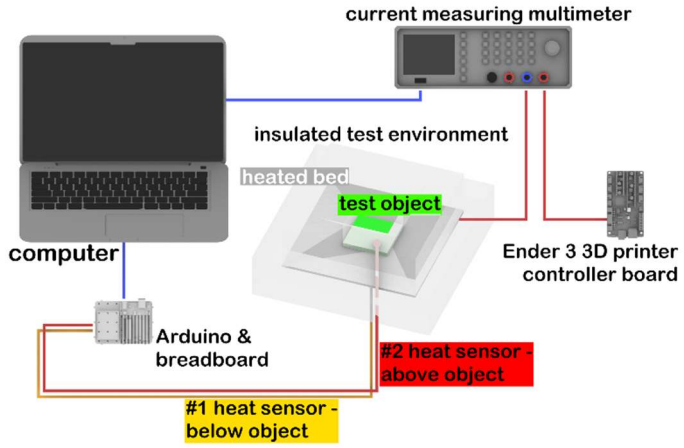

Figure 1. Schematic representation of the experimental setup used for thermal conductivity measurements [49].

The measurements were performed in five stages in the case of both glass and resin samples: (i) 35°C for 45 min; (ii) 37°C for 35 min; (iii) 44°C for 30 min; (iv) 49°C for 25 min; and (v) 58°C for 20 min. The duration of a full heating cycle was 155 min. During the entire measurement cycle the heating bed was completely surrounded with polystyrene (except the 7 cm × 7 cm opening); thus, heat conductivity could be determined by measuring the loss of the current (for details, see below). Further data processing was performed in the Origin software (OriginLab Corporation, Northampton, MA, USA). After reaching the thermodynamic equilibrium in each phase, the difference between the two thermosensors was determined by averaging the difference data obtained in three full heating cycles.

Heat flow was calculated on the basis of the ratio of the maximum usable current and the current related to the actual heating consumed over the three cycles, and then the amount of heat loss was deducted from this value. After that, the following equation was used:

$$\lambda = \left| \frac{\dot{Q}}{A \cdot \frac{T_2 - T_1}{\delta}} \right|$$

where Q - heat flow (W), A - cross-section of the test specimen (m^2), T_1, T_2 - temperatures measured on both sides of the test specimen (°C), δ - thickness of the test specimen (m). The measured and calculated values were fitted to an exponential curve that was determined by the following equation:

$$\boldsymbol{y = A \cdot e^{-\frac{x}{t}} + y_0}$$

where A, t, y_0 are constants and x marks the temperature.

The zero point correction factor of the device was determined by the following equation:

$$\boldsymbol{k = \frac{\lambda_{reference}}{\lambda_{measured}}}$$

where k is the correction factor and $\lambda_{reference}$ and $\lambda_{measured}$ are the heat conductions for the reference material as determined by the manufacturer and as measured in our experiments at 23 °C, respectively. The correction was made at the ambient temperature at which the measurement was performed (23 °C).

3.2.7 DSC-TGA

LabSys Evo device (Setaram Ltd., Caluire-et-Cuire, France) was used to perform these experiments. The calibration of the instrument was recently performed by the manufacturer. The measurements were carried out under 100 mL/min nitrogen atmosphere and the mass of each sample was set between 5.2–5.5 mg. The applied temperature range for the measurements started at 30°C, ended at 750°C, and was increased at a rate of 10°C/min. Because of the high temperatures, uncovered Al2O3 crucibles (Setaram Ltd., Caluire-et-Cuire, France) with a volume of 100 µL were used. The rate of the sample's spontaneous cooling was sufficient for the measurements; thus, the application of an external cooler was not necessary. Data processing was performed using Origin 2021 software (OriginLab Corporation, Northampton, MA, USA).

3.2.8 Digital Microscopy

Images were taken of both the intact and broken surface of the specimens used in the Charpy test to evaluate the structure of the resin material with a König digital

microscope (König Electronic GmbH, Reichelsheim, Germany) with 35× magnification.

3.2.9 Fabrication of the Heat-exchange Device

The instrument was designed using Rhinoceros 6 CAD (computer-aided design) software (Robert McNeel & Associates, Seattle, WA, USA). The size of the final product was 75 mm × 120 mm × 7 mm, the cooling pipes were 10.5 mm long with a 5 mm inner and 7 mm outer diameter and were interspaced from each other by 1 mm (Figure 2). The slicing process was performed by the PreForm slicing software (Formlabs Inc., Somerville, MA, USA). The layer height was set to 50 µm, and the device was in "Y" printing orientation on the printing bed. The overall printing time was 13 h and 15 min and it required a total volume of 46 mL resin. The post-processing included bathing in isopropyl alcohol for 10 min and UV curing at 60 °C for 15 min.

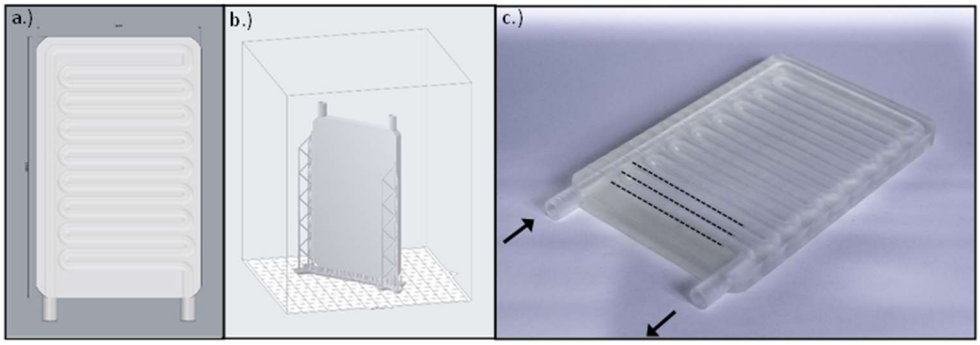

Figure 2. a) The CAD model of the cooling plate created with Rhinoceros 6 CAD software. b) The .stl model uploaded in the slicer software. c) The manufactured cooling plate using a 3D printer. The arrows indicate the inflow and outflow pipes of the plate, and the dotted lines represent the parallel cooling pipes [49].

3.3. Experimental Procedures of Wire Myography

3.3.1. Experimental Animals and Their Housing

The experiments are conducted at the Institute for Translational Medicine, Medical School, University of Pecs. Adult Wistar rats and *Trpa1*$^{+/+}$ and *Trpa1*$^{-/-}$ mice were used in the experiments. All animals were housed at standard conditions, with food and water *ad libitum*.

3.3.2 Testing of Wire Myograph Measurements in the Dynamic Temperature Range

According to the manufacturer's instruction, the temperature in the chambers of the DMT during the experiments should be stable, as the changing temperature might import big errors in the measurements due to temperature drift. Because limiting temperature to a single point is a big constraint in investigating the role of TRP receptors, we wanted to evaluate these temperature effects to see if it is possible to isolate these effects with precision high enough to reliably estimate the vessel's response. For that purpose, the device was calibrated to the starting temperature of 37°C and the 40 μm tungsten wire was mounted alone while the temperature was gradually increased from 35°C to 42°C or decreased from 37°C to 20°C, each in 5 replicates. The maximum change in force and SDs of measurements at each temperature were calculated for each chamber individually, and these measurements were compared to measurements obtained in animal experiments.

3.3.3. Surgical Preparation

Anesthesia was induced by ketamine-xylazine cocktail (81.7 and 9.3mg/kg, respectively). For isolation of tail arteries, lateral incisions were made, and the skin from the top of the tail was carefully removed. Thin entomological needles were used to separate the tail artery from the connective tissue and long segments of arteries were excised while holding one end with the forceps. The surgical removal of tail arteries was performed under a surgical microscope (model SZX7; Olympus, Tokyo, Japan). Common carotid arteries from mice and rats were ligated before the excision and excised between ligations. The animals were euthanized with pentobarbital (100 mg/kg) after the surgery. Extracted arteries were placed in a Petri dish with a gel-covered bottom, containing Krebs solution that was infused with 5% CO_2 and 95% O_2. The arteries were excised to four pieces of 2 mm length, which were mounted on corresponding DMT chambers prefilled with 5ml Krebs solution *via* tungsten wires of 15-micrometer diameter for mouse tail arteries or 40-micrometer diameter for mouse carotid arteries, rat tail arteries, and rat carotid arteries. In the Petri dish containing the mouse tail artery, some SNP would be added to dilate them for easier protrusion of the tungsten wires and minimum endothelium damage. The chambers were heated or cooled

to a designated temperature and oxygenated for at least an hour before the vessels were placed in them.

3.3.4. Experimental Procedure

Before each series of experiments, the calibration of DMT chambers was performed at the designated temperature. The low temperatures were achieved with previously constructed heat-exchange plates, as described above [49]. The experiments were performed either at normal body temperature, 37°C or cold. Different temperatures for cold were used in rats and mice. The mouse arteries were not viable at 17°C, so the experiments were conducted at 20°C, while the experiments with rat arteries were conducted at 17°C. The vessels were mounted and left to rest for 30 minutes. The tension of vessels was normalized to standardized conditions to yield optimal constriction that is comparable between separate measurements and the vessels were left to rest for an additional 30 minutes. The vessels were precontracted with either PE (10^{-5} M for mice, 10^{-4} M for rats) or 90 M KCl. Endothelium-dependent vasodilation was evaluated with acetylcholine (AC, 10^{-4} M for rats, 10^{-5} M for mice), and endothelium-independent vasodilation was evaluated with SNP (10^{-4} M for rats, 10^{-5} M for mice).

The precontraction before adding Na_2S or distilled water as control was always made with PE, as it was expected that the ratio of potassium ions might affect Na_2S-induced activation. 50 µl of Na_2S solution was added in consecutive order to reach concentrations of Na_2S of 10^{-6},10^{-5},10^{-4}, 10^{-3}, and 10^{-2} M in the bath solution of the vessel. Likewise, distilled water was added five times in consecutive order in the control experiments. After each series of treatments, the chamber was washed three times with Krebs solution. At the end of the experiments, the viability of vessels was evaluated again with KCl and acetylcholine.

4. Results

4.1. Meta-analysis

Altogether 4,420 studies were retrieved from the PubMed, EMBASE, and CENTRAL databases. After filtering for human and clinical trials and removing duplicates with EndNote, 121 remaining papers were screened on title and abstract. 36 full-text articles were reviewed for compliance with inclusion criteria, yielding 11 studies that were eligible for qualitative synthesis. Searching through the references, an additional 3 studies were found. However, the final number of analyzed papers was 10, as one was excluded for suspicion of being performed on the same set of data as another study that was already included, two had data inappropriate for analysis, and one used supplementation with a low dose of TRPV1 agonist, nonivamide, which doesn't belong to the capsinoid family and has only half of the potency of capsaicin.

Out of 10 studies, 8 were with parallel placebo control and 2 with crossover designs. One study was non-randomized, and according to the risk of bias analysis, 6 studies were considered to have a high risk of bias, 2 studies had a moderate risk of bias, and 2 studies were at low risk of bias. Due to differences in study design and methodology, considerably high between-study heterogeneity (indicated by an I^2 of 46-96%) was observed in our analysis.

Studies that used capsaicinoids only and capsaicinoids combined with other substances were included as separate subgroups in the forest plot for serum total cholesterol (Figure 3). Dietary capsaicinoid supplementation markedly ($p = 0.004$) reduced serum total cholesterol compared to the controls (SMD = -0.57; CI, -0.95, -0.18). With regards to capsaicinoid-containing mixtures, both of the included studies seemed to decrease serum total cholesterol, however, there was no significant effect in the individual studies or on average (SMD = -0.32; CI, -0.75, 0.11; $p = 0.141$). The overall effect of all capsaicinoid supplementations (i.e., alone and in combination; $n = 195$) was a significant ($p = 0.001$) decrease in serum total cholesterol, as compared to the control groups ($n = 203$) with an SMD of -0.52 (CI, -0.83, -0.21).

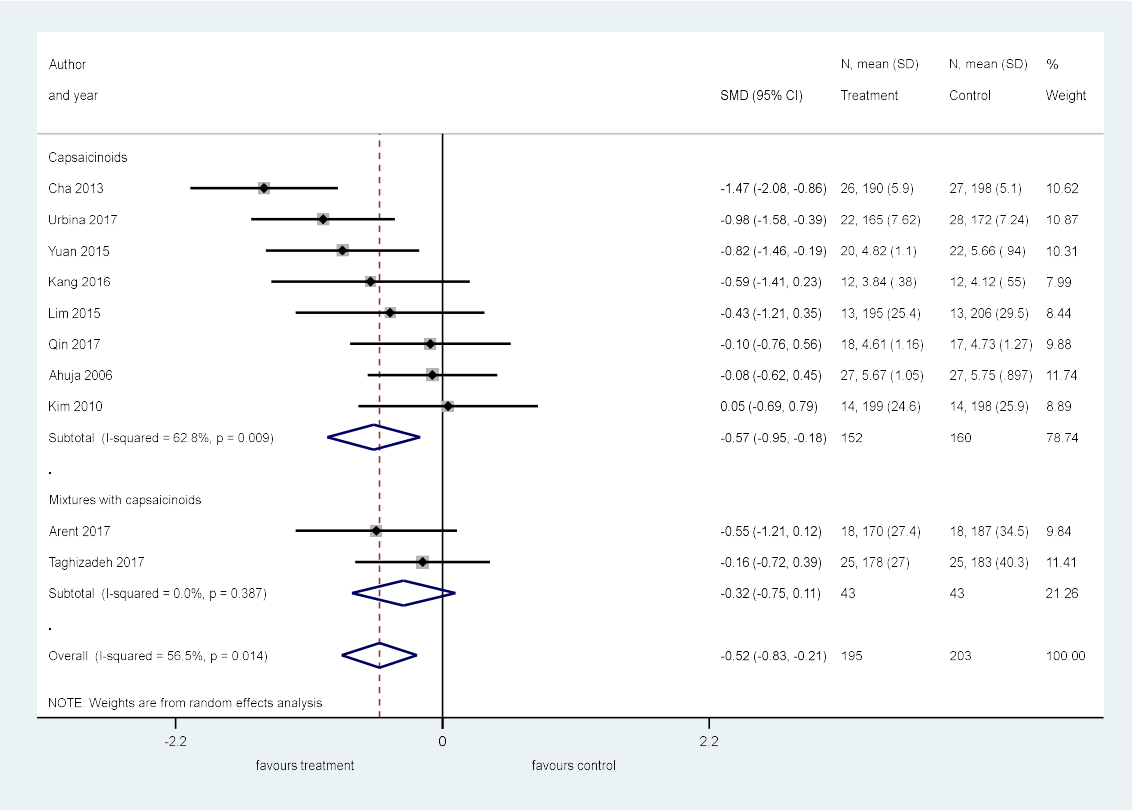

Figure 3. Capsaicinoid supplementation reduced serum total cholesterol [50].

We found sufficient data to analyze the changes in LDL, triglyceride, and HDL levels in response to dietary capsaicinoid supplementation. At the end of the trials, the LDL level was lower (as indicated by a negative SMD) in the capsaicinoid-treated groups than in controls in most of the studies, whereas it was higher in two studies (Figure 4). The averaged SMD was not significantly different in either the capsaicinoid alone or mixture subgroups. However, the overall average SMD, calculated from all 10 studies, was -0.30 (CI -0.97, - 0.02), showing a statistically significant decrease ($p = 0.035$).

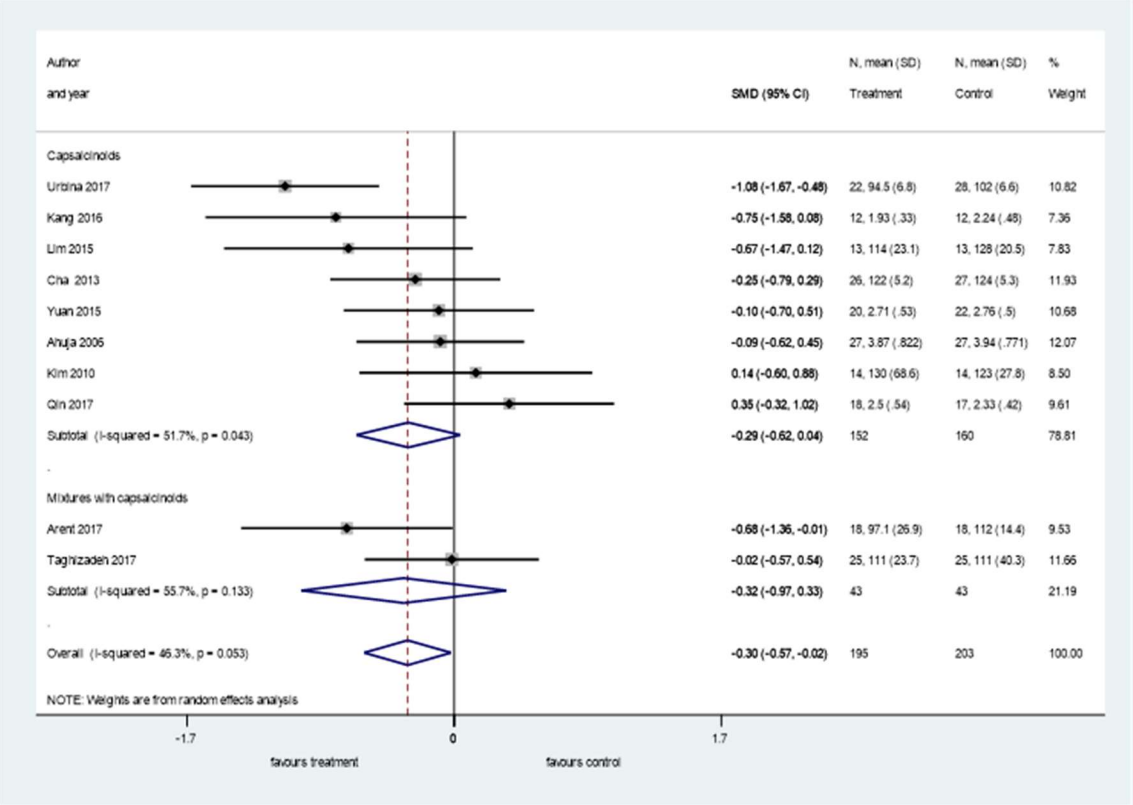

Figure 4. Capsaicinoid oral supplementation reduced serum LDL [50].

Capsaicinoids did not have a significant effect on serum triglyceride levels when administered alone (SMD = -0.46; CI, -1.49, 0.57) or in a mixture (SMD = -0.19; CI, -0.62, 0.23) (Figure 5). The overall effect (including both subgroups) was also not meaningful (SMD = -0.39; CI, -1.15, 0.37). When we compared serum HDL levels between the capsaicinoid-treated and control groups, we found no significant change in SMD, regardless of whether the capsaicinoids were administered alone (SMD = 0.05; CI, -0.37, 0.47) or in combination with other substances (SMD = -0.31; CI, -0.82, 0.21) (Figure 6). The overall effect was negligible (SMD = -0.03, CI -0.37, 0.32).

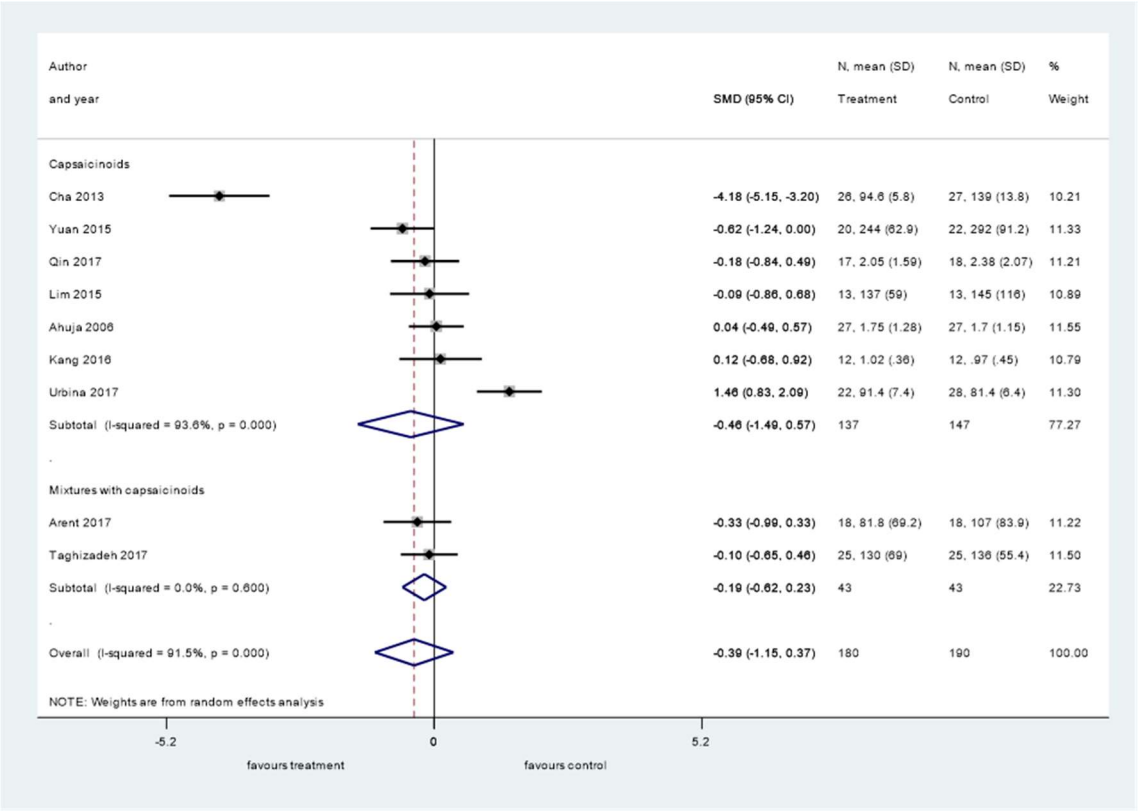

Figure 5. Capsaicinoid oral supplementation did not affect serum triglycerides [50].

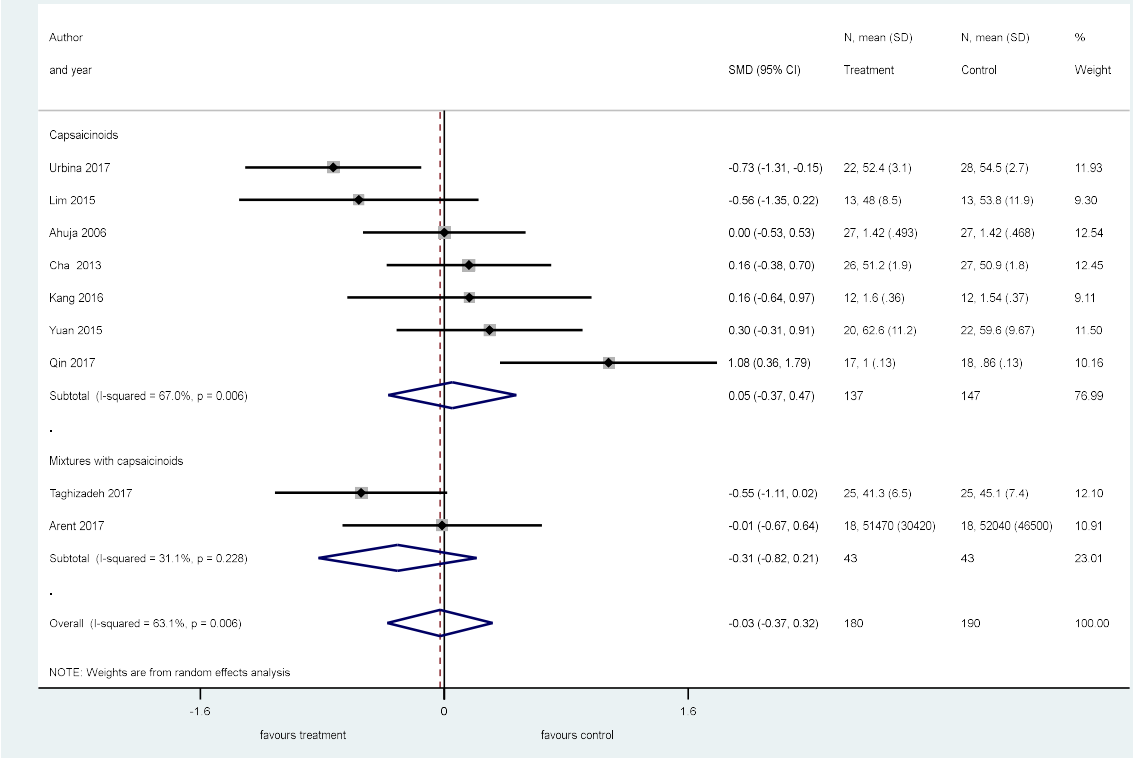

Figure 6. Capsaicinoid oral supplementation did not affect serum HDL [50].

4.2 Fabrication of a Novel Heat Exchange Device

4.2.1 Mechanical Characterization

The results of the mechanical characterization underlined that the selected resin is hard, durable, and can withstand the planned experiments after the fabrication of the heat-exchange device (Table 2). The average value of tensile strength was 67.66 ± 1.31 MPa, the flexural stress at standard deflection was measured as 78.82 ± 1.17 MPa, while the Charpy impact test resulted in 20.70 ± 2.30 kJ/m^2. The shore D hardness was found to be 83.00 ± 0.47.

In an earlier study, Epon 828® resin, a commonly used epoxy polymer, exhibited a tensile strength of 69 MPa and a tensile Young's modulus of 2750 MPa [41], which are slightly higher values than what we found for the resin used in the present study (Table 2). A recent summary of the tensile strength and modulus of fused filament fabrication 3D-printed PLA parts indicated that if the design parameters were similar (*i.e.*, XYZ build orientation; 0–45° raster angle; 0.15–0.20 mm layer thickness), then tensile strength varied between 41 and 59 MPa and the tensile modulus ranged from 3130 to 3520 MPa [30]. In the same study, the authors fabricated a PLA specimen with the same technology and similar design parameters (XYZ build orientation, 0.14 mm layer thickness), which had a tensile strength of 31–58 MPa and tensile modulus of 2900-3130 MPa depending from the raster angle (0–90°) [30]. The tensile strength of the investigated material in the present study was higher, but it was also more elastic (Table 2).

Table 2. The results of the mechanical characterization of the fabricated heat exchanger [49].

		Mean	SD
Tensile Young's modulus	(MPa)	2304.80	42.90
Tensile strength	(MPa)	67.66	1.31
Flexural Young's modulus	(MPa)	2246.80	66.70
Flexural stress at standard deflection	(MPa)	78.82	1.17
Charpy impact	(kJ/m^2)	20.70	2.30
Shore D hardness		83.00	0.47

4.2.2 Thermal Conductivity of the Resin Material

The thermal conductivity measurements were performed on the transparent resin. Glass was used as a reference material. The measured data points of resin, which were 0.314 W/mK at 35°C, 0.311 W/mK at 37°C, 0.361 W/mK at 44°C, 0.351 W/mK at 49°C, and 0.490 W/mK at 58°C, a curve was fitted, and then the results were extrapolated based on the previously determined correction factor (k=0.931). After the calibration of the setup, the heat conduction parameters were measured at 35, 37, 44, 49, and 58°C, which resulted in heat conduction of 0.314, 0.311, 0.361, 0.351, and 0.490 W/mK, respectively (Figure 7).

The corrected average of heat conduction for the tested resin material was 0.280 W/mK, which was considered constant at all temperatures. To our knowledge, this is the first study that reports the thermal conductivity of SLA 3D-printed clear resin ($\lambda_{clear\ resin}$ = 0.280 W/mK), which is similar to the thermal conductivity of epoxy resin ($\lambda_{epoxy\ resin}$ = 0.202 W/mK) as determined earlier by other authors [20].

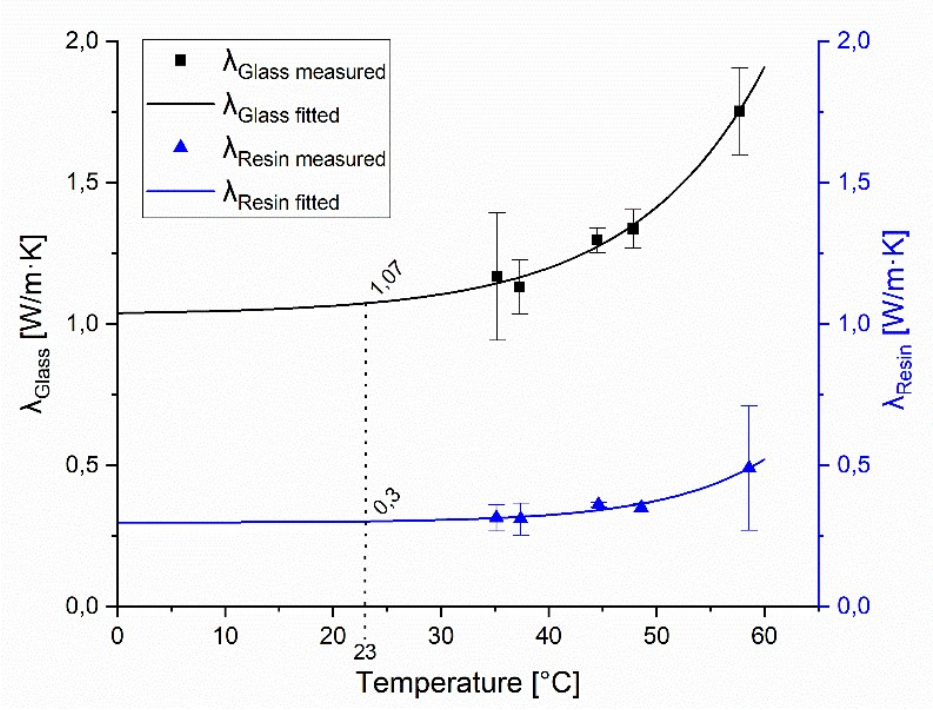

Figure 7. Measured and fitted heat conduction parameters of the tested materials. Heat conduction of the reference glass material is represented by the black curve; the squares show the average values with standard deviations measured at the indicated temperatures. Heat conduction parameters of the resin material are represented by the blue curve; triangles show the measured average values with standard deviations measured at the indicated temperatures [49].

4.2.3 Thermal Characterization of the Transparent Resin

The characterization of the thermal properties of the transparent resin samples revealed a relatively high heat stability of the printouts (Figure 8 and Table 3). According to the manufacturer, there is no significant change in the thermal properties of these samples until 250°C, which has now also been confirmed with the results of our DSC-TGA (Figure 8). It should be noted, however, that a slight gradual loss of sample mass was present already from the beginning of the heating of the sample. The same tendency could be observed with ABS samples, though, in that case, the gradual decrease in sample mass started at higher temperatures [101]. Interestingly the TGA curve of the tested Clear resin (Figure 4) is very similar to that of PLA shown in a previous study [101]. However, while PLA and other PLA-based composites usually have a melting temperature of approx. 150-170°C [43], the clear resin stayed solid at that temperature and even far above (Table 3). Of note, other photopolymers, such as thermally cured structural self-adhesive tapes have much less thermal stability [38]. Such good thermal stability as the one observed in the case of the SLA 3D-printed resin can be achieved in the case of several polymer materials only by the addition of nanoparticles or cellulose nanofibers to their structure, which can enhance various properties, including thermal stability [3, 81]. Our collaborator research group has previously examined the thermal properties of 3D printouts from many composites, such as PLA, ABS, polyamide, high-impact polystyrene, and polyethylene terephthalate glycol and none of these materials had the glass transition (Tg) and melting phases at such high temperatures as the transparent resin. However, the appearance of the fast phase of mass decrease at around 300°C suggests that resin quickly destabilizes and loses its previous rigid structure above this temperature (Figure 8).

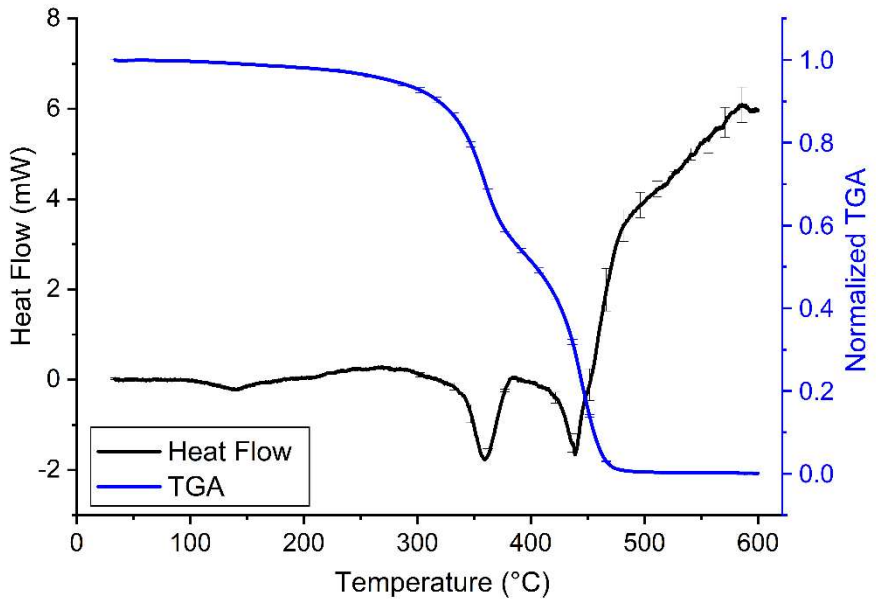

Figure 8. Heating curves of Clear resin V4 (30–600 °C, black line) combined with TGA of the samples (30–600 °C, blue line) on a common temperature scale (i.e., abscissa) at a heating rate of 10 °C/min. On the heating curves, the endothermic process (i.e., when the sample melts) causes a drop in heat flow. A decrease in normalized TGA indicates a loss of sample mass. The error bars show the standard error of means from at least 3 independent measurements [49].

The quick phase change is confirmed by the synchronicity of the prompt decrease in sample mass with the endothermic reaction (*i.e.*, the melting of the sample). This indicates that pyrolysis and the melting of the sample are parallel. Based on our TGA, at around 500°C, the majority of the sample was pyrolyzed (Figure 8).

Table 3. Corresponding temperature values of the characteristic DSC peaks in the heating cycle of the transparent resin samples (where T_{on} is the initial temperature, T_g is the glass transition temperature, and T_{end} is the final temperature of the phase). The data are shown in the mean ± standard error format [49].

T_{on} (°C)	T_g (°C)	T_{end} (°C)	Melting (°C)	Decomposition (°C)
100.82 ± 3.55	122.09 ± 4.15	138.96 ± 1.07	359.11 ± 0.27	438.93 ± 0.38

4.2.4 Digital Microscopy

The images taken with the digital microscope revealed important information about the structure of the resin material. The fabricated material had an extremely smooth, glass-like surface, and a glassy breaking pattern. The layers were not clearly visible; they could not be separated visually with the used 35× magnification. The

material was nearly transparent and, therefore, ideal for the production of heat-exchange devices. On the intact surface, small bumps with 0.5 mm diameter could be observed. The raft, which is fundamental in this technology was connected to these protrusions, which must be considered during the 3D modeling and printing processes (Figure 9).

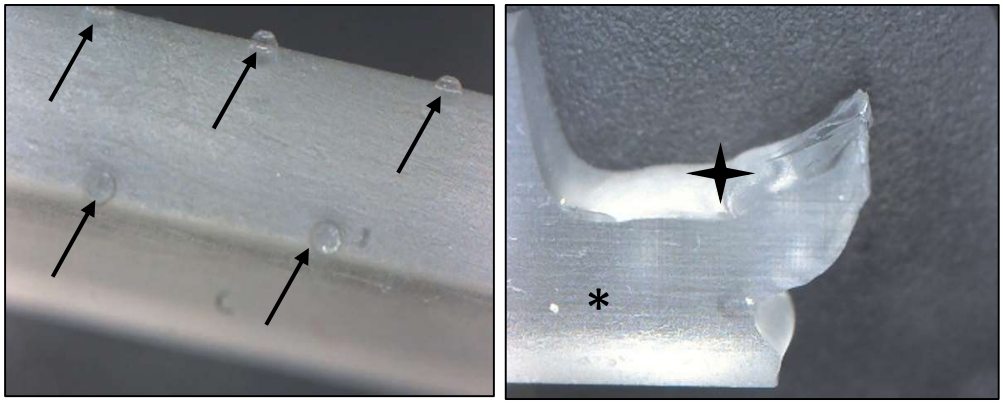

a b

Figure 9. Images of the fabricated resin material taken with a digital microscope. (**a**) Intact test specimen, surface on the edge. The black arrows point to the protrusions, which are the remains of the raft. (**b**) Broken test specimen. The black star indicates the broken, and the asterisk marks the intact surface, where the glassy-like structure can be observed. Magnification: 35× [49].

4.3 Experimental Results from Wire Myography

4.3.1 Force Transducer Measurements in the Dynamic Temperature Range

The force measurements changed in all 4 chambers in both scenarios, during heating or cooling (Figure 10). The mean change of force at the end of each experiment in cooling ranged from -2.86 to 0.754, and in heating from -2.01 to 0.870. The maximum change was significantly changed between the chambers, as shown by two-way ANOVA ($F(3,1,3,32) = 17.544$, $p = 6.47e\text{-}07$) and borderline insignificant between the cooling and the heating treatment ($F(3,1,3,32) = 3.518$, $p = 0.0699$). Trajectories of measurements were similar within each chamber for each scenario. However, the standard error was significantly different between the chambers and within the chambers or treatments, suggesting high fluctuations during the experiment.

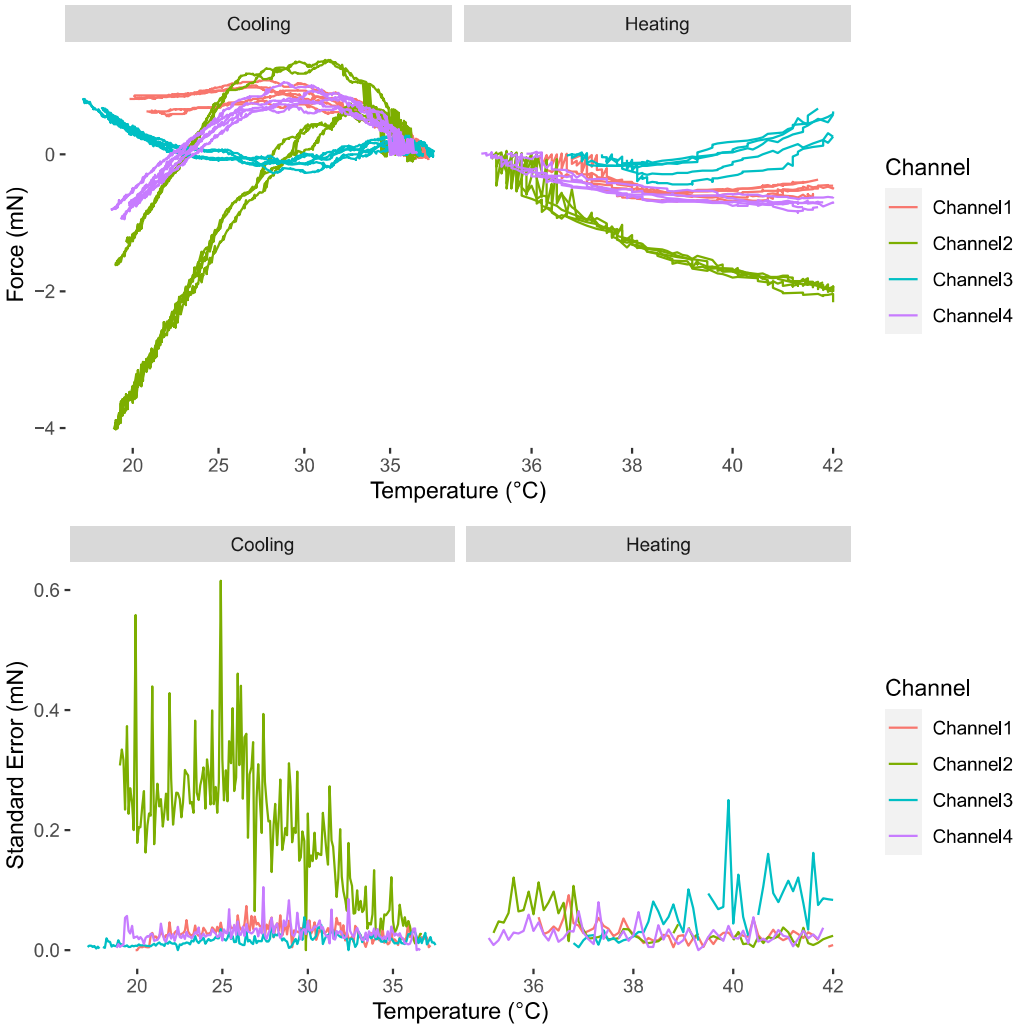

Figure 10. Mock experiments with changing temperature. Each chamber showed a distinct trend, but the measurement errors introduced due to changing temperature would significantly affect our conclusions; this kind of experimental setup was deemed not practical [Kelava et al., unpublished].

4.3.2 Effects of Classical Vasoconstrictors on Rat Tail Arteries in Cold

In our preliminary research, the temperature didn't have a significant effect on the vasoconstriction induced by 10^{-4} M phenylephrine. However, the KCl-induced vasoconstriction at 16°C decreased by ~4.5 mN, compared to 36°C, as Welch one-way ANOVA shows ($p = 0.002$). Increasing the concentration of KCl from 60 to 90 mM at 16°C, we found a significant ($p = 0.041$) increase in the isometric force of the tail artery (Figure 11).

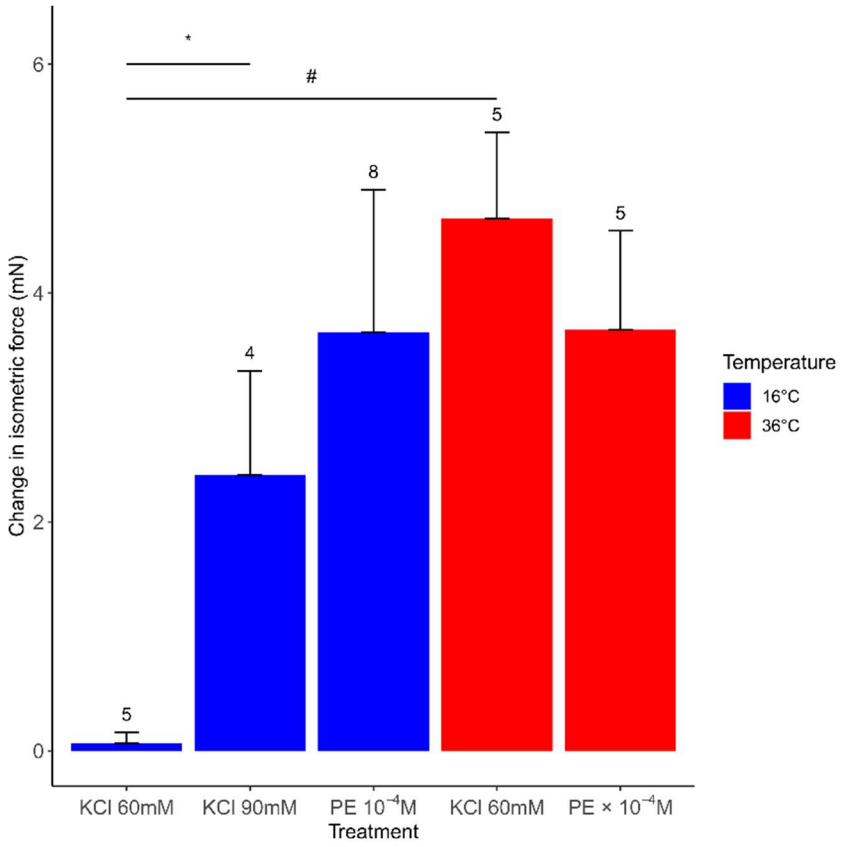

Figure 11. Vasoconstriction in rat tail artery at different temperatures. # - significant effect of temperature ; * - significant effect of differing KCl concentrations [49].

4.3.3 The Effects of Temperature on Acetylcholine Response

Temperature inhibited the acetylcholine-induced vasodilation in all 4 studied vessel types (Figure 12). In mice, the response to acetylcholine was independent of genotype at both temperatures. In rat carotids (Figure 12a), at 37°C acetylcholine reduced carotid artery precontraction by 84.3±15.4%, compared to 22.1±4.0% at 17°C ($F(1,12)=11.51$, $p=0.00535$), while in rat tail arteries (Figure12b) it decreased precontraction by 16.6±4.0% at 37°C, compared to only 3.7±1.5% at 17°C ($F(1,14)=9.465$, $p=0.00821$). In mice carotids (Figure12c), precontraction was reduced by 56.9±8.8% at 37°C, and by 31.2±11.2% at 20°C ($F(1,1,1, 24)=4.991$, $p=0.0351$), while in tail arteries (Figure 12d), it was decreased by 40.4±9.3% at 37°C and 14.3±4.1% at 20°C ($F(1,1,1, 28)=7.297$, $p=0.0116$). There was no significant difference between TRPA1 WT and KO mice in the response to acetylcholine (Figure 12).

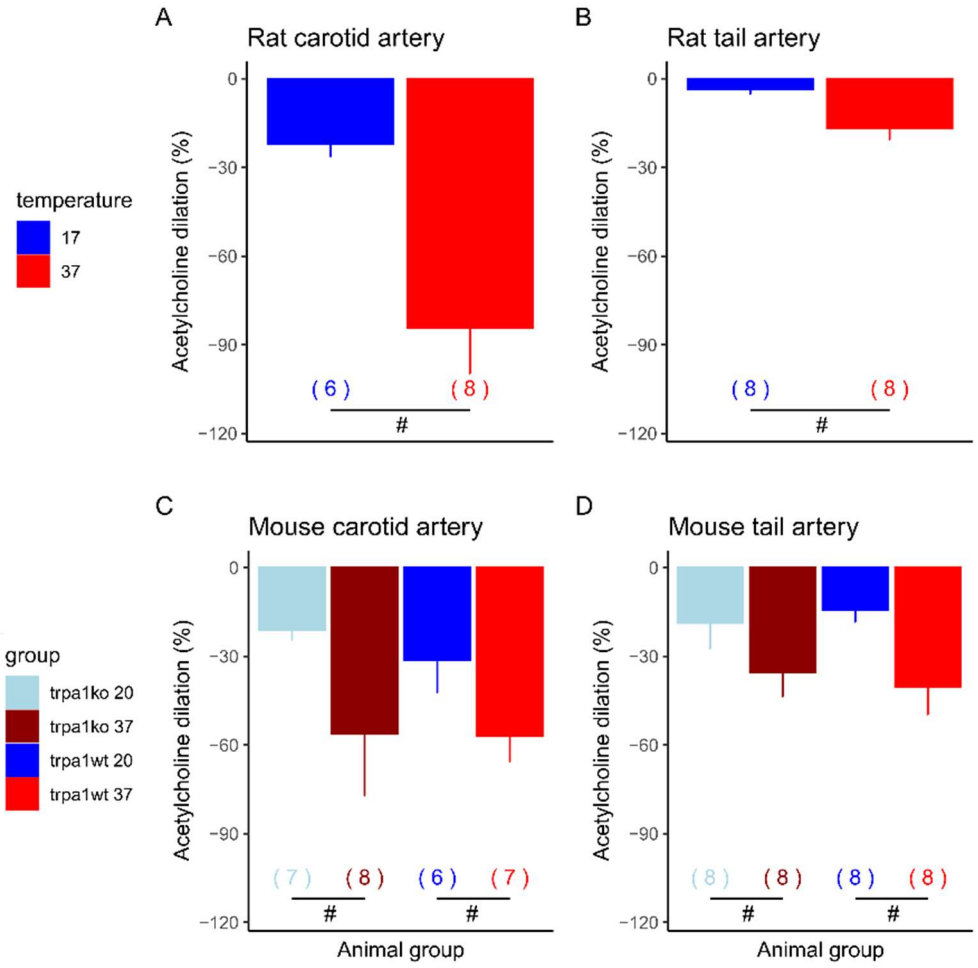

Figure 12. The effect of temperature on acetylcholine-induced vasodilation. # - significant effect of temperature [Kelava et al. 2024; manuscript in preparation].

4.3.4 The Effects of Temperature on the Response to SNP

Unlike acetylcholine, the temperature didn't have a significant effect on response to direct NO donor, SNP, in any of the 4 studied vessel types, even though there seemed to be some decrease in carotid arteries (Figure 13).

The SNP-induced dilation was somewhat reduced in the cold in rat carotid arteries ($F(1,12)=1.6211888$; $p=0.227$), but the effect was statistically insignificant. The dilation was -76.9±33.6 at 17°C and -131.4 ± 27.3 at 37°C (Figure 13a). In rat tail arteries, there was no effect of the temperature ($F(1,14)=0.249$; $p=0.626$), with dilation of -56.7 ± 16.1 at 17 °C and -48.5 ± 3.3 at 37°C (Figure 13b).

A similar trend was observed in mice, where the effect of temperature was also observed in carotid arteries, albeit statistically insignificant (F(1,1,1,23)=1.791; p=0.194), and there was no effect of genotype (Figure 13c). The dilation in the TRPA1 WT mice was 79.0 ± 22.0 at 37°C and -38.6±10.9 at 20°C, while in KO mice it was -44.9± 8.5 at 37°C and -47.7 ± 8.1 at 20°C (Figure 13c).

In mice tail arteries, there was no difference at two different temperatures (F (1,1,1,27)=0.44; p=0.513) and no effect of genotype (Figure 13d). The dilation in the WT mice was -65.5±18.3 at 37°C, and -58.4 ± 19.7 at 20°C, while in TRPA1 KO mice it was -42.7 ± 5.3 at 37°C and -89.7±54.5 at 20°C.

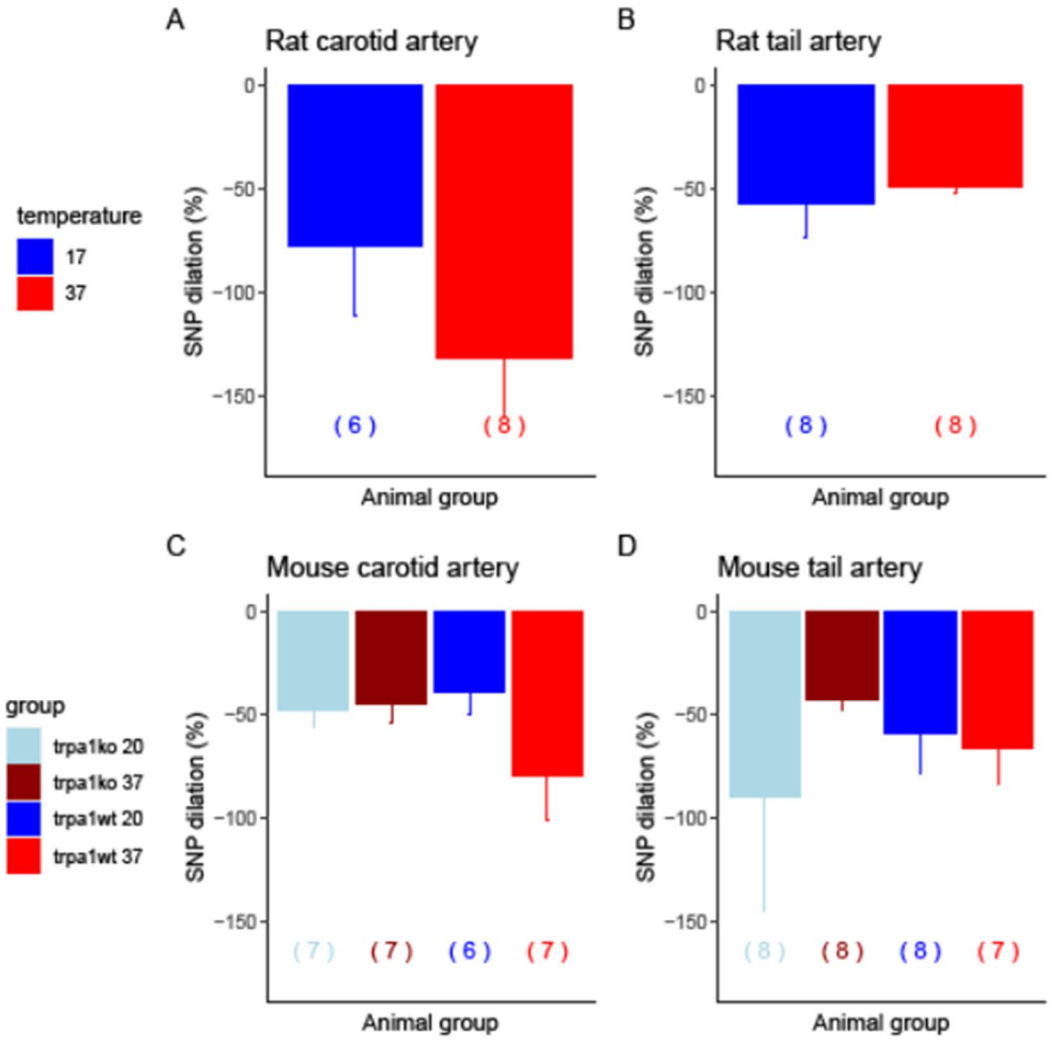

Figure 13. The effect of temperature on sodium-nitroprusside-induced vasodilation [Kelava *et al.* 2024; manuscript in preparation].

4.3.5 The Effect of H_2S in the Tail and Carotid Arteries of Rats and Mice at Different Temperatures

H_2S caused vasomotor responses in the range from 10^{-4} to 10^{-2} M. The responses varied and depended on the species, arterial bed, temperature, and genotype (Figure 13).

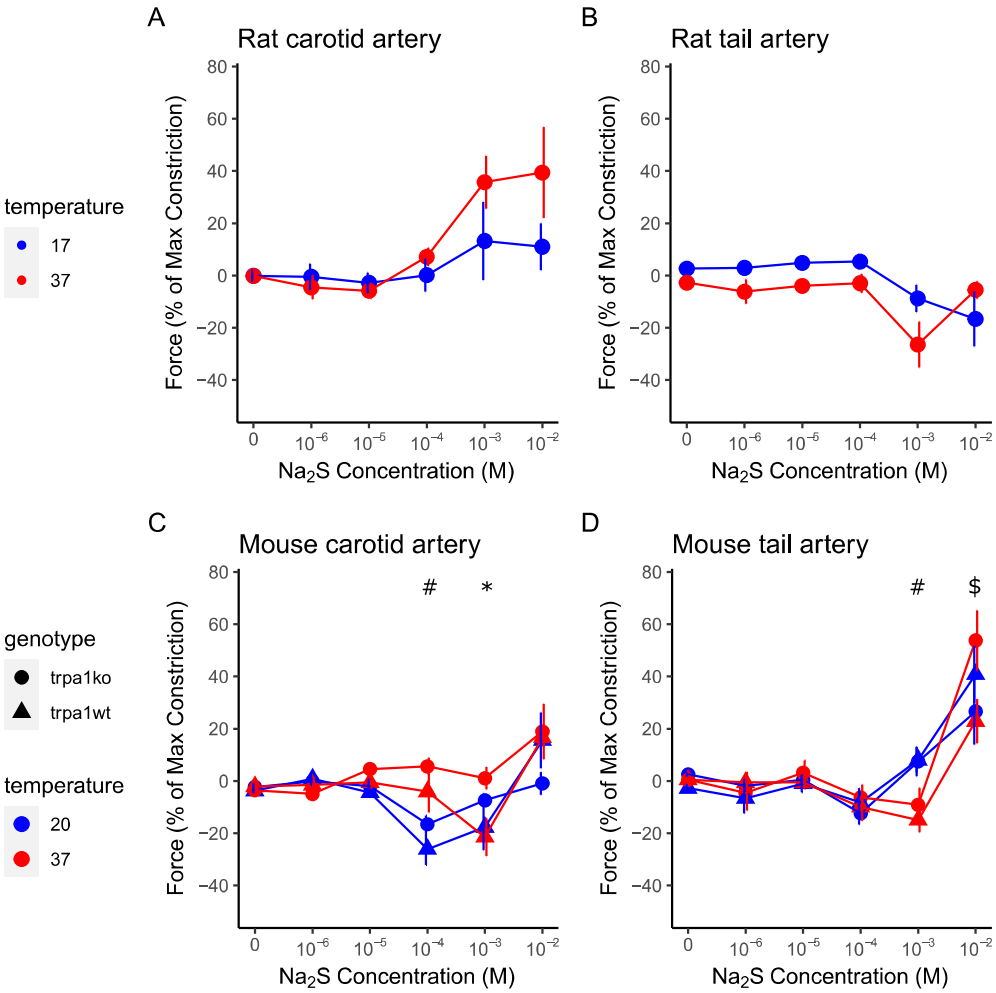

Figure 14. The effects of Na_2S on vasomotor responses at different temperatures. # - significant effect of temperature to Na_2S response, *- significant effect of presence of TRPA1 on Na_2S response, $ - significant interaction between temperature and presence of TRPA1 on Na_2S response [Kelava et al. 2024; manuscript in preparation].

In rats, Na_2S caused a response at 10^{-4}, 10^{-3} M and10^{-2} M. The carotid arteries showed dose-dependent vasoconstriction, that was decreased at 17°C at either concentration, even though the decrease was statistically not significant between 37 vs 17°C (Figure 13a): 10^{-4} M (7.2±3.5% vs. 0.2±6.3%), 10^{-3} M (35.7±10.1% vs. 13.2 ± 14.9%) and 10^{-2} M (39.4± 17.4% vs 11.0± 9.0%).

In rat tail artery experiments, the effects of Na_2S were observed at concentrations of 10^{-3} M and 10^{-2} M, with responses that seemed to be temperature-dependent at the lower concentration (Figure 13b). At 10^{-3} M, dilation was higher at 37°C (-26.5 ± 8.7%) compared to 17°C (-8.7 ± 5.2%), as indicated by borderline insignificant main effect of temperature ($F(1, 14) = 3.27$, $p=0.0922$). However, at the higher concentration the values were reversed, with stronger vasodilation being observed at 17°C (-16.6±10.5) than at 37°C (-5.5±3.3), however, there was still no statistical significance.

In mice, Na_2S caused a response at 10^{-4}, 10^{-3} M, and 10^{-2}M, which was dependent on temperature. In the carotid artery, WT mice showed dose-dependent vasodilation that was reversed to vasoconstriction at 10^{-2} M. At 10^{-4} M, there was a significant difference at different temperatures ($F(1,1,1, 24) =16.606$, $p =0.000436$), with stronger vasodilation at 20°C than at 37°C (-26.1±6.1% vs -4.1±8.0%). At 10^{-3} M, there was no difference at different temperatures, but the TRPA1 KO mice showed significantly weaker vasodilation than the WT controls ($F(1,1,1, 24) =8.263$, $p =0.00835$), with marked difference at 37°C (-21.4±7.2% vs 1.1±4.3%) and not so marked difference at 20°C (-17.7±8.7% vs -7.4±2.6%).

In the tail artery, Na_2S elicited responses at 10^{-3} M and 10^{-2} M, with temperature dependency observed primarily at 10^{-3} M ($F(1,1,1, 28) =12.949$, $p =0.00122$) (Figure 13a). At this concentration, vasodilation occurred at 37°C (-14.9±4.7%) and constriction at 20°C (8.1 ± 4.9%). At 10^{-2} M, vessels constricted at both temperatures, with a significant interaction between genotype and temperature ($F(1,1,1, 28) =4.212$, $p =0.0496$). While differences were not statistically significant between the two temperatures or the two genotypes, the TRPA1 KO mice exhibited higher constriction than the WT mice at 37°C (53.8± 11.5% vs 22.9±8.5%), and this was reversed at 20°C, where KO mice showed lower constriction compared to WT controls (26.6±12.6% vs 40.8±10.9%).

5. Discussion

The important findings related to cardiometabolic and -vascular responses to TRP stimulation by chemical agents or noxious cold exposure are: 1) oral supplementation of TRPV1 agonists reduces total serum cholesterol and LDL levels; 2) H_2S can cause both vasoconstriction and vasodilation depending on concentration, temperature, vascular bed, and concentration; 3) at physiological concentrations of H_2S and normal temperature, common carotid arteries of rats and mice show opposite responses: while mouse carotids dilate, the rat carotids constrict; 4) TRPA1 is responsible for H_2S induced vasodilation in carotid arteries in mice; 5) cold increases vasodilation in mouse carotid arteries; and 6) presence of TRPA1 affects the response of isolated mouse tail arteries, depending on the temperature.

5.1 Effects of Oral Capsaicinoids on Total Serum Cholesterol

Our meta-analysis showed that overall, oral capsaicinoid supplementation reduced total serum cholesterol, which was attributed to a decrease in LDL, while HDL remained unchanged and triglycerides were slightly reduced. The studies showed high heterogeneity in the response. This is due to differences in the duration of trials, ranging from 4 to 12 months; selection criteria, since some studies recruited healthy participants and some included overweight individuals; differences in treatments, since one study was supplemented with exercise routines; and different compounds and formulations, because 2 studies included herbal mixtures in a powder that contained capsaicinoids, while others included pills and different quantities of the total intake.

As LDL is a major prognostic factor in the development of atherosclerosis, capsaicinoids might have beneficial effects on the prevention of cardiovascular disease. The mechanisms of the observed reduction in total serum cholesterol and LDL are unclear. There may be some direct mechanism of cholesterol control, but indirect mechanisms, through control of other lipids and energy intake/expenditure, are more likely. The mechanisms are in part challenging to study because capsaicin is a lipophilic compound, that may reach all tissues. Most of capsaicin is metabolized in the liver, but

it was shown that it can also rapidly enter the central nervous system and kidneys, depending on the route of administration, while unmetabolized capsaicin lingers longest in the lungs [75]. One likely target is BAT. Research on mice demonstrated TRPV1 expression in BAT and protection against obesity and hypercholesterolemia, which might be a result of the interaction of capsaicinoids with BAT [9]. Further, BAT thermogenesis is stimulated *via* the sympathetic pathway. This sympathetic activation could happen through capsaicin's effects in CNS, but it could also happen through the inhibition of ghrelin release, a hunger hormone that was shown to inhibit thermogenesis [57, 60]. Interestingly, in one of the analyzed studies, ghrelin concentrations were measured and capsaicin-treated groups had decreased levels compared to the control [47], while in several papers, appetite suppression was reported [21, 102], which could also be an effect of reduced ghrelin levels.

Many authors report an association between BAT activation and reduction of serum cholesterol, although the findings are mixed. In an experiment with mice, the mobilization of fats in BAT for energy production increased liver uptake of delipidated, cholesterol-enriched lipoprotein remnants, thus clearing cholesterol from blood [11]. Similar effects are observed in cold exposure, wherein BAT is activated. A recent human trial showed that cold exposure increases free fatty acids in serum, while triglycerides are transiently increased, but then return to normal, suggesting fat mobilization. However, the authors measured only transient effects on lipid profile, and in 120 minutes upon cold exposure, serum cholesteryl esters were slightly increased [92]. Separate studies have shown that lipoprotein lipase, the enzyme that degrades triglycerides, also promotes cholesterol efflux from adipocytes in BAT to HDL in blood where it is subsequently hydrolyzed by endothelial lipase, taken up by the liver through scavenger B1 receptor, and excreted with the bile [8, 83, 113]. Therefore, even though triglycerides are the primary fuel for heat production, BAT recruitment likely affects serum cholesterol as well.

5.2 Development of heat exchange device

The successful development of heat-exchange plates underlined that resins with desktop SLA 3D printers can be potentially used for the fabrication of efficient and durable heat-exchange devices to be used in vascular physiology experiments. Mechanical tests revealed that the studied resin material is sufficiently hard and brite, with a Shore D hardness value of 83.0 ± 0.5. The results of the mechanical testing were supported by images taken with digital microscopy: the structure of the resin sample showed a glass-like, smooth surface both on the intact and broken surfaces. According to the thermal analysis of the sample, the heat stability was shown up to slightly above 250°C, although melting and sample decomposition occurred relatively quickly above that temperature range. These findings confirm that the transparent resin material can be reliably used in biomedical applications. Furthermore, with thermal conductivity measurements, we found that a relatively effective heat insulation can be achieved by using the studied resin material. In addition, we also showed that the application of the fabricated heat-exchange device can maintain a nearly constant temperature in vascular physiology measurements.

The wire myograph was also operational at lower temperatures, as demonstrated in our first experiments. However, the instrument could not be reliably used in experiments involving temperature change. Mock experiments with mounted wires without vessels showed that measurements during temperature change fluctuated significantly between the chambers. Two chambers had very high fluctuations during temperature change, while the other two showed somewhat consistent change, but even within these two, the standard error between the measurements varied over time, reaching around 0.1 mN at different time points. The reason behind these fluctuations is likely the electrical circuit that is responsible for force transducer measurements, which is positioned adjacent to the chambers and is not well thermally insulated. It uses Wheatstone bridge design, which is commonly used in sensor applications. In this circuit, one end generates electricity that is proportional to the force created by the vessel, while the other end changes the voltage to balance out that electricity. The temperature change in Wheatstone bridge affects the resistance of its resistors, which comprise both sensory elements, as well as reference resistors, and so it has to be calibrated to the specific temperature of the experiment before it starts. Change in

temperature during the experiment reduces the reliability of the measurements and that is why the setup could not be used to study the responses of vessels while the change is occurring [18]. We have concluded that the results obtained in this manner could not be reliable and reproducible in our case, thus we decided to focus on experiments at different fixed temperatures. Perhaps with better thermal isolation of the force transducers, artifacts introduced in the measurements would be more predictable and after their subtraction, measurements of real-time response to temperature change would be achievable. Alternatively to wire myography, pressure myography might be a more appropriate method to evaluate such real-time responses, as there, the vascular diameter is continuously monitored with high-resolution cameras.

5.3 Effects of Cold on KCl and Phenylephrine Constriction in Rat Tail Arteries

Preliminary experiments were performed on rat tail arteries. It was shown that at a lower temperature of 13°C, vasoconstriction through KCl-induced depolarization was significantly inhibited, while PE vasoconstriction and SNP-induced relaxation were unchanged. Increasing the amount of KCl to 90 mM produced a stronger response, but it still didn't reach the extent of responses at higher (deep body temperature range) temperature. These results were in accordance with the results previously obtained in different vessels at lower temperatures by using different instruments [16, 85], thus confirming the reliability of our measurements. As temperature affects the speed of diffusion as well as chemical reactions, including active transport of ionic species, new ionic equilibrium is the likely reason for the changes in KCl response. The investigation of this new ionic equilibrium was out of the scope of our research, but it may offer interesting subjects for future research. In the literature, there were only some modest attempts to explain why this happens.

One group suggested that reduced membrane permeability to calcium at cold disables VSMC contraction [16]. We propose that inhibition of the sodium-potassium-ATP pump, which occurs at cold [61], prevents cells from maintaining normal cell membrane potential and leads to more positive charges inside the cells, along with higher-than-normal extracellular potassium. This would require higher electromotive force for potassium to enter cells, thus preventing its entrance. In this manner, there

would be not enough depolarization to activate voltage-gated sodium channels and subsequent calcium entrance and VSMC contraction. It should be noted that this might not happen *in vivo*, as the cells in *in vitro* experiments are exposed to a relatively higher volume of extracellular fluid, so they may be more affected by its constituents. Indeed, a recent analysis of patients who underwent therapeutic hypothermia demonstrated the occurrence of hypokalemia in cold, presenting with risks of hyperkalemia on rewarming. However, the hypothermia in these cases was milder than in our experiments, never reaching temperatures below 32°C [14]. A meta-analysis that included 50 studies in animals and humans found hypokalemia in 39 studies, while in 11 studies there was hyperkalemia. The authors suggested that accidental hypothermia, which is usually more severe, leads to hyperkalemia [17]. Similar results were observed in a recent paper [28].

In vivo, experiments with rats showed that decreasing core temperature to 22°C causes hypokalemia. The authors measured serum potassium 4 times in each rat while decreasing the temperature from normothermic animals and produced a curve that showed temperature-dependent hypokalemia. This is in contrast to our suggestions and to what is expected if the Na^+/K^+-ATP-ase is inhibited. This response may be reversed at even lower temperatures of 17°C, corresponding to human data where hypokalemia occurs at first with hypothermia, but with lowering temperature further hyperkalemia ensues. In addition to this explanation and our previous explanation of discrepancies between *in vivo* and *in vitro* experiments, the authors also suggested that tissue redistribution of potassium might be the cause of hypokalemia, suggesting that the liver accumulates excess potassium. They haven't measured it, but cite several other papers that have observed increases in hepatocellular potassium during hypothermia [88]. This tissue redistribution might be a mechanism of protection against hyperkalemia that would be expected to happen when cold inhibits Na^+/K^+ ATPase.

5.4 Vasomotor Effects of Na_2S in Carotid and Tail Arteries in Mice and Rat

The effect of Na_2S was first observed at 10^{-4} M, which is in accordance with previous papers that suggested this concentration is needed in experiments performed *in vitro* to observe major changes in biological function [55]. The initially observed

vasodilation was reversed to vasoconstriction after 5 minutes which might have been caused by evaporation of H_2S and the effect of increased sodium concentrations. Indeed, it was suggested that the halftime of 10^{-4} M H_2S in myograph chambers containing air-bubbled water solution of 5 ml is 2.46 sec, suggesting that ~80 % of H_2S is removed from the chamber by the 5th minute [25]. Furthermore, even during *in vivo* experiments, the effects of Na_2S are shortlasting. In experiments with a closed cranial window, Na_2S caused vasodilation in the dural and pial arteries. The effect was observed within 1 minute and was extinguished in less than 1 minute. Interestingly, in dural arteries, the dilation was dependent on TRPA1, while in pial arteries, it was dependent on KCa3.1 channels. Both of these arteries express TRPA1 in endothelium [39].

At 37°C, tail and carotid arteries in mice showed a correlation in Na_2S response: vasodilation at 10^{-4} M and 10^{-3} M, while vasoconstriction at 10^{-2} M. This was not the case in rats, where 10^{-3} M of Na_2S caused vasodilation in tail artery, but vasoconstriction in carotid arteries, whereas 10^{-2} M of Na_2S caused vasoconstriction in both.

The reasons underlying this difference might be multifaceted, reflecting many differences in the biology of the two species. As H_2S causes vasodilation in common carotids from other mammalian species, including mice and rabbits [20], this might be a special adaptation in rats, which could promote shunting of the H_2S-rich blood towards the liver, where the three-enzyme pathway enables the oxidation and clearance of sulfide from the blood [40]. Likewise, there are underlying differences in the thermoregulatory systems between the two species. Mice can enter torpor, a hypometabolic state where their core temperature, activity, and oxygen consumption drop, and which is affected by ambient temperature, nutritional status, and food availability [87]. Rats do not use this ability on such a regular basis and there is controversy about whether they use it at all, or whether it is just survivable accidental hypothermia that is observed in several rat species [69]. H_2S is suggested to be an important controller in the activation of this energy-conserving mechanism [42]. During a torpor bout, the peripheral vascular resistance increases, so the tail arteries would be expected to constrict while mean arterial pressure drops, suggesting dilation of the central arteries, such as carotids. Torpor is also associated with a decrease in heart rate [95]. Peripheral resistance increases in exposure to cold (without torpor) as well, but this is typically associated with increases in heart rate, so the mean arterial pressure also increases in both mice and rats [96].

5.5 Temperature Modulation of H_2S-induced Vasomotor Responses

5.5.1 Tail Arteries in Mice and Rats

Regarding the tail arteries, our findings suggest that ambient temperature had a more pronounced effect on Na_2S response in mice than in rats. Although the dilation was still reduced in both species in cold, in mice it was even reversed to constriction. At higher Na_2S concentration (10^{-2} M), the rat tail artery continued to dilate at cold, while it continued to constrict in mice. This different response in cold might be attributable to more stringent management of heat dissipation in mice that are at higher risk of dropping their core temperature in cold environment due to their smaller size. In particular, our research suggests that mice might have more control over local cooling events than rats as our experimental setup doesn't allow the investigation of systemic responses. H_2S, as a potent vasodilator, induces paradoxical vasodilation in the rat tail artery in cold, which would contribute to further cooling, while in the mouse tail artery, the mild constriction it induced could help to withstand the harmful effect of cooling.

5.5.2 Carotid Arteries in Mice and Rats

Compared to tail arteries, cold had the opposite effect on H_2S-induced responses in the carotid arteries of both species: it increased the vessel diameter. This translates to reduced H_2S-induced vasoconstriction in rat carotids and increased H_2S-induced vasodilation in mouse carotids. Previous research has demonstrated cooling-induced vasodilation in carotid arteries from rabbits and humans [66]. We couldn't have measured this effect, as the vessels would have been immersed in the cold for a while before starting the measurements, but our research has shown that acetylcholine vasodilation was inhibited in cold, and although non-significant, there seemed to have been inhibition of SNP-induced vasodilation in cold as well.

5.6 The Role of TRPA1 in H_2S-induced Vasomotor Responses in Mice

5.6.1 Tail Artery

There was no difference in the response to H_2S between the genotypes. This is in contrast with two *in vivo* experiments on mouse cutaneous arteries from ears and paws, where the first one showed a difference between $TRPA1^{+/+}$ and $TRPA1^{-/-}$ mice stimulated by topical H_2S donor and the other one showed the difference between the genotypes upon cold stimulation [6, 73]. This could be due to differences in vascular beds or the experiment design. According to the literature, TRPA1 can be expressed in either endothelial cells, such as pial and dural arteries, or in perivascular neurons. The wire myography is usually used to assess the functions of ECs and VSMCs. Several groups have reported that functional nerve endings might be present as well. However, these neurons would be expected to be damaged and equilibrated with the bath solution, so it is difficult to imagine that activation of ion channels could stimulate synaptic transmission. Indeed, papers that demonstrate the presence of neurons in wire myography bath chambers usually used calcium-independent activators and inhibitors of synaptic transmission, tyramine [109] and guanethidine [105], respectively. Thus, perhaps there is no TRPA1 in ECs and VSMCs in mice tail arteries, but we can't exclude its presence in perivascular neurons.

Interaction between temperature and genotype was observed at a high 10^{-2} M (*i.e.*, beyond physiological) dose of Na_2S, at which TRPA1 KO mice had smaller vasoconstriction than WT mice at 20°C, but higher vasoconstriction at 37°C. The explanations for this might be physiological adaptations to the lack of TRPA1 in perivascular neurons. The two aforementioned papers showed that these responses to H_2S and cold are likely mediated by TRPA1 in perivascular neurons [6, 73]. Both research groups showed that TRPA1-dependent vasodilation was mediated by CGRP, a peptide released by sensory neurons, and Aubdool *et al*. additionally showed substance P dependency as well as the importance of NO release [6]. Regarding vasoconstriction, Aubdool *et al*. proposed that TRPA1 activation causes the generation of ROS [6]. Previous research in mice tail arteries suggested that cold-induced generation of ROS from mitochondria promotes translocation of α2C-adrenoceptors from the Golgi to the surface membrane in VSMC in a ROCK-dependent fashion [7].

H_2S might also increase the generation of ROS [44], even though the studies show biphasic effects. At lower doses, H_2S protects mitochondria in hypoxia by providing an alternative electron acceptor for oxidative phosphorylation, while at higher doses, H_2S inhibits cytochrome c oxidase and thus prevents electron transport. In the same manner, research has suggested that H_2S might cause both increases and decreases in ROS. Thus, possibly due to the lack of TRPA1 in KO mice, VSMCs do not contain as many vesicles with α2C-adrenoceptors as the WT mice, thereby ROS cannot activate translocation of as many receptors to the surface. The experimental confirmation of this hypothesis remains the subject for future studies.

Previous research in mouse tail arteries had shown that acetylcholine-induced dilation at physiological deep body temperatures is mediated predominantly by NO and prostacyclin (PGI_2) production [33]. However, the acetylcholine-induced dilation at cold (28°C) was not affected by either NO or PGI_2 inhibitors. Thus, the researchers concluded that the NO/PGI_2-independent endothelial dilator mechanism is responsible for acetylcholine response in cold. They showed that inhibition of small-conductance or intermediate-conductance calcium-dependent potassium channels (SK, IK), reduced acetylcholine dilation in cold, thus concluded that endothelial hyperpolarization through myo-endothelial coupling is the predominant mechanism of acetylcholine dilation in cold [33]. Our experiments were performed at a lower temperature (20°C) and we observed smaller responses to acetylcholine at this temperature in both rat and mouse arteries. These discoveries are in accordance with the previous findings showing that the tail has different thermoregulatory functions in rats and mice [86]. It was shown that rats cannot thermoregulate successfully when their tail is amputated, while mouse thermoregulation is not affected by the removal of their tail. Furthermore, it was suggested that the mouse tail contributes modestly to thermoregulation, with an overall impact of around 7% [86].

5.6.2 Carotid Artery

The H_2S-induced vasodilation at 10^{-3} M was reduced in the mouse carotid artery at both temperatures in the absence of the TRPA1 channel. This was a surprise, since we expected that TRPA1, as a cold receptor, would have a more prominent role at the periphery. The effect of TRPA1 presence was partly diminished at 20°C, mostly due to

smaller vasodilation in the WT mice. This could be explained by cold-induced desensitization of TRPA1. Previous research has shown that slow cooling can bring about TRPA1 desensitization [24]. While we did not employ gradual cooling in our protocol, the temperature slightly above the reported 17°C threshold of TRPA1 activation might have produced a similar effect. This temperature should have been enough to activate some TRPA1 receptors, as the channel open probability is a function that starts increasing as soon as the temperature drops below 25°C [24]. The same authors reported potentiation of agonist-induced TRPA1 activation upon cooling and stimulation with AITC, but this increased sensitivity was not observed in our experiments. The vessels did indeed show increased sensitivity to H_2S in cold, reacting at lower concentrations of 10^{-4} M, but this was observed in both $TRPA1^{+/+}$ and $TRPA1^{-/-}$ mice, so it was not TRPA1 dependent. The increased vasodilation at cold was specific to H_2S, as acetylcholine- and SNP-induced vasodilation was reduced in cold.

The presence of TRPA1 in the carotid artery presents itself as a possible mechanism of how cold-induced vasodilation ensues. Mustafa *et al*. investigated cold-induced vasodilation in several animal models since 2002[66]. In 2023, they published an extensive review, where they elucidated this response was not endothelium-dependent, was not neurogenic or myogenic, did not involve NO or CO, nor did it involve any vasodilator compound released from vessels, as the addition of more vessel segments to chambers did not increase the response. They concluded that unknown thermal receptors in VSMCs mediate this response [65]. TRPA1 might be a candidate molecule for such a response. In support of this hypothesis, hyperpolarization and subsequent vasodilation were shown to be mediated through calcium entry *via* ROS-activated TRPA1 channels in the cerebral artery [93].

5.7 Conclusions

The research presented here highlights the important contributions of two TRP receptors, TRPV1 and TRPA1, to cardiovascular system functions. Our meta-analysis suggests that activation of TRPV1 can protect from hypercholesterolemia. We developed and validated a novel heat-exchange device that enables wire myography experiments to be performed in a wide range of temperatures. Our basic research shows that TRPA1 is responsible for H_2S-induced vasodilation in the carotid arteries of mice, but not for the vasodilation in the tail arteries. We demonstrate the striking difference in carotid arteries from rats, where H_2S caused vasoconstriction, which is an important consideration in translational research. Furthermore, we demonstrate that decreasing temperature increases H_2S-induced vasodilation in the carotid artery of mice, but restricts it in the mouse tail artery, where the effect is even reversed to vasoconstriction. Cold changed the responses in rat arteries in the same direction, albeit the effect was smaller there.

6. Peer-reviewed Publications by the Author

1. Publications related to the thesis

Kelava, L., Nemeth, D., Hegyi, P., Keringer, P., Kovacs, D.K., Balasko, M., Solymar, M., Pakai, E., Rumbus, Z. and Garami, A., 2022. Dietary supplementation of transient receptor potential vanilloid-1 channel agonists reduces serum total cholesterol level: a meta-analysis of controlled human trials. Critical Reviews in Food Science and Nutrition, 62(25), pp.7025-7035. **(IF:10.3)**

Kelava, L., Ivić, I., Pakai, E., Fekete, K., Maroti, P., Told, R., Ujfalusi, Z. and Garami, A., 2022. Stereolithography 3D printing of a heat exchanger for advanced temperature control in wire myography. Polymers, 14(3), p.471. **(IF:4.9)**

Kelava, L., Pakai, E., Fekete, K., and Garami, A., 2024. Vascular effects of hydrogen sulfide at normal body temperature and cold in the isolated tail and carotid arteries from rats, TRPA1+/+, and TRPA1-/- mice. Biomedicines (in preparation).

2. Publications not related to the thesis

Olah, E., Rumbus, Z., Kormos, V., Tekus, V., Pakai, E., Wilson, H.V., Fekete, K., Solymar, M., Kelava, L., Keringer, P. and Gaszner, B., 2021. The hypothermic effect of hydrogen sulfide is mediated by the transient receptor potential ankyrin-1 channel in mice. Pharmaceuticals, 14(10), p.992. (**IF:4.6**)

Toldi, J., **Kelava, L.,** Marton, S., Muhl, D., Kustan, P., Feher, Z., Maar, K., Garai, J., Pakai, E. & Garami, A. (2023). Distinct patterns of serum and urine macrophage migration inhibitory factor kinetics predict death in sepsis: a prospective, observational clinical study. Scientific Reports, 13(1), 588. **(IF:4.3)**

Song, Y., **Kelava, L.,** Zhang, L., & Kiss, I. (2022). Microarray data analysis to identify miRNA biomarkers and construct the lncRNA-miRNA-mRNA network in lung adenocarcinoma. Medicine, 101(36), e30393. **(IF:1.6)**

Kovács, D.K., Farkas, N., Soós, A., Hegyi, P., **Kelava, L.,** Eitmann, S., Schekk, A., Molnár, Z., Erőss, B. and Balaskó, M., 2021. Assessment of clinical data on urocortins and their therapeutic potential in cardiovascular diseases: A systematic review and meta-analysis. Clinical and Translational Science, 14(6), pp.2461-2473. **(IF:3.6)**

Keringer, P., Furedi, N., Gaszner, B., Miko, A., Pakai, E., Fekete, K., Olah, E., **Kelava, L.,** Romanovsky, A.A., Rumbus, Z. and Garami, A., 2022. The hyperthermic effect of central cholecystokinin is mediated by the cyclooxygenase-2 pathway. American Journal of Physiology-Endocrinology and Metabolism, 322(1), pp.E10-E23. **(IF:4.5)**

Koren, T., Koller Šarić, K. and **Kelava, L.,** 2022. The first records of Trithemis annulata

(Palisot de Beauvois, 1807)(Odonata: Libellulidae) in Croatia. Natura Croatica: Periodicum Musei Historiae Naturalis Croatici, 31(2), pp.293-302. **(IF:0.42)**

Song, Y., **Kelava, L.** and Kiss, I., 2023. MiRNAs in Lung Adenocarcinoma: Role, Diagnosis, Prognosis, and Therapy. International Journal of Molecular Sciences, 24(17), p.13302. **(IF:5.6)**

Cumulative impact factor of publications related to the thesis: 15.2
Cumulative impact factor of all publications: 48.628
Total number of publications: 9

7. Acknowledgments

I would like to express gratitude to my mentor, Dr. András Garami for giving me the opportunity to conduct this PhD research at his department and for guiding me through the process. He was always there with good advice when needed, and was very calm and patient, even through difficult times.

I thank all the current and former members of the Department of Thermophysiology for their technical assistance, they did an excellent work, with kindness, and were always helpful (in alphabetical order): Roland Bakos, Zsuszanna Dudas, Kata Fekete, Dr. Eszter Garaminé Pákai, Dr. Patrik Kéringer, Dr. Zoltán Rumbus, and Anikó Várnagyné Rózsafi.

I thank Dr. Péter Tóth for granting me access to his laboratory to conduct experimental research and to the 3D Printing and Visualization Center led by Dr. Péter Maróti for our successful collaboration.

I thank Kinga Kurucz and Andrea Mihálffyné Jech for their kindness and help with administrative tasks, and I thank all the members of the Institute for Translational Medicine in Pécs, and student researcher, Kazushi Ogasawara.

Finally, I thank my family and friends, especially my parents, Vesna Rosandić-Kelava and Vitomir Kelava, for their support in life and everything related, and my friends and collaborators Ivan Ivić, Toni Koren, and Yongan Song.

8. References

[1] S.S. Abdalla, A.A. Harb, I.M. Almasri, Y.K. Bustanji, The interaction of TRPV1 and lipids: Insights into lipid metabolism, Frontiers in physiology, 13 (2022) 1066023.

[2] K. Abe, H. Kimura, The possible role of hydrogen sulfide as an endogenous neuromodulator, The Journal of neuroscience : the official journal of the Society for Neuroscience, 16 (1996) 1066-1071.

[3] M. Alexandre, P. Dubois, Polymer-layered silicate nanocomposites: preparation, properties and uses of a new class of materials, Materials science and engineering: R: Reports, 28 (2000) 1-63.

[4] S.F. Ang, S.W. Sio, S.M. Moochhala, P.A. MacAry, M. Bhatia, Hydrogen sulfide upregulates cyclooxygenase-2 and prostaglandin E metabolite in sepsis-evoked acute lung injury via transient receptor potential vanilloid type 1 channel activation, Journal of immunology (Baltimore, Md. : 1950), 187 (2011) 4778-4787.

[5] H. Aslami, A. Heinen, J.J. Roelofs, C.J. Zuurbier, M.J. Schultz, N.P. Juffermans, Suspended animation inducer hydrogen sulfide is protective in an in vivo model of ventilator-induced lung injury, Intensive care medicine, 36 (2010) 1946-1952.

[6] A.A. Aubdool, R. Graepel, X. Kodji, K.M. Alawi, J.V. Bodkin, S. Srivastava, C. Gentry, R. Heads, A.D. Grant, E.S. Fernandes, S. Bevan, S.D. Brain, TRPA1 is essential for the vascular response to environmental cold exposure, Nature communications, 5 (2014) 5732.

[7] S.R. Bailey, S. Mitra, S. Flavahan, N.A. Flavahan, Reactive oxygen species from smooth muscle mitochondria initiate cold-induced constriction of cutaneous arteries, American journal of physiology. Heart and circulatory physiology, 289 (2005) H243-250.

[8] A. Bartelt, C. John, N. Schaltenberg, J.F.P. Berbée, A. Worthmann, M.L. Cherradi, C. Schlein, J. Piepenburg, M.R. Boon, F. Rinninger, M. Heine, K. Toedter, A. Niemeier, S.K. Nilsson, M. Fischer, S.L. Wijers, W. van Marken Lichtenbelt, L. Scheja, P.C.N. Rensen, J. Heeren, Thermogenic adipocytes promote HDL turnover and reverse cholesterol transport, Nature communications, 8 (2017) 15010.

[9] P. Baskaran, V. Krishnan, K. Fettel, P. Gao, Z. Zhu, J. Ren, B. Thyagarajan, TRPV1 activation counters diet-induced obesity through sirtuin-1 activation and PRDM-16 deacetylation in brown adipose tissue, International journal of obesity (2005), 41 (2017) 739-749.

[10] M. Benítez-Angeles, S.L. Morales-Lázaro, E. Juárez-González, T. Rosenbaum, TRPV1: Structure, Endogenous Agonists, and Mechanisms, International journal of molecular sciences, 21 (2020).

[11] J.F. Berbée, M.R. Boon, P.P. Khedoe, A. Bartelt, C. Schlein, A. Worthmann, S. Kooijman, G. Hoeke, I.M. Mol, C. John, C. Jung, N. Vazirpanah, L.P. Brouwers, P.L. Gordts, J.D. Esko, P.S. Hiemstra, L.M. Havekes, L. Scheja, J. Heeren, P.C. Rensen, Brown fat activation reduces hypercholesterolaemia and protects from atherosclerosis development, Nature communications, 6 (2015) 6356.

[12] K.J. Bigiarelli, Rodent Thermoregulation: Considerations for Tail-Cuff Blood Pressure Measurements, Journal of the American Association for Laboratory Animal Science : JAALAS, 61 (2022) 406-411.

[13] E. Blackstone, M. Morrison, M.B. Roth, H2S induces a suspended animation-like state in mice, Science (New York, N.Y.), 308 (2005) 518.

[14] K. Boubes, D. Batlle, Serum potassium changes during hypothermia and rewarming: a case series and hypothesis on the mechanism, Clinical kidney journal, 16 (2023) 827-834.

[15] J.C. Brasen, C. de Wit, C.M. Sorensen, Myoendothelial coupling through Cx40 contributes to EDH-induced vasodilation in murine renal arteries: evidence from experiments and modelling, Acta physiologica (Oxford, England), 222 (2018).

[16] S.P. Bruttig, D.E. Roberts. Cold-Induced Changes in Arterial Sensitivity. Available online: https://apps.dtic.mil/sti/citations/ADA239493. Accessed (29 December 2021).

[17] S. Buse, M. Blancher, D. Viglino, M. Pasquier, M. Maignan, P. Bouzat, T. Annecke, G. Debaty, The impact of hypothermia on serum potassium concentration: A systematic review, Resuscitation, 118 (2017) 35-42.

[18] E. Cao, J.F. Cordero-Morales, B. Liu, F. Qin, D. Julius, TRPV1 channels are intrinsically heat sensitive and negatively regulated by phosphoinositide lipids, Neuron, 77 (2013) 667-679.

[19] M.J. Caterina, M.A. Schumacher, M. Tominaga, T.A. Rosen, J.D. Levine, D. Julius, The capsaicin receptor: a heat-activated ion channel in the pain pathway, Nature, 389 (1997) 816-824.

[20] J.M. Centeno, M.A. López-Morales, A. Aliena-Valero, T. Jover-Mengual, M.C. Burguete, M. Castelló-Ruiz, F.J. Miranda, Potassium channels contribute to the increased sensitivity of the rabbit carotid artery to hydrogen sulfide in diabetes, European journal of pharmacology, 853 (2019) 33-40.

[21] Y.S. Cha, S.R. Kim, J.A. Yang, H.I. Back, M.G. Kim, S.J. Jung, W.O. Song, S.W. Chae, Kochujang, fermented soybean-based red pepper paste, decreases visceral fat and improves blood lipid profiles in overweight adults, Nutrition & metabolism, 10 (2013) 24.

[22] M.A. Chotani, S. Flavahan, S. Mitra, D. Daunt, N.A. Flavahan, Silent alpha(2C)-adrenergic receptors enable cold-induced vasoconstriction in cutaneous arteries, American journal of physiology. Heart and circulatory physiology, 278 (2000) H1075-1083.

[23] D.E. Clapham, C. Miller, A thermodynamic framework for understanding temperature sensing by transient receptor potential (TRP) channels, Proceedings of the National Academy of Sciences of the United States of America, 108 (2011) 19492-19497.

[24] D. del Camino, S. Murphy, M. Heiry, L.B. Barrett, T.J. Earley, C.A. Cook, M.J. Petrus, M. Zhao, M. D'Amours, N. Deering, G.J. Brenner, M. Costigan, N.J. Hayward, J.A. Chong, C.M. Fanger, C.J. Woolf, A. Patapoutian, M.M. Moran, TRPA1 contributes to cold hypersensitivity, The Journal of neuroscience : the official journal of the Society for Neuroscience, 30 (2010) 15165-15174.

[25] E.R. DeLeon, G.F. Stoy, K.R. Olson, Passive loss of hydrogen sulfide in biological experiments, Analytical biochemistry, 421 (2012) 203-207.

[26] R. DerSimonian, N. Laird, Meta-analysis in clinical trials, Controlled clinical trials, 7 (1986) 177-188.

[27] S. Earley, TRPA1 channels in the vasculature, British journal of pharmacology, 167 (2012) 13-22.

[28] M.E. Elsayed, B. Schick, A. Woywodt, B.F. Palmer, The hypokalaemia that came from the cold, Clinical kidney journal, 16 (2023) 768-772.

[29] A. Eskilsson, K. Shionoya, S. Enerbäck, D. Engblom, A. Blomqvist, The generation of immune-induced fever and emotional stress-induced hyperthermia in mice does not involve brown adipose tissue thermogenesis, FASEB journal : official publication of the Federation of American Societies for Experimental Biology, 34 (2020) 5863-5876.

[30] K. Fayazbakhsh, M. Movahedi, J. Kalman, The impact of defects on tensile properties of 3D printed parts manufactured by fused filament fabrication, Materials today communications, 18 (2019) 140-148.

[31] E.S. Fernandes, M.A. Fernandes, J.E. Keeble, The functions of TRPA1 and TRPV1: moving away from sensory nerves, British journal of pharmacology, 166 (2012) 510-521.

[32] R.A.R. Fernández, R.N. Soriano, H.D.C. Francescato, J.P. Sabino, T.M. Coimbra, L.G.S. Branco, Cryogenic role of central endogenous hydrogen sulfide in the rat model of endotoxic shock, Brain research, 1650 (2016) 218-223.

[33] S. Flavahan, N.A. Flavahan, Cooling-induced dilatation of cutaneous arteries is mediated by increased myoendothelial communication, American journal of physiology. Heart and circulatory physiology, 319 (2020) H123-h132.

[34] A. Garami, E. Pakai, H.A. McDonald, R.M. Reilly, A. Gomtsyan, J.J. Corrigan, E. Pinter, D.X.D. Zhu, S.G. Lehto, N.R. Gavva, P.R. Kym, A.A. Romanovsky, TRPV1 antagonists that cause hypothermia, instead of hyperthermia, in rodents: Compounds' pharmacological profiles, in vivo targets, thermoeffectors recruited and implications for drug development, Acta physiologica (Oxford, England), 223 (2018) e13038.

[35] A. Garami, Y.P. Shimansky, Z. Rumbus, R.C.L. Vizin, N. Farkas, J. Hegyi, Z. Szakacs, M. Solymar, A. Csenkey, D.A. Chiche, R. Kapil, D.J. Kyle, W.D. Van Horn, P. Hegyi, A.A. Romanovsky, Hyperthermia induced by transient receptor potential vanilloid-1 (TRPV1) antagonists in human clinical trials: Insights from mathematical modeling and meta-analysis, Pharmacology & therapeutics, 208 (2020) 107474.

[36] K. Gintner, P2. 8 Simultaneous measurement of resistance and temperature changes in bridge circuits, Tagungsband, (2019) 708-714.

[37] C.J. Gordon, The mouse thermoregulatory system: Its impact on translating biomedical data to humans, Physiology & behavior, 179 (2017) 55-66.

[38] K. Gziut, A. Kowalczyk, B. Schmidt, Free-radical bulk-photopolymerization process as a method of obtaining thermally curable structural self-adhesive tapes and effect of used type I photoinitiators, Polymers (Basel), 12 (2020).

[39] A.K. Hansted, L.J. Jensen, J. Olesen, I. Jansen-Olesen, Localization of TRPA1 channels and characterization of TRPA1 mediated responses in dural and pial arteries in vivo after intracarotid infusion of Na2S, Cephalalgia : an international journal of headache, 40 (2020) 1310-1320.

[40] T.M. Hildebrandt, M.K. Grieshaber, Three enzymatic activities catalyze the oxidation of sulfide to thiosulfate in mammalian and invertebrate mitochondria, The FEBS journal, 275 (2008) 3352-3361.

[41] S.Y. Hong, Y.C. Kim, M. Wang, H.-I. Kim, D.-Y. Byun, J.-D. Nam, T.-W. Chou, P.M. Ajayan, L. Ci, J. Suhr, Experimental investigation of mechanical properties of UV-Curable 3D printing materials, Polymer, 145 (2018) 88-94.

[42] B.S. Jensen, A. Fago, Sulfide metabolism and the mechanism of torpor, Journal of experimental biology, 224 (2021).

[43] S. Jia, D. Yu, Y. Zhu, Z. Wang, L. Chen, L. Fu, Morphology, crystallization and thermal behaviors of PLA-based composites: wonderful effects of hybrid GO/PEG via dynamic impregnating, Polymers (Basel), 9 (2017).

[44] J. Jiang, A. Chan, S. Ali, A. Saha, K.J. Haushalter, W.-L.M. Lam, M. Glasheen, J. Parker, M. Brenner, S.B. Mahon, Hydrogen sulfide—mechanisms of toxicity and development of an antidote, Scientific reports, 6 (2016) 20831.

[45] L. Jin, G. Jagatheesan, L. Guo, M. Nystoriak, M. Malovichko, P. Lorkiewicz, A. Bhatnagar, S. Srivastava, D.J. Conklin, Formaldehyde Induces Mesenteric Artery Relaxation via a Sensitive Transient Receptor Potential Ankyrin-1 (TRPA1) and Endothelium-Dependent Mechanism: Potential Role in Postprandial Hyperemia, Frontiers in physiology, 10 (2019) 277.

[46] J.M. Johnson, C.T. Minson, D.L. Kellogg, Jr., Cutaneous vasodilator and vasoconstrictor mechanisms in temperature regulation, Comprehensive Physiology, 4 (2014) 33-89.

[47] C. Kang, Y. Zhang, X. Zhu, K. Liu, X. Wang, M. Chen, J. Wang, H. Chen, S. Hui, L. Huang, Q. Zhang, J. Zhu, B. Wang, M. Mi, Healthy Subjects Differentially Respond to Dietary Capsaicin Correlating with Specific Gut Enterotypes, The Journal of clinical endocrinology and metabolism, 101 (2016) 4681-4689.

[48] Y. Karashima, K. Talavera, W. Everaerts, A. Janssens, K.Y. Kwan, R. Vennekens, B. Nilius, T. Voets, TRPA1 acts as a cold sensor in vitro and in vivo, Proceedings of the National Academy of Sciences of the United States of America, 106 (2009) 1273-1278.

[49] L. Kelava, I. Ivić, E. Pakai, K. Fekete, P. Maroti, R. Told, Z. Ujfalusi, A. Garami, Stereolithography 3D Printing of a Heat Exchanger for Advanced Temperature Control in Wire Myography, Polymers, 14 (2022) 471.

[50] L. Kelava, D. Nemeth, P. Hegyi, P. Keringer, D.K. Kovacs, M. Balasko, M. Solymar, E. Pakai, Z. Rumbus, A. Garami, Dietary supplementation of transient receptor potential vanilloid-1 channel agonists reduces serum total cholesterol level: a meta-analysis of controlled human trials, Critical reviews in food science and nutrition, 62 (2022) 7025-7035.

[51] P. Kiekkas, D. Aretha, G.I. Baltopoulos, The continuing question of how fever duration is associated with patient outcome, Critical care (London, England), 16 (2012) 166.

[52] A.-P. Koivisto, M.G. Belvisi, R. Gaudet, A. Szallasi, Advances in TRP channel drug discovery: from target validation to clinical studies, Nature reviews drug discovery, 21 (2022) 41-59.

[53] M. Košir, M. Podbregar, Advances in the Diagnosis of Sepsis: Hydrogen Sulfide as a Prognostic Marker of Septic Shock Severity, The electronic journal of the International Federation of Clinical Chemistry and Laboratory Medicine, 28 (2017) 134-141.

[54] W.J. Laursen, E.O. Anderson, L.J. Hoffstaetter, S.N. Bagriantsev, E.O. Gracheva, Species-specific temperature sensitivity of TRPA1, Temperature (Austin, Tex.), 2 (2015) 214-226.

[55] M.D. Levitt, M.S. Abdel-Rehim, J. Furne, Free and acid-labile hydrogen sulfide concentrations in mouse tissues: anomalously high free hydrogen sulfide in aortic tissue, Antioxidants & redox signaling, 15 (2011) 373-378.

[56] T. Li, C.T. Saito, T. Hikitsuchi, Y. Inoguchi, H. Mitsuishi, S. Saito, M. Tominaga, Diverse sensitivities of TRPA1 from different mosquito species to thermal and chemical stimuli, Scientific reports, 9 (2019) 20200.

[57] L. Lin, J.H. Lee, O.Y. Bongmba, X. Ma, X. Zhu, D. Sheikh-Hamad, Y. Sun, The suppression of ghrelin signaling mitigates age-associated thermogenic impairment, Aging, 6 (2014) 1019-1032.

[58] C.J. Madden, S.F. Morrison, Central nervous system circuits that control body temperature, Neuroscience letters, 696 (2019) 225-232.

[59] E. Magli, E. Perissutti, H(2)S Donors and Their Use in Medicinal Chemistry, Biomolecules, 11 (2021).

[60] A. Mano-Otagiri, H. Ohata, A. Iwasaki-Sekino, T. Nemoto, T. Shibasaki, Ghrelin suppresses noradrenaline release in the brown adipose tissue of rats, The Journal of endocrinology, 201 (2009) 341-349.

[61] M. Marjanovic, J.S. Willis, ATP dependence of Na(+)-K+ pump of cold-sensitive and cold-tolerant mammalian red blood cells, The Journal of physiology, 456 (1992) 575-590.

[62] T. Miyamoto, A.E. Dubin, M.J. Petrus, A. Patapoutian, TRPV1 and TRPA1 mediate peripheral nitric oxide-induced nociception in mice, PloS one, 4 (2009) e7596.

[63] L. Moparthi, V. Sinica, V.K. Moparthi, M. Kreir, T. Vignane, M.R. Filipovic, V. Vlachova, P.M. Zygmunt, The human TRPA1 intrinsic cold and heat sensitivity involves separate channel structures beyond the N-ARD domain, Nature communications, 13 (2022) 6113.

[64] S.L. Morales-Lázaro, T. Rosenbaum, Cholesterol as a Key Molecule That Regulates TRPV1 Channel Function, Advances in experimental medicine and biology, 1135 (2019) 105-117.

[65] S. Mustafa, The effect of temperature on vascular smooth muscle: cooling-induced vasodilation in deep arteries and veins, Pflugers Archiv : European journal of physiology, 475 (2023) 1089-1095.

[66] S. Mustafa, O. Thulesius, Cooling-induced carotid artery dilatation: an experimental study in isolated vessels, Stroke, 33 (2002) 256-260.

[67] Y. Nakamura, T. Yahiro, Prostaglandin EP3 receptor-expressing preoptic neurons bidirectionally control body temperature via tonic GABAergic signaling, Science advances, 8 (2022) eadd5463.

[68] M.G. Netea, B.J. Kullberg, J.W.M. Van der Meer, Circulating Cytokines as Mediators of Fever, Clinical infectious diseases, 31 (2000) S178-S184.

[69] J. Nowack, C. Turbill, Survivable hypothermia or torpor in a wild-living rat: rare insights broaden our understanding of endothermic physiology, Journal of comparative physiology. B, Biochemical, systemic, and environmental physiology, 192 (2022) 183-192.

[70] E. Olah, Z. Rumbus, V. Kormos, The Hypothermic Effect of Hydrogen Sulfide Is Mediated by the Transient Receptor Potential Ankyrin-1 Channel in Mice, Pharmaceuticals (Basel, Switzerland), 14 (2021).

[71] E.M. Outzen, M. Zaki, B. Abdolalizadeh, A. Sams, H.C. Boonen, M. Sheykhzade, Translational value of mechanical and vasomotor properties of mouse isolated mesenteric resistance-sized arteries, Pharmacology research & perspectives, 3 (2015) e00200.

[72] C.K. Park, Z.Z. Xu, T. Berta, Q. Han, G. Chen, X.J. Liu, R.R. Ji, Extracellular microRNAs activate nociceptor neurons to elicit pain via TLR7 and TRPA1, Neuron, 82 (2014) 47-54.

[73] G. Pozsgai, Z. Hajna, T. Bagoly, M. Boros, Á. Kemény, S. Materazzi, R. Nassini, Z. Helyes, J. Szolcsányi, E. Pintér, The role of transient receptor potential ankyrin 1 (TRPA1) receptor activation in hydrogen-sulphide-induced CGRP-release and vasodilation, European journal of pharmacology, 689 (2012) 56-64.

[74] F.S. Quan, G.J. Lee, Analytical Methods for Detection of Gasotransmitter Hydrogen Sulfide Released from Live Cells, Biochemistry research international, 2021 (2021) 5473965.

[75] W.D. Rollyson, C.A. Stover, K.C. Brown, H.E. Perry, C.D. Stevenson, C.A. McNees, J.G. Ball, M.A. Valentovic, P. Dasgupta, Bioavailability of capsaicin and its implications for drug delivery, Journal of controlled release : official journal of the Controlled Release Society, 196 (2014) 96-105.

[76] A.A. Romanovsky, The thermoregulation system and how it works, Handbook of clinical neurology, 156 (2018) 3-43.

[77] A.A. Romanovsky, M.C. Almeida, A. Garami, A.A. Steiner, M.H. Norman, S.F. Morrison, K. Nakamura, J.J. Burmeister, T.B. Nucci, The transient receptor potential vanilloid-1 channel in thermoregulation: a thermosensor it is not, Pharmacological reviews, 61 (2009) 228-261.

[78] A.A. Romanovsky, A.I. Ivanov, Y.P. Shimansky, Selected contribution: ambient temperature for experiments in rats: a new method for determining the zone of thermal neutrality, Journal of applied physiology (Bethesda, Md. : 1985), 92 (2002) 2667-2679.

[79] A.A. Romanovsky, M. Székely, Fever and hypothermia: two adaptive thermoregulatory responses to systemic inflammation, Medical hypotheses, 50 (1998) 219-226.

[80] Z. Rumbus, R. Matics, P. Hegyi, C. Zsiboras, I. Szabo, A. Illes, E. Petervari, M. Balasko, K. Marta, A. Miko, A. Parniczky, J. Tenk, I. Rostas, M. Solymar, A. Garami, Fever Is Associated with Reduced, Hypothermia with Increased Mortality in Septic Patients: A Meta-Analysis of Clinical Trials, PloS one, 12 (2017) e0170152.

[81] N. Saba, A. Safwan, M. Sanyang, F. Mohammad, M. Pervaiz, M. Jawaid, O. Alothman, M. Sain, Thermal and dynamic mechanical properties of cellulose nanofibers reinforced epoxy composites, International journal of biological macromolecules, 102 (2017) 822-828.

[82] J.I. Sbodio, S.H. Snyder, B.D. Paul, Regulators of the transsulfuration pathway, British journal of pharmacology, 176 (2019) 583-593.

[83] N. Schaltenberg, C. John, M. Heine, F. Haumann, F. Rinninger, L. Scheja, J. Heeren, A. Worthmann, Endothelial Lipase Is Involved in Cold-Induced High-Density Lipoprotein Turnover and Reverse Cholesterol Transport in Mice, Frontiers in cardiovascular medicine, 8 (2021) 628235.

[84] K. Schmidt, C. de Wit, Endothelium-Derived Hyperpolarizing Factor and Myoendothelial Coupling: The in vivo Perspective, Frontiers in physiology, 11 (2020) 602930.

[85] J.T. Shepherd, N.J. Rusch, P.M. Vanhoutte, Effect of cold on the blood vessel wall, General pharmacology, 14 (1983) 61-64.

[86] V. Škop, N. Liu, J. Guo, O. Gavrilova, M.L. Reitman, The contribution of the mouse tail to thermoregulation is modest, American journal of physiology, endocrinology and metabolism, 319 (2020) E438-e446.

[87] M. Soto, L. Orliaguet, M.L. Reyzer, M.L. Manier, R.M. Caprioli, C.R. Kahn, Pyruvate induces torpor in obese mice, Proceedings of the National Academy of Sciences of the United States of America, 115 (2018) 810-815.

[88] J. Sprung, E.Y. Cheng, S. Gamulin, J.P. Kampine, Z.J. Bosnjak, Effects of acute hypothermia and beta-adrenergic receptor blockade on serum potassium concentration in rats, Critical care medicine, 19 (1991) 1545-1551.

[89] C. Statzer, J. Meng, R. Venz, M. Bland, S. Robida-Stubbs, K. Patel, D. Petrovic, R. Emsley, P. Liu, I. Morantte, C. Haynes, W.B. Mair, A. Longchamp, M.R. Filipovic, T.K. Blackwell, C.Y. Ewald, ATF-4 and hydrogen sulfide signalling mediate longevity in response to inhibition of translation or mTORC1, Nature communications, 13 (2022) 967.

[90] A.A. Steiner, V.F. Turek, M.C. Almeida, J.J. Burmeister, D.L. Oliveira, J.L. Roberts, A.W. Bannon, M.H. Norman, J.C. Louis, J.J. Treanor, N.R. Gavva, A.A. Romanovsky, Nonthermal activation of transient receptor potential vanilloid-1 channels in abdominal viscera tonically inhibits autonomic cold-defense effectors, The Journal of neuroscience : the official journal of the Society for Neuroscience, 27 (2007) 7459-7468.

[91] G.M. Story, A.M. Peier, A.J. Reeve, S.R. Eid, J. Mosbacher, T.R. Hricik, T.J. Earley, A.C. Hergarden, D.A. Andersson, S.W. Hwang, P. McIntyre, T. Jegla, S. Bevan, A. Patapoutian, ANKTM1, a TRP-like channel expressed in nociceptive neurons, is activated by cold temperatures, Cell, 112 (2003) 819-829.

[92] M.E. Straat, L. Jurado-Fasoli, Z. Ying, K.J. Nahon, L.G.M. Janssen, M.R. Boon, G.F. Grabner, S. Kooijman, R. Zimmermann, M. Giera, P.C.N. Rensen, B. Martinez-Tellez, Cold exposure induces dynamic changes in circulating triacylglycerol species, which is dependent on intracellular lipolysis: A randomized cross-over trial, EBioMedicine, 86 (2022) 104349.

[93] M.N. Sullivan, A.L. Gonzales, P.W. Pires, A. Bruhl, M.D. Leo, W. Li, A. Oulidi, F.A. Boop, Y. Feng, J.H. Jaggar, D.G. Welsh, S. Earley, Localized TRPA1 channel Ca2+ signals stimulated by reactive oxygen species promote cerebral artery dilation, Science signaling, 8 (2015) ra2.

[94] M.N. Sullivan, P. Thakore, V. Krishnan, S. Alphonsa, W. Li, Y. Feng Earley, S. Earley, Endothelial cell TRPA1 activity exacerbates cerebral hemorrhage during severe hypertension, Frontiers in molecular biosciences, 10 (2023) 1129435.

[95] S.J. Swoap, M.J. Gutilla, Cardiovascular changes during daily torpor in the laboratory mouse, American journal of physiology. Regulatory, integrative and comparative physiology, 297 (2009) R769-774.

[96] S.J. Swoap, J.M. Overton, G. Garber, Effect of ambient temperature on cardiovascular parameters in rats and mice: a comparative approach, American journal of physiology. Regulatory, integrative and comparative physiology, 287 (2004) R391-396.

[97] N. Takahashi, Y. Mori, TRP Channels as Sensors and Signal Integrators of Redox Status Changes, Frontiers in pharmacology, 2 (2011) 58.

[98] K. Talavera, J.B. Startek, J. Alvarez-Collazo, B. Boonen, Y.A. Alpizar, A. Sanchez, R. Naert, B. Nilius, Mammalian Transient Receptor Potential TRPA1 Channels: From Structure to Disease, Physiological reviews, 100 (2020) 725-803.

[99] E.A. Tansey, C.D. Johnson, Recent advances in thermoregulation, Advances in physiology education, 39 (2015) 139-148.

[100] Ø. Tøien, J. Blake, D.M. Edgar, D.A. Grahn, H.C. Heller, B.M. Barnes, Hibernation in black bears: independence of metabolic suppression from body temperature, Science (New York, N.Y.), 331 (2011) 906-909.

[101] Z. Ujfalusi, A. Pentek, R. Told, A. Schiffer, M. Nyitrai, P. Maroti, Detailed thermal characterization of acrylonitrile butadiene styrene and polylactic acid based carbon composites used in additive manufacturing, Polymers (Basel), 12 (2020) 2960.

[102] S.L. Urbina, M.D. Roberts, W.C. Kephart, K.B. Villa, E.N. Santos, A.M. Olivencia, H.M. Bennett, M.D. Lara, C.A. Foster, M. Purpura, R. Jäger, L.W. Taylor, C.D. Wilborn, Effects of twelve weeks of capsaicinoid supplementation on body composition, appetite and self-reported caloric intake in overweight individuals, Appetite, 113 (2017) 264-273.

[103] F. Ushikubi, E. Segi, Y. Sugimoto, T. Murata, T. Matsuoka, T. Kobayashi, H. Hizaki, K. Tuboi, M. Katsuyama, A. Ichikawa, T. Tanaka, N. Yoshida, S. Narumiya, Impaired febrile response in mice lacking the prostaglandin E receptor subtype EP3, Nature, 395 (1998) 281-284.

[104] R. Wang, Physiological implications of hydrogen sulfide: a whiff exploration that blossomed, Physiological reviews, 92 (2012) 791-896.

[105] Y. Wang, R.D. Bukoski, Distribution of the perivascular nerve Ca2+ receptor in rat arteries, British journal of pharmacology, 125 (1998) 1397-1404.

[106] Z. Winter, P. Gruschwitz, S. Eger, F. Touska, K. Zimmermann, Cold Temperature Encoding by Cutaneous TRPA1 and TRPM8-Carrying Fibers in the Mouse, Frontiers in molecular neuroscience, 10 (2017) 209.

[107] J.H. Xu, T.H. He, N.P. Wang, W.M. Gao, Y.J. Cheng, Q.F. Ji, S.H. Wu, Y.L. Wei, Y. Tang, W.Z. Yang, J. Zhang, Thermoregulatory pathway underlying the pyrogenic effects of prostaglandin E(2) in the lateral parabrachial nucleus of male rats, Acta pharmacologica Sinica, 45 (2024) 1832-1847.

[108] V. Yadav, X.H. Gao, B. Willard, M. Hatzoglou, R. Banerjee, O. Kabil, Hydrogen sulfide modulates eukaryotic translation initiation factor 2α (eIF2α) phosphorylation status in the integrated stress-response pathway, The Journal of biological chemistry, 292 (2017) 13143-13153.

[109] X.P. Yang, S. Chiba, Effects of prolonged cold storage on purinergic and adrenergic components of sympathetic co-transmission in isolated canine splenic arteries, Japanese journal of pharmacology, 81 (1999) 163-169.

[110] H. Zhang, C. Wang, K. Zhang, P.M. Kamau, A. Luo, L. Tian, R. Lai, The role of TRPA1 channels in thermosensation, Cell insight, 1 (2022) 100059.

[111] H. Zhang, L. Zhi, S. Moochhala, P.K. Moore, M. Bhatia, Hydrogen sulfide acts as an inflammatory mediator in cecal ligation and puncture-induced sepsis in mice by upregulating

the production of cytokines and chemokines via NF-kappaB, American journal of physiology. Lung cellular and molecular physiology, 292 (2007) L960-971.

[112] H. Zhang, L. Zhi, P.K. Moore, M. Bhatia, Role of hydrogen sulfide in cecal ligation and puncture-induced sepsis in the mouse, American journal of physiology. Lung cellular and molecular physiology, 290 (2006) L1193-1201.

[113] T. Zhang, J. Chen, X. Tang, Q. Luo, D. Xu, B. Yu, Interaction between adipocytes and high-density lipoprotein:new insights into the mechanism of obesity-induced dyslipidemia and atherosclerosis, Lipids in health and disease, 18 (2019) 223.

CRITICAL REVIEWS IN FOOD SCIENCE AND NUTRITION
2022, VOL. 62, NO. 25, 7025–7035
https://doi.org/10.1080/10408398.2021.1910138

Taylor & Francis
Taylor & Francis Group

REVIEW

Dietary supplementation of transient receptor potential vanilloid-1 channel agonists reduces serum total cholesterol level: a meta-analysis of controlled human trials

Leonardo Kelava[a], David Nemeth[b], Peter Hegyi[b,c,d], Patrik Keringer[a], Dora K. Kovacs[b], Marta Balasko[b], Margit Solymar[a], Eszter Pakai[a], Zoltan Rumbus[a], and Andras Garami[a]

[a]Department of Thermophysiology, Institute for Translational Medicine, Medical School, University of Pecs, Pecs, Hungary; [b]Institute for Translational Medicine, Medical School, University of Pecs, Pecs, Hungary; [c]Szentagothai Research Centre, University of Pecs, Pecs, Hungary; [d]Department of Translational Medicine, First Department of Medicine, Medical School, University of Pecs, Pecs, Hungary

ABSTRACT

Abnormal cholesterol level is a major risk factor in the development of atherosclerosis, which is a fundamental derangement in cardiovascular diseases. Any efforts should be undertaken to lower blood cholesterol levels. Among dietary interventions, capsaicinoid supplementation is also considered as a novel cholesterol-lowering approach, but human studies concluded contradictory results about its effectiveness. The present meta-analysis aimed at determining the effects of capsaicinoids on serum lipid profile in humans. We searched the PubMed, EMBASE, and CENTRAL databases from inception to February 2021. We included 10 controlled studies, which involved 398 participants. We found that dietary capsaicinoid supplementation alone or in combination with other substances significantly ($p = 0.004$ and 0.001, respectively) reduced serum total cholesterol level compared to controls with an overall standardized mean difference of −0.52 (95% confidence interval: −0.83, −0.21). Capsaicinoids also decreased low-density lipoprotein level significantly ($p = 0.035$), whereas no effect was observed on serum levels of high-density lipoprotein and triglycerides. Our findings provide novel quantitative evidence for the efficacy of dietary capsaicin supplementation in lowering serum total cholesterol and low-density lipoprotein levels in humans. To validate our conclusion, further randomized controlled trials in a diverse population of adult humans receiving dietary capsaicinoid supplementation are warranted.

KEYWORDS

Capsaicin; chili; LDL; lipid profile; lipoprotein; TRPV1

Introduction

Atherosclerosis represents a significant challenge for patients and healthcare worldwide, including developed and developing countries alike (Herrington et al. 2016), and it is a main underlying cause of ischemic heart disease and stroke, which, respectively, accounted for about 9 and 6 million deaths globally in 2015 (Roth et al. 2017). The development of atherosclerosis entails the formation of fatty deposits (plaques) in the vascular wall, which thickens the wall, but, in turn, narrows the lumen of the vessels, therefore reducing the blood flow and tissue blood supply (Lusis 2000).

Cholesterol is a key substance, which contributes to the buildup of plaques, hence high cholesterol level is a well-acknowledged risk factor for cardiovascular diseases, including atherosclerosis (Ference et al. 2017). Different pharmacological therapies, for example, statins, selective cholesterol absorption inhibitors, and resins, are used to decrease abnormally high serum cholesterol (Ray et al. 2019), but lifestyle changes are also fundamental in controlling cholesterol levels. Important advantages of changes in lifestyle (e.g., diet and physical activity) are the better compliance of the patients and the absence of possibly severe, adverse effects (e.g., liver failure, myopathy, and diabetes mellitus), both of which can hinder pharmacological therapies (Thompson, Clarkson, and Karas 2003; Sattar et al. 2010). Currently, there are different dietary recommendations that aim at reducing serum cholesterol levels (Arnett et al. 2019), but the hunt for novel and effective, cholesterol-lowering natural ingredients is still ongoing.

A candidate among such natural ingredients is capsaicin, which is the first known agonist of the transient receptor potential vanilloid-1 (TRPV1) channel, formerly also known as the capsaicin receptor [for a review, see Romanovsky et al. (2009)]. TRPV1 contributes to the maintenance of energy metabolism in humans through different mechanisms, including the regulation of energy expenditure (Ludy, Moore, and Mattes 2012), body temperature (Garami et al. 2020), and body mass (Zsiboras et al. 2018). Data from animal experiments also suggest that TRPV1 activation

CONTACT Andras Garami andras.garami@aok.pte.hu Department of Thermophysiology, Institute for Translational Medicine, Medical School, University of Pecs, 12 Szigeti Str., Pecs H7624, Hungary.

Supplemental data for this article is available online at http://dx.doi.org/10.1080/10408398.2021.1910138.

increases fat oxidation in rodents (Leung 2014), and that capsaicin administration decreases serum levels of cholesterol and triglycerides in small mammals, such as mice, rats, hamsters, and rabbits, although it should be also noted that the beneficial effect was not shown in some studies [for a recent systematic review, see Sanati, Razavi, and Hosseinzadeh (2018)]. At present, the results about the effect of TRPV1 agonists on serum cholesterol in human studies are inconclusive. In different trials, TRPV1 agonists caused a decrease (Yuan et al. 2016; Taghizadeh et al. 2017), no effect (Kim et al. 2010; Hochkogler et al. 2017) or an increase (Urbina et al. 2017) in serum cholesterol levels. In the present meta-analysis, we wanted to amalgamate the available data from human studies in order to determine the effects of the TRPV1 agonist capsaicinoids on serum cholesterol levels.

Methods

This meta-analysis was conducted in accordance with the PRISMA (Preferred Reporting Items for Systematic reviews and Meta-Analyses) guidelines (Moher et al. 2009) (Supplementary material Table S1). The question was raised in the PICO (Population, Intervention, Control, Outcome) format: in adult human subjects we wanted to compare the effect of TRPV1 agonists with placebo on serum total cholesterol level (as the primary outcome). Secondary outcome measures included triglyceride, lipoprotein component, fasting glucose and insulin levels. This meta-analysis has been registered with PROSPERO International Prospective Register of Systematic Reviews (registration number: CRD42020162735).

Search strategy

We searched the PubMed, EMBASE, and CENTRAL (Cochrane Central Register of Controlled Trials) databases from inception until February 20, 2021 to identify eligible papers for the meta-analysis. The used search term was "(capsa* OR capsi* OR TRPV1 OR vanilloid) AND (LDL OR HDL OR lipoprotein OR triglyceride OR cholester* OR "lipid")." The search was limited to human trials without language and publication date restrictions. Two authors (LK, AG) conducted the search separately; disagreements were resolved by consensus, if needed, with the help of a third party (ZR).

Selection of studies and data extraction

Two authors (LK, ZR) assessed study eligibility and extracted data from the selected studies independently. Studies were required to include the following: controlled human trial design; a group with TRPV1 agonist administration; a placebo group; serum cholesterol level among the outcome measures. The following data were extracted from the eligible studies: author names, publication year, age, body mass index (BMI), and number of the participants, as well as, different outcome measures, *viz.*, serum levels of total cholesterol, high- and low-density lipoproteins (HDL and LDL, respectively), triglycerides, as well as, fasting glucose and insulin.

Evaluation of risk of bias and quality of evidence

The risk of bias was evaluated for all analyzed outcome measures, i.e., serum levels of total cholesterol, HDL, LDL, and triglycerides, as well as, for fasting plasma glucose and insulin levels, within the studies. According to the revised tool for assessing risk of bias in randomized trials (Rob 2) (Sterne et al. 2019), we assessed the bias in the following domains: randomization process, deviations from intended intervention, missing outcome data, measurement of the outcome, and selection of the reported result (Supplementary material Tables S2–S5). If the trial was not randomized, risk of bias was assessed with the ROBINS-I (Risk Of Bias In Non-randomized Studies of Interventions) tool (Supplementary material Table S6). The results of the assessments were visualized with the "robvis" tool (McGuinness and Higgins 2021).

The Grading of Recommendations Assessment, Development and Evaluation (GRADE) approach was used to evaluate the applicability of the evidence. According to the GRADE system (Atkins et al. 2004), each outcome was tested based on the following factors: study design, risk of bias, indirectness, inconsistency, imprecision, and publication bias. The overall quality of the evidence for each outcome could be "high," "moderate," "low," or "very low." The basal grade was high for randomized controlled studies and it was decreased by 1 grade for serious concerns or by 2 for very serious concerns.

Statistical analysis

The statistical analysis was performed according to the standard methods of meta-analysis by using the Stata/IC 16.0 software (StataCorp LLC, College Station, TX, USA). Subjects were grouped as either administered with a TRPV1 agonist (i.e., intervention group) or not (i.e., controls). We used standardized mean differences (SMDs) with 95% confidence intervals (CIs) between intervention and control groups as primary measure of the effect size on serum lipid, glucose, and insulin level response at the end of the substance administration. For standardization, the differences in means were divided by their corresponding pooled standard deviation (SD) values, which was required because the different measuring methods, reported units, and TRPV1 agonist dose ranges could result in different variances among the study groups, and, therefore, influence the results. SMD values were compared by using the random effect model by DerSimonian and Laird (1986), and then presented as "forest plots".

Statistical heterogeneity was determined by the I^2 statistical test ($p < 0.1$ indicating significant heterogeneity), as previously (Olah et al. 2018). As an attempt to reduce heterogeneity, subgroups administered with capsaicin (and its derivates) only and with capsaicinoids in mixture of other supposedly active ingredients were analyzed separately. As

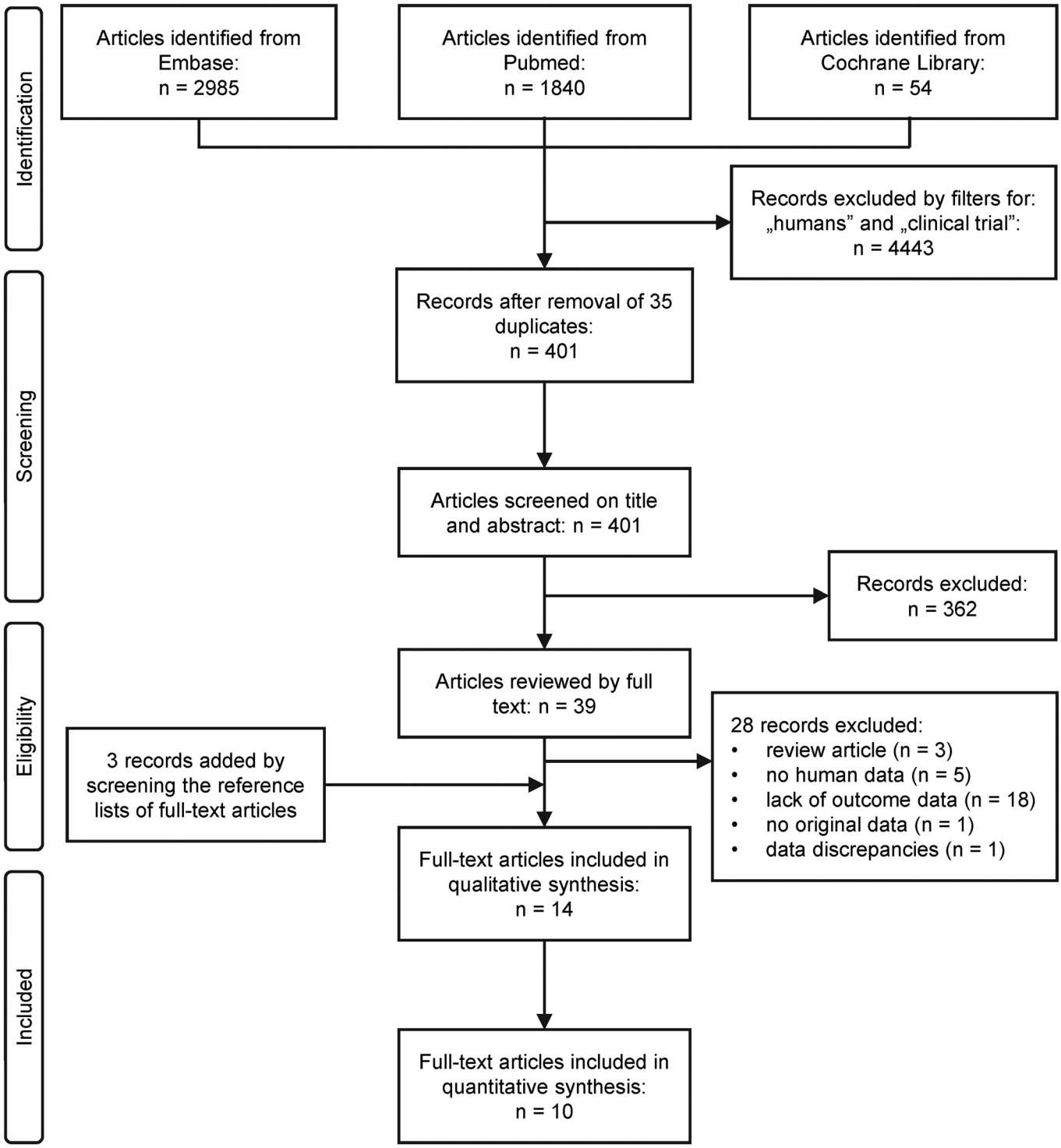

Figure 1. Flow chart of study selection and inclusion.

in our recent study (Csenkey et al. 2019), publication bias was assessed by the visual inspection of funnel plots (Supplementary material Figures S3–S8). Quantitative evaluation by Egger's test (Egger et al. 1997) could be performed only for total serum cholesterol and LDL levels, because in case of the other outcome parameters the number of eligible studies was lower than ten, which is the minimal number of studies recommended for the test by the Cochrane Handbook (Higgins et al. 2021).

Results

Search results

The search identified altogether 4,879 studies from the PubMed, EMBASE, and CENTRAL databases (Figure 1). We used built-in filters available on the website of the databases to limit our search to humans and clinical trials, which resulted in exclusion of 4,443 records. After removing 35 duplicates, 401 papers remained, which were manually screened on title

Table 1. Summary of study characteristics for publications included in the meta-analyses.

First author (year)	Study design	Country	Control/ treatment (n)	Age[a] (years)	BMI[a] (kg/m^2)	Administered substance	Dosage of capsaicin (mg/day)	Duration (weeks)
Ahuja and Ball (2006)	RCRT	Australia	27/27	46.0 (12.0)	26.6 (4.9)	Chili supplement	approx. 22[b]	4
Arent et al. (2018)	RCT	USA	18/18	36.9 (10.2)	NR	METABO pill[c]	NR	8
Cha et al. (2013)	RCT	China	30/30	42.6 (1.9)	27.1 (0.7)	Kochujang pill	NR	12
Kang et al. (2016)	NRCRT	China	12/12	27.8 (3.8)	22.4 (3.2)	Chili supplement[d]	5	6
Kim et al. (2010)	RCT	China	14/14	NR	26.4 (2.5)	Chili supplement	NR	12
Lim et al. (2015)	RCT	China	13/13	42.0 (7.7)	26.9 (4.5)	Kochujang pill	NR	12
Qin et al. (2017)	RCT	China	17/18	43.5 (5.4)	26.3 (2.9)	Pod pepper powder	4	12
Taghizadeh et al. (2017)	RCT	Iran	25/25	33.7 (7.2)	32.4 (4.6)	Dietary supplement[e]	100	8
Urbina et al. (2017)	RCT	USA	28/22	29.0 (2.0)	27.5 (6.0)	Chili supplement	4	12
Yuan et al. (2016)	RCT	China	22/20	30.4 (4.5)	27.0 (3.6)	Chili powder	4	4

BMI, body mass index; NR, not reported; NRCRT, non-randomized cross-over trial; RCRT, randomized cross-over trial; RCT, randomized controlled trial.
[a]Data are reported as mean (standard deviation).
[b]Based on the reported capsaicin concentrations in cayenne pepper (Al Othman et al. 2011).
[c]Containing capsaicin, caffeine, raspberry ketone, garlic organosulfur, vitamin B, chromium, and gingerols.
[d]Containing 1.05 mg/g capsaicin, 0.58 mg/g dihydrocapsaicin, and 0.12 mg/g nordihydrocapsaicin.
[e]Consisting of 125 mg green tea, 25 mg capsaicin, and 50 mg ginger.

and abstract for inclusion criteria. Full texts of 39 articles were obtained and reviewed, which resulted in the selection of 11 studies that were found eligible for qualitative synthesis (Ahuja and Ball 2006; Inoue et al. 2007; Kim et al. 2010; Kang et al. 2016; Yuan et al. 2016; Hochkogler et al. 2017; Lee et al. 2017; Qin et al. 2017; Taghizadeh et al. 2017; Urbina et al. 2017; Arent et al. 2018). Manual search of the reference lists of the eligible articles lead to the identification of three additional studies (Snitker et al. 2009; Cha et al. 2013; Lim et al. 2015), thereby increasing the total number of eligible studies to 14. However, four of these studies could not be included in the quantitative analysis, because they did not report appropriate data for meta-analysis (Inoue et al. 2007; Snitker et al. 2009), or the authors (Lee et al. 2017) analyzed the same participants' data as an earlier study by Cha et al. (2013), which was already included in our meta-analysis, or because the subjects did not receive capsaicin, but instead they were administered with a low dose (0.15 mg/day) of nonivamide (Hochkogler et al. 2017), which has a potency of half of that of capsaicin (Skofitsch, Donnerer, and Lembeck 1984). As a result, 10 studies were included in the meta-analyses (Ahuja and Ball 2006; Kim et al. 2010; Cha et al. 2013; Lim et al. 2015; Kang et al. 2016; Yuan et al. 2016; Qin et al. 2017; Taghizadeh et al. 2017; Urbina et al. 2017; Arent et al. 2018). We confirmed that our search algorithm was sensitive enough by also adding "paprika species" and "herbal mixtures" to the search key, which extended search did not identify any additional studies eligible for quantitative synthesis.

Study characteristics and quality

The descriptive characteristics of the analyzed studies are presented in Table 1. All 10 studies were controlled trials: 8 with parallel placebo control (Kim et al. 2010; Yuan et al. 2016; Qin et al. 2017; Taghizadeh et al. 2017; Urbina et al. 2017; Arent et al. 2018), and 2 with crossover designs (Ahuja and Ball 2006; Kang et al. 2016). Except for one trial (Kang et al. 2016), all studies were randomized. The duration of the trials varied from 4 to 12 weeks, but all of them could be considered as short term, lasting for less than three months. Apart from a BMI of 26-32, the subjects had no diagnosed health issues, except for one study (Yuan et al. 2016), which recruited women with postprandial diabetes mellitus. With regards to substance administration, capsaicin was used in all studies, but in two trials (Taghizadeh et al. 2017; Arent et al. 2018), it was combined with other biologically active compounds (Table 1). The daily dose range of capsaicin (4-5 mg) was similar in four of the analyzed studies (Kang et al. 2016; Yuan et al. 2016; Qin et al. 2017; Urbina et al. 2017), while 100 mg was used in the study by Taghizadeh et al. (2017) and 22 mg by Ahuja and Ball (2006). The applied dosage was not reported in four papers (Kim et al. 2010; Cha et al. 2013; Lim et al. 2015; Arent et al. 2018).

According to the risk of bias analysis (Supplementary material Tables S2–S6), six studies were considered overall as high risk (Ahuja and Ball 2006; Kim et al. 2010; Cha et al. 2013; Lim et al. 2015; Urbina et al. 2017; Arent et al. 2018), two studies as moderate risk (Kang et al. 2016; Qin et al. 2017), and two studies as low risk (Yuan et al. 2016; Taghizadeh et al. 2017).

By using the GRADE approach, the overall quality of evidence was evaluated as low in case of lipid parameters, while as very low in case of glucose and insulin. The summary of findings and the detailed evaluation using the GRADE system are shown in Supplementary material Tables S7 and S8. It should be noted, however, that despite the suitability of GRADE for developing clinical guidelines, its applicability is questionable in food-based dietary guidelines, in which field there are still inconsistencies for rating evidence quality (Blake et al. 2018). Therefore, our GRADE results should be taken with care.

Effects on lipid parameters and other outcomes

First, we analyzed the effect of dietary capsaicin supplementation on the serum total cholesterol level by comparing the cholesterol levels between the intervention and control groups at the end of the trials. Studies which used capsaicinoids only (Ahuja and Ball 2006; Kim et al. 2010; Cha et al.

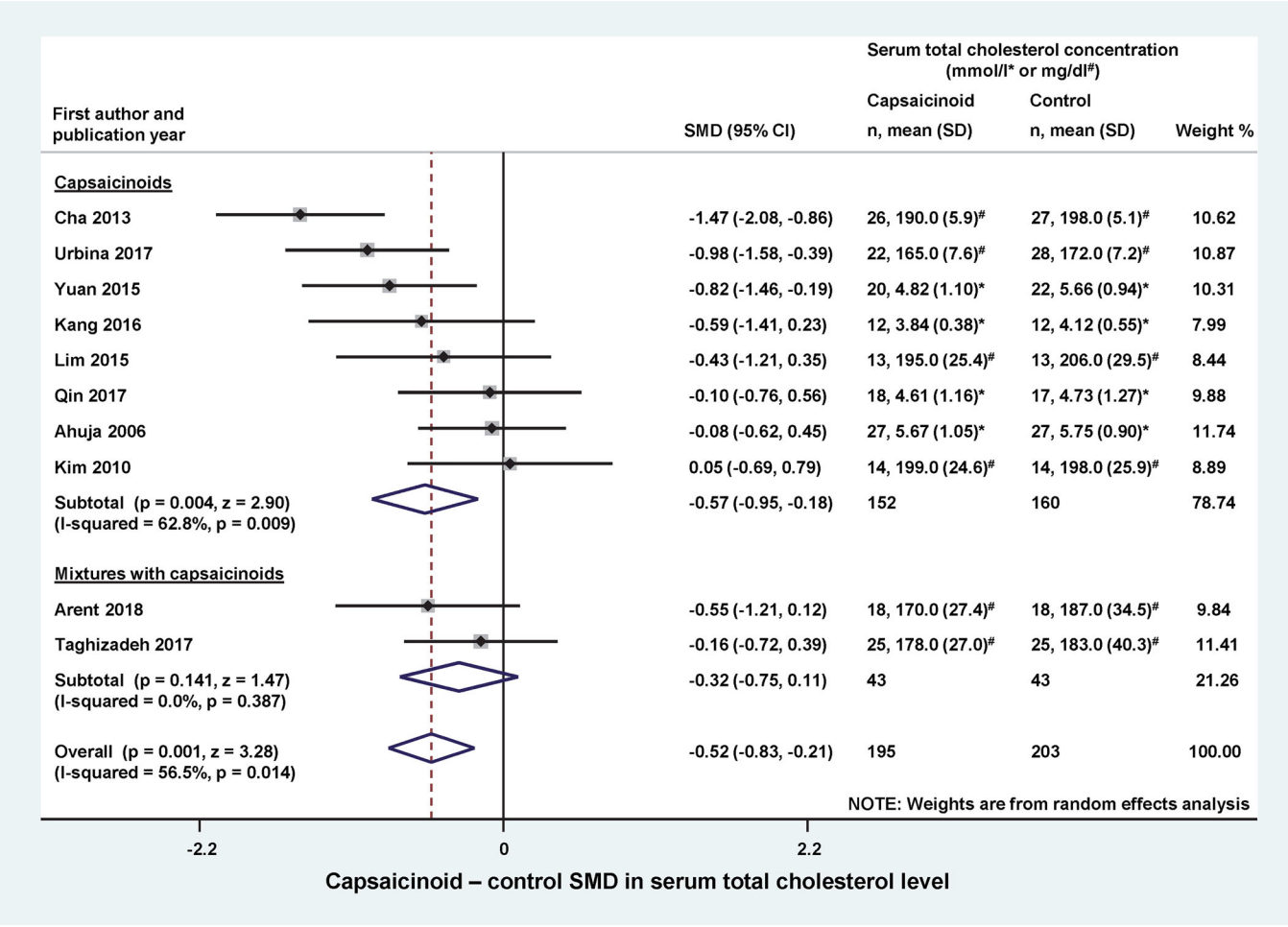

Figure 2. Forest plot of the effects of capsaicinoids (top) and capsaicinoid-containing mixtures (bottom) on serum total cholesterol level. Here, and in Figures 3–5, for each study, we calculated the difference between serum cholesterol levels in the capsaicinoid-treated group and the control group at the end of the intervention period. For all studies, the differences in means were standardized (based on variances) to obtain standardized mean differences (SMDs). The SMDs and 95% confidence intervals (CI) are used as primary measures of effect size and are shown in the forest plot. Black circles represent the SMD for each study, while the left and right horizontal arms of the circles indicate the corresponding CI. The size of the gray box is proportional to the sample size and inversed variance. The rhombus represents the average SMD calculated from the SMDs of the individual studies in a subgroup (top and middle) and in all studies (bottom). The horizontal diagonal of the rhombus represents the CI, while the vertical diagonal of the rhombus points at the SMD value of the subgroup or of all studies. The dashed line is determined by the vertical diagonal of the bottom rhombus and indicates the SMD of all studies in the forest plot. There was no significant difference between the two subgroups (Q = 0.709; $p = 0.400$). SD, standard deviation.

2013; Lim et al. 2015; Kang et al. 2016; Yuan et al. 2016; Qin et al. 2017; Urbina et al. 2017) and capsaicinoids combined with other active ingredients (Taghizadeh et al. 2017; Arent et al. 2018) were included as separate subgroups in the forest plot (Figure 2). Dietary capsaicinoid supplementation markedly ($p = 0.004$) reduced serum total cholesterol compared to the controls (SMD = −0.57; CI, −0.95, −0.18). With regards to capsaicinoid-containing mixtures, both of the included studies seemed to decrease serum total cholesterol, however, there was no significant effect in the individual studies or on average (SMD = −0.32; CI, −0.75, 0.11; $p = 0.141$). The overall effect of all capsaicionoid supplementations (i.e., alone and in combination; n = 195) was a significant ($p = 0.001$) decrease in serum total cholesterol, as compared to the control groups (n = 203) with an SMD of −0.52 (CI, −0.83, −0.21).

Next, we wanted to know which component of total cholesterol is affected the most by capsaicionoids. We found sufficient data to analyze the changes in LDL, triglyceride, and HDL levels in response to dietary capsaicinoid supplementation. Similarly as in Figure 2, in the remaining forest plots we also analyzed the capsaicinoid alone and mixture subgroups separately, if applicable. At the end of the trials, the LDL level was lower (as indicated by a negative SMD) in the capsaicinoid-treated groups than in controls in the most of the studies (Ahuja and Ball 2006; Cha et al. 2013; Lim et al. 2015; Kang et al. 2016; Yuan et al. 2016; Urbina et al. 2017), whereas it was higher in two studies (Kim et al. 2010; Qin et al. 2017) (Figure 3). The averaged SMD was not significantly different in either the capsaicinoid alone or mixture subgroups. However, the overall average SMD, calculated from all 10 studies, was −0.30 (CI −0.57, −0.02), indicating a significant ($p = 0.035$) decrease in the capsaicinoid-treated group.

Capsaicinoids did not have a significant effect on serum triglyceride levels, when administered alone (SMD = −0.46; CI, −1.49, 0.57) or in a mixture (SMD = −0.19; CI, −0.62, 0.23) (Figure 4). The overall effect (including both subgroups) was also not statistically significant (SMD = −0.39; CI, −1.15, 0.37). When we compared serum HDL levels

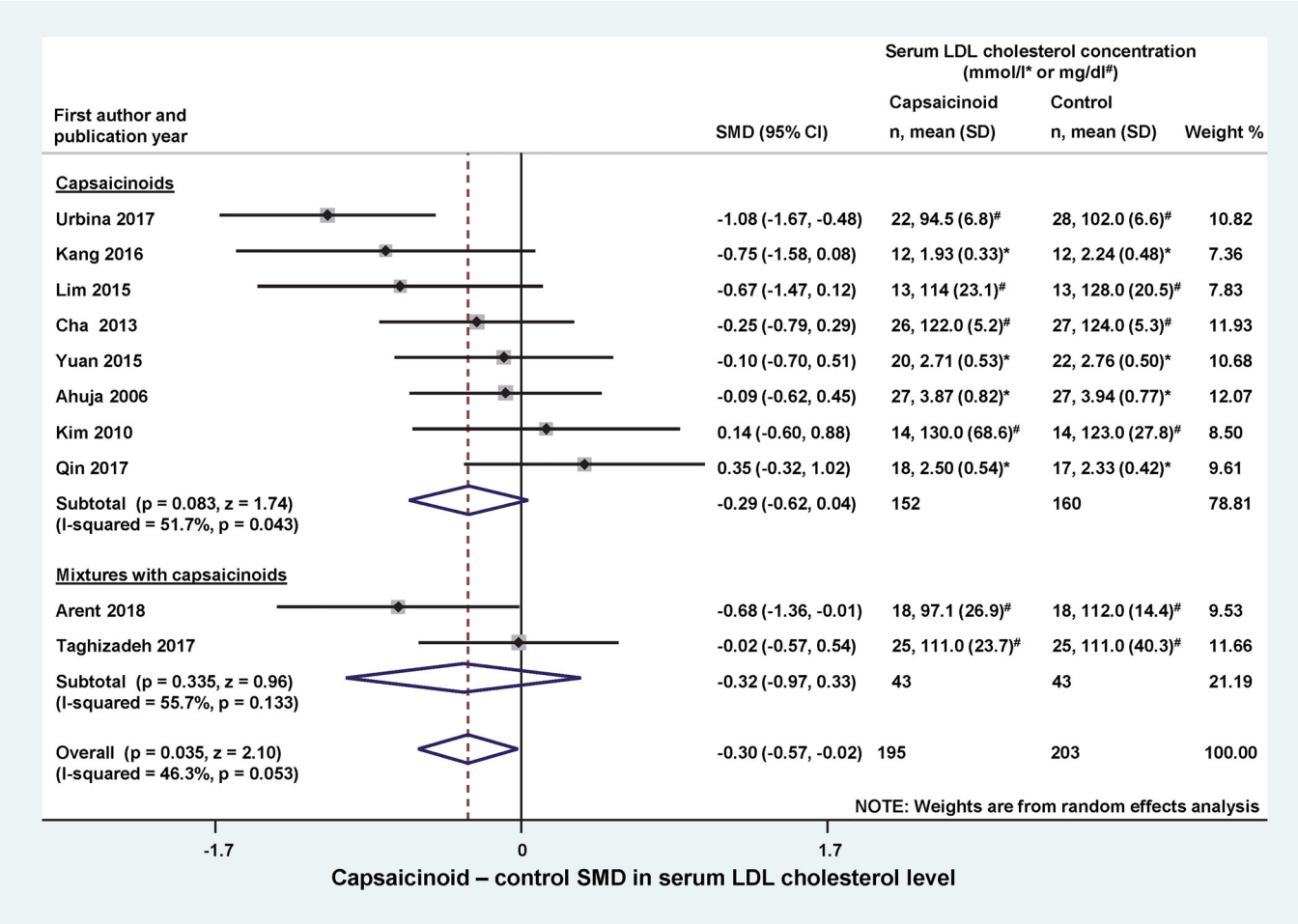

Figure 3. Forest plot of the effects of capsaicinoids (top) and capsaicinoid-containing mixtures (bottom) on serum low-density lipoprotein (LDL) cholesterol level. There was no significant difference between the two subgroups (Q = 0.006; $p = 0.940$). CI, confidence interval; SD, standard deviation; SMD, standardized mean difference.

between the capsaicinoid-treated and control groups, we found no significant change in SMD, regardless from whether the capsaicinoids were administered alone (SMD = 0.05; CI, −0.37, 0.47) or in combination with other substances (SMD = −0.31; CI, −0.82, 0.21) (Figure 5). The overall effect was negligible (SMD = −0.03; CI, −0.37, 0.32).

In addition to the lipid parameters, we also analyzed two indicators of carbohydrate metabolism: fasting blood glucose and insulin. We did not find a significant effect of dietary capsaicinoid supplementation on either of these parameters as compared to the placebo group (Supplementary material Figures S1 and S2). The SMDs between capsaicinoid-treated and control groups were 0.41 (CI, −0.26, 1.07) for glucose and 0.28 (CI, −0.25, 0.82) for insulin.

Qualitative synthesis

Four studies were not included in the meta-analysis, but were retained for qualitative review. All four studies had randomized controlled design. In one of these articles, Lee et al. (2017) analyzed the data from the same participants as a previous study by Cha et al. (2013), which was included in the meta-analysis. Accordingly, the study design and characteristics of participants were the same in the two studies, and the effects of capsaicinoids on the outcome parameters were also similar.

In two studies, the authors stated that TRPV1 agonist supplementation did not have a significant effect on lipid parameters (total cholesterol, LDL, HDL, and triglyceride), but factual information about blood levels was not reported (Inoue et al. 2007; Snitker et al. 2009). Despite the lack of a significant effect on blood lipid parameters, both of these studies reported a beneficial effect of TRPV1 agonists on body fat mass. Inoue et al. (2007) assigned 44 subjects into 3 groups: ingestion of non-pungent capsinoids at 3 or 10 mg/kg, or placebo, and showed that capsinoids enhance energy expenditure and fat oxidation. In the study by Snitker et al. (2009), 80 subjects were assigned into a capsinoid-treated (6 mg) or placebo group, and the authors found that capsinoids caused an augmented abdominal fat loss and a near significant increase in fat oxidation.

Hochkogler et al. (2017) studied the effects of nonivamide at a low dose of 0.15 mg/day (versus a control group) in 18 participants. Although the potency of nonivamide is only half of that of capsaicin (Skofitsch, Donnerer, and Lembeck 1984), it prevented dietary-induced fat accumulation even at the applied low dose. The authors hypothesized

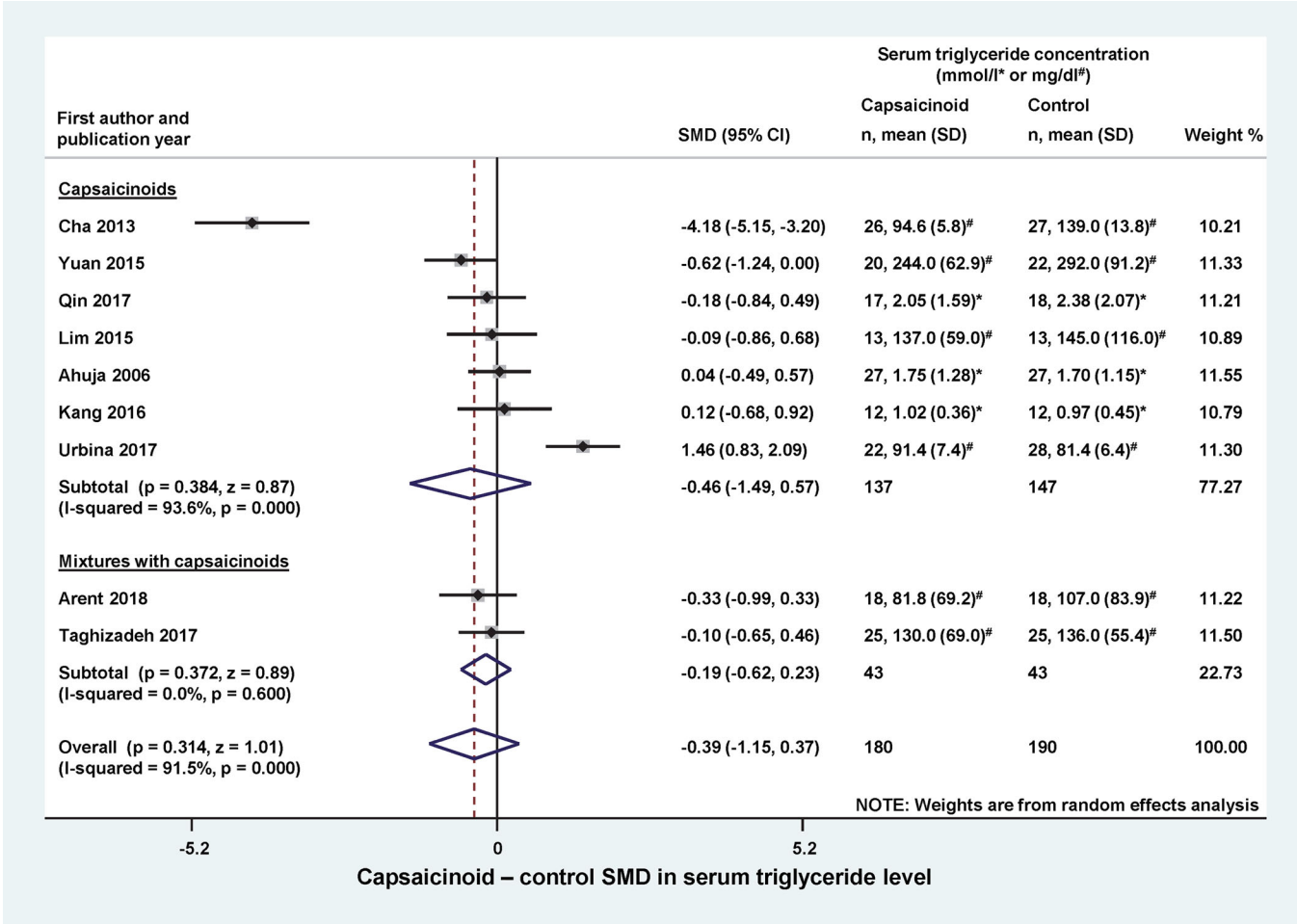

Figure 4. Forest plot of the effects of capsaicinoids (top) and capsaicinoid-containing mixtures (bottom) on total serum triglyceride level. There was no significant difference between the two subgroups (Q = 0.216; $p = 0.642$). CI, confidence interval; SD, standard deviation; SMD, standardized mean difference.

that nonivamide affects lipid assimilation by reducing adipogenesis, however, significant change in blood lipid parameters was not detected (Hochkogler et al. 2017).

Discussion

In the present study, we show that dietary intake of TRPV1 agonists reduced serum total cholesterol and LDL levels in humans, to our knowledge for the first time, with meta-analysis of the available controlled trials, including a total of 10 studies with 398 subjects.

High serum cholesterol is a main risk factor for atherosclerotic cardiovascular disease (Stone and Grundy 2019), which is the major component of cardiovascular diseases responsible for over 4 million deaths in Europe annually (Townsend et al. 2015). Lowering cholesterol levels reduces the risk for atherosclerosis, which explains why current guidelines recommend substantial reduction in serum cholesterol level, most of all in that of LDL (Mach et al. 2020). While different cholesterol-lowering pharmacological treatments are available, evidence on the influence of lifestyle changes and functional foods on lipoproteins is growing. Lifestyle changes, alone or in combination with drugs, are still among the recommended intervention strategies of reducing cardiovascular risk (Mach et al. 2020).

A beneficial effect of TRPV1 agonists, particularly capsaicin, on blood cholesterol has been long sought based on data obtained in animal experiments showing that capsaicin improved obesity-related metabolic disorders, also including dyslipidemia (Panchal, Bliss, and Brown 2018; Li et al. 2020). Human studies, however, lead to contradictory findings, thereby questioning whether the cholesterol-lowering effects of TRPV1 agonists observed in experimental models are applicable for humans. Indeed, the effect of dietary supplementation with capsaicinoids on serum cholesterol in humans ranged from beneficial to neutral to unfavorable. However, the number of the controlled human studies on the effect of capsaicinoids on cholesterol serum levels was too small until recently for a quantitative synthesis of their overall result, since six trials eligible for such synthesis were published in the last five years (Kang et al. 2016; Yuan et al. 2016; Qin et al. 2017; Taghizadeh et al. 2017; Urbina et al. 2017; Arent et al. 2018). In the present meta-analysis, we performed the long-sought quantitative synthesis of the available data and showed that dietary capsaicinoid supplementation lowers blood cholesterol levels in humans. When we looked at the lipid components, we found that capsaicinoids significantly decreased LDL levels, while the levels of triglycerides and HDL were not affected by the treatment. These findings indicate that the capsaicinoid-induced

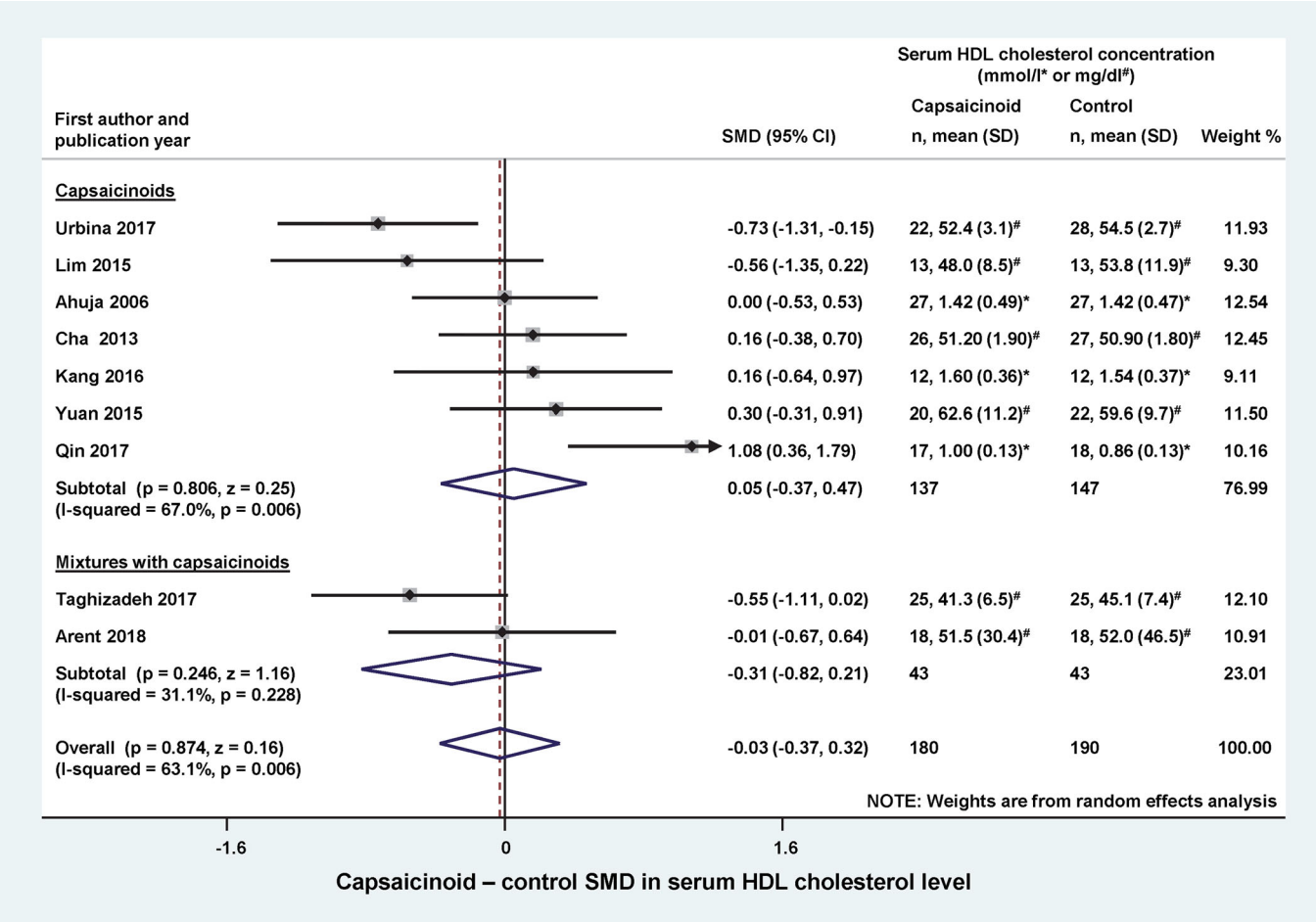

Figure 5. Forest plot of the effects of capsaicinoids (top) and capsaicinoid-containing mixtures (bottom) on serum high-density lipoprotein (HDL) cholesterol level. There was no significant difference between the two subgroups ($Q = 1.115$; $p = 0.291$). CI, confidence interval; SD, standard deviation; SMD, standardized mean difference.

reduction of total cholesterol is associated with a beneficial alteration in lipid components, inasmuch as LDL, the harmful component (Ference et al. 2017), decreases, while HDL, the protective component (Rosenson et al. 2018), does not change. Unfortunately, there was not enough data available to study further lipid components (e.g., chylomicron, very-low- and intermediate-DL).

The exact mechanism by which TRPV1 agonists affect cholesterol levels could not be studied in the present work (due to its meta-analysis nature) and remains subject for further research. It is notable, however, that in healthy human subjects, capsaicin ingestion increased thermogenesis and activation of the sympathetic nervous system (Matsumoto et al. 2000) and augmented fat oxidation during exercise (Shin and Moritani 2007). Capsaicin and capsiate were also shown to increase energy expenditure in humans and proposed as novel therapeutic agents in obesity (Zsiboras et al. 2018). A site for thermogenesis in humans is the brown adipose tissue (Nedergaard and Cannon 2018), which can be stimulated via the sympathetic nervous system (e.g., in cold). It has been shown that adrenergic activation of brown fat is protective against hypercholesterolemia in mice (Berbee et al. 2015), and that its cold-induced activation by means of cold acclimation improved cholesterol metabolism in human patients with hypercholesterolemia (De Lorenzo et al. 1998). Adrenergic brown fat stimulation can trigger intracellular mechanisms capable of increasing the activation of lipases, which are responsible for the mobilization of fatty acids that can be used for thermogenesis (Xu and Lopez 2018). These findings suggest a link between capsaicin-induced thermogenesis, possibly via sympathetic activation in brown fat, and the reduction in blood cholesterol levels. It should be also noted that TRPV1 expression was described in brown and white adipocytes, therefore capsaicin can even directly (i.e., independently of adrenergic activation) regulate thermogenesis, adipocyte differentiation, and expression of uncoupling proteins [for a recent review, see Uchida et al. (2018)].

Alternative interactions between the TRPV1 channel and cholesterol level may include the hunger hormone ghrelin. Studies in mice and rats suggested that ghrelin inhibits thermogenesis (Mano-Otagiri et al. 2009; Lin et al. 2014). Interestingly, one of the studies, which was included in our analysis, found that capsaicin administration markedly ($p < 0.01$) decreased serum ghrelin concentration in the participants (Kang et al. 2016). The presence of TRPV1 channels was shown in the human stomach (Faussone-Pellegrini et al. 2005), which is the main site of ghrelin production (Kojima and Kangawa 2005). Hence, a potential inhibitory action of capsaicin on ghrelin production can not be

excluded. Moreover, a direct effect of cholesterol on TRPV1 was also suggested, as in cholesterol depletion the membrane trafficking of TRPV1 channels is negatively affected, while in cholesterol enrichment the activation of TRPV1 by capsaicin is inhibited (Morales-Lazaro and Rosenbaum 2019). However, the physiological significance of this interaction remains unknown.

The cholesterol-reducing effects of dietary TRPV1 agonists, as also shown here, are of high importance, especially considering that these compounds were found to evoke further advantageous effects on human bodily homeostasis. For instance, decreased body mass (Leung 2014), increased energy expenditure (Zsiboras et al. 2018), reduced blood pressure (Sanati, Razavi, and Hosseinzadeh 2018), as well as, lower blood sugar and increased insulin sensitivity (Panchal, Bliss, and Brown 2018) were all reported in response to the administration of different TRPV1 agonists. Moreover, potent and selective pharmacological agents for the modulation of TRPV1 activity were also developed and subjected to in-vivo testing. Depending on their pharmacological profiles against the TRPV1 channel, these compounds caused an increase, no change, or a decrease in the body temperature of laboratory animals (Garami et al. 2018) and humans (Garami et al. 2020). This raises the possibility that through targeted modulation of the TRPV1 channel, and thereby energy expenditure, some of the compounds might be also used in the control of lipid metabolism.

Some limitations of our study must be also mentioned. Although the number of studies was sufficient for meta-analysis, it was still relatively small. Only 10 controlled human studies (9 randomized and 1 non-randomized) could be included in the quantitative synthesis despite the extensive literature search. Consequently, we could not perform some of the planned analysis (e.g., subgroup analysis for sex and food intake) in our study because of data unavailability. Due to differences in study design and methodology, considerably high between-study heterogeneity (indicated by an I^2 of 46-96%) was observed in our analysis (Figures 3–5, Supplementary material Figures S1 and S2). To account for the presence of heterogeneity, we used the random-effects model in all forest plots of our meta-analyses and performed subgroup analysis. However, when we divided these studies into subgroups in some cases heterogeneity was still present and only two studies remained in a group, which does not allow one to draw firm conclusions about the overall results of such small subgroups. Based on visual inspection of the funnel plots (Supplementary material Figures S3–S8), some asymmetry may be present, indicating the possible existence of publication bias, although when Egger's test could be performed, its results contradicted the presence of publication bias ($p = 0.973$ for total cholesterol and $p = 0.523$ for LDL). Nevertheless, two studies were identified by the literature search, but could not be included in the quantitative synthesis, because the authors opted not to report the results due to the lack of statistically significant difference between the treatment groups (Inoue et al. 2007; Snitker et al. 2009). Finally, it should be also noted that the overall risk of bias was judged as high in six of the ten analyzed studies (Supplementary material Tables S2–S5), and the GRADE certainty rating was low for the analyzed lipid parameters (Supplementary material Tables S7 and S8). It is possible that, despite all of our approaches to reduce methodological errors, the low number, different design and quality, and occasionally high heterogeneity of the analyzed studies may have negatively impacted our results.

In conclusion, the present study provides novel quantitative support to the beneficial effects of dietary capsaicin supplementation on serum total cholesterol and LDL levels in humans. Although the quantitative synthesis of the available data is, to our knowledge, the most extensive in its field, we also have to point out that the quality of evidence was evaluated as low in case of the analyzed lipid parameters and that a few studies which might argue against our results could not be included in the meta-analysis only in qualitative synthesis. Consequently, further randomized controlled trials are warranted to validate our findings and prove unequivocally that dietary intake of TRPV1 agonists is an effective intervention for lowering blood cholesterol levels.

Funding

This study was supported by "Hungarian National Research, Development and Innovation Office (grant FK 124483), the Medical School, University of Pecs (grant KA-2019-27), the New National Excellence Program of the Hungarian Ministry of Human Capacities (grants UNKP-20-3-II-PTE-877 and UNKP-20-5-PTE-736), the Janos Bolyai Research Scholarship of the Hungarian Academy of Sciences, Economic Development and Innovation Operative Program Grants (GINOP 2.3.2-15-2016-00048) and a Human Resources Operative Program (EFOP-3.6.1.-16-2016-00004) of the National Research, Development and Innovation Office."

ORCID

Andras Garami http://orcid.org/0000-0003-2493-0571

References

Ahuja, K. D., and M. J. Ball. 2006. Effects of daily ingestion of chilli on serum lipoprotein oxidation in adult men and women. *British Journal of Nutrition* 96 (2):239–42. doi: 10.1079/BJN20061788.

Al Othman, Z. A., Y. B. Ahmed, M. A. Habila, and A. A. Ghafar. 2011. Determination of capsaicin and dihydrocapsaicin in Capsicum fruit samples using high performance liquid chromatography. *Molecules* 16 (10):8919–29. doi: 10.3390/molecules16108919.

Arent, S. M., A. J. Walker, J. K. Pellegrino, D. J. Sanders, B. A. McFadden, T. N. Ziegenfuss, and H. L. Lopez. 2018. The combined effects of exercise, diet, and a multi-ingredient dietary supplement on body composition and adipokine changes in overweight adults. *Journal of the American College of Nutrition* 37 (2):111–20. doi: 10.1080/07315724.2017.1368039.

Arnett, D. K., R. S. Blumenthal, M. A. Albert, A. B. Buroker, Z. D. Goldberger, E. J. Hahn, C. D. Himmelfarb, A. Khera, D. Lloyd-Jones, J. W. McEvoy, et al. 2019. 2019 ACC/AHA guideline on the primary prevention of cardiovascular disease: A report of the American College of Cardiology/American Heart Association task force on clinical practice guidelines. *Circulation* 140 (11):e596–e646. doi: 10.1161/cir.0000000000000678.

Atkins, D., D. Best, P. A. Briss, M. Eccles, Y. Falck-Ytter, S. Flottorp, G. H. Guyatt, R. T. Harbour, M. C. Haugh, D. Henry, et al. 2004.

Grading quality of evidence and strength of recommendations. *BMJ* 328 (7454):1490 doi: 10.1136/bmj.328.7454.1490.

Berbee, J. F., M. R. Boon, P. P. Khedoe, A. Bartelt, C. Schlein, A. Worthmann, S. Kooijman, G. Hoeke, I. M. Mol, C. John, et al. 2015. Brown fat activation reduces hypercholesterolaemia and protects from atherosclerosis development. *Nature Communications* 6:6356. doi: 10.1038/ncomms7356.

Blake, P., S. Durao, C. E. Naude, and L. Bero. 2018. An analysis of methods used to synthesize evidence and grade recommendations in food-based dietary guidelines. *Nutrition Reviews* 76 (4):290–300. doi: 10.1093/nutrit/nux074.

Cha, Y. S., S. R. Kim, J. A. Yang, H. I. Back, M. G. Kim, S. J. Jung, W. O. Song, and S. W. Chae. 2013. Kochujang, fermented soybean-based red pepper paste, decreases visceral fat and improves blood lipid profiles in overweight adults. *Nutrition & Metabolism* 10 (1): 24. doi: 10.1186/1743-7075-10-24.

Csenkey, A., G. Jozsa, N. Gede, E. Pakai, B. Tinusz, Z. Rumbus, A. Lukacs, Z. Gyongyi, P. Hamar, R. Sepp, et al. 2019. Systemic antibiotic prophylaxis does not affect infectious complications in pediatric burn injury: A meta-analysis. *PLoS One* 14 (9):e0223063. doi: 10.1371/journal.pone.0223063.

De Lorenzo, F., M. Mukherjee, Z. Kadziola, R. Sherwood, and V. V. Kakkar. 1998. Central cooling effects in patients with hypercholesterolaemia. *Clinical Science* 95 (2):213–7. doi: 10.1042/CS19980091.

DerSimonian, R., and N. Laird. 1986. Meta-analysis in clinical trials. *Controlled Clinical Trials* 7 (3):177–88. doi: 10.1016/0197-2456(86)90046-2.

Egger, M., G. D. Smith, M. Schneider, and C. Minder. 1997. Bias in meta-analysis detected by a simple, graphical test. *BMJ* 315 (7109): 629–34. doi: 10.1136/bmj.315.7109.629.

Faussone-Pellegrini, M. S., A. Taddei, E. Bizzoco, M. Lazzeri, M. G. Vannucchi, and P. Bechi. 2005. Distribution of the vanilloid (capsaicin) receptor type 1 in the human stomach. *Histochemistry and Cell Biology* 124 (1):61–8. doi: 10.1007/s00418-005-0025-9.

Ference, B. A., H. N. Ginsberg, I. Graham, K. K. Ray, C. J. Packard, E. Bruckert, R. A. Hegele, R. M. Krauss, F. J. Raal, H. Schunkert, et al. 2017. Low-density lipoproteins cause atherosclerotic cardiovascular disease. 1. Evidence from genetic, epidemiologic, and clinical studies. A consensus statement from the European Atherosclerosis Society Consensus Panel. *European Heart Journal* 38 (32):2459–72. doi: 10.1093/eurheartj/ehx144.

Garami, A., E. Pakai, H. A. McDonald, R. M. Reilly, A. Gomtsyan, J. J. Corrigan, E. Pinter, D. X. D. Zhu, S. G. Lehto, N. R. Gavva, et al. 2018. TRPV1 antagonists that cause hypothermia, instead of hyperthermia, in rodents: Compounds' pharmacological profiles, in vivo targets, thermoeffectors recruited and implications for drug development. *Acta Physiologica* 223 (3):e13038. doi: 10.1111/apha.13038.

Garami, A., Y. P. Shimansky, Z. Rumbus, R. C. L. Vizin, N. Farkas, J. Hegyi, Z. Szakacs, M. Solymar, A. Csenkey, D. A. Chiche, et al. 2020. Hyperthermia induced by transient receptor potential vanilloid-1 (TRPV1) antagonists in human clinical trials: Insights from mathematical modeling and meta-analysis. *Pharmacology & Therapeutics* 208:107474. doi: 10.1016/j.pharmthera.2020.107474.

Herrington, W., B. Lacey, P. Sherliker, J. Armitage, and S. Lewington. 2016. Epidemiology of atherosclerosis and the potential to reduce the global burden of atherothrombotic disease. *Circulation Research* 118 (4):535–46. doi: 10.1161/circresaha.115.307611.

Higgins, J. P. T., J. Thomas, J. Chandler, M. Cumpston, T. Li, M. J. Page, and V. A. Welch, eds. 2021. *Cochrane handbook for systematic reviews of interventions* (version 6.2), updated February Cochrane, 2021. http://www.training.cochrane.org/handbook

Hochkogler, C. M., B. Lieder, P. Rust, D. Berry, S. M. Meier, M. Pignitter, A. Riva, A. Leitinger, A. Bruk, S. Wagner, et al. 2017. A 12-week intervention with nonivamide, a TRPV1 agonist, prevents a dietary-induced body fat gain and increases peripheral serotonin in moderately overweight subjects. *Molecular Nutrition & Food Research* 61 (5):1600731. doi: 10.1002/mnfr.201600731.

Inoue, N., Y. Matsunaga, H. Satoh, and M. Takahashi. 2007. Enhanced energy expenditure and fat oxidation in humans with high BMI scores by the ingestion of novel and non-pungent capsaicin analogues (capsinoids). *Bioscience, Biotechnology, and Biochemistry* 71 (2):380–9. doi: 10.1271/bbb.60341.

Kang, C., Y. Zhang, X. Zhu, K. Liu, X. Wang, M. Chen, J. Wang, H. Chen, S. Hui, L. Huang, et al. 2016. Healthy subjects differentially respond to dietary capsaicin correlating with specific gut enterotypes. *The Journal of Clinical Endocrinology and Metabolism* 101 (12):4681–9. doi: 10.1210/jc.2016-2786.

Kim, Y., Y. J. Park, S. O. Yang, S. H. Kim, S. H. Hyun, S. Cho, Y. S. Kim, D. Y. Kwon, Y. S. Cha, S. Chae, et al. 2010. Hypoxanthine levels in human urine serve as a screening indicator for the plasma total cholesterol and low-density lipoprotein modulation activities of fermented red pepper paste. *Nutrition Research* 30 (7):455–61. doi: 10.1016/j.nutres.2010.06.014.

Kojima, M., and K. Kangawa. 2005. Ghrelin: Structure and function. *Physiological Reviews* 85 (2):495–522. doi: 10.1152/physrev.00012.2004.

Lee, Y., Y. S. Cha, Y. Park, and M. Lee. 2017. PPARγ2 C1431T polymorphism interacts with the antiobesogenic effects of Kochujang, a Korean fermented, soybean-based red pepper paste, in overweight/obese subjects: A 12-week, double-blind randomized clinical trial. *Journal of Medicinal Food* 20 (6):610–7. doi: 10.1089/jmf.2016.3911.

Leung, F. W. 2014. Capsaicin as an anti-obesity drug. In *Progress in drug research. Fortschritte der Arzneimittelforschung. Progres des recherches pharmaceutiques*, eds O. Abdel-Salam, Vol. 68, 171–9. Basel: Springer doi: 10.1007/978-3-0348-0828-6_7.

Li, D., T. Zhang, J. Lu, C. Peng, and L. Lin. 2020. Natural constituents from food sources as therapeutic agents for obesity and metabolic diseases targeting adipose tissue inflammation. *Critical Reviews in Food Science and Nutrition*, 1–19. doi: 10.1080/10408398.2020.1768044.

Lim, J. H., E. S. Jung, E. K. Choi, D. Y. Jeong, S. W. Jo, J. H. Jin, J. M. Lee, B. H. Park, and S. W. Chae. 2015. Supplementation with Aspergillus oryzae-fermented kochujang lowers serum cholesterol in subjects with hyperlipidemia. *Clinical Nutrition* 34 (3):383–7. doi: 10.1016/j.clnu.2014.05.013.

Lin, L., J. H. Lee, O. Y. Bongmba, X. Ma, X. Zhu, D. Sheikh-Hamad, and Y. Sun. 2014. The suppression of ghrelin signaling mitigates age-associated thermogenic impairment. *Aging* 6 (12):1019–32. doi: 10.18632/aging.100706.

Ludy, M. J., G. E. Moore, and R. D. Mattes. 2012. The effects of capsaicin and capsiate on energy balance: Critical review and meta-analyses of studies in humans. *Chemical Senses* 37 (2):103–21. doi: 10.1093/chemse/bjr100.

Lusis, A. J. 2000. Atherosclerosis. *Nature* 407 (6801):233–41. doi: 10.1038/35025203.

Mach, F., C. Baigent, A. L. Catapano, K. C. Koskinas, M. Casula, L. Badimon, M. J. Chapman, G. G. De Backer, V. Delgado, B. A. Ference, et al. 2020. 2019 ESC/EAS guidelines for the management of dyslipidaemias: Lipid modification to reduce cardiovascular risk. *European Heart Journal* 41 (1):111–88. doi: 10.1093/eurheartj/ehz455.

Mano-Otagiri, A., H. Ohata, A. Iwasaki-Sekino, T. Nemoto, and T. Shibasaki. 2009. Ghrelin suppresses noradrenaline release in the brown adipose tissue of rats. *The Journal of Endocrinology* 201 (3): 341–9. doi: 10.1677/joe-08-0374.

Matsumoto, T., C. Miyawaki, H. Ue, T. Yuasa, A. Miyatsuji, and T. Moritani. 2000. Effects of capsaicin-containing yellow curry sauce on sympathetic nervous system activity and diet-induced thermogenesis in lean and obese young women. *Journal of Nutritional Science and Vitaminology* 46 (6):309–15. doi: 10.3177/jnsv.46.309.

McGuinness, L. A., and J. P. T. Higgins. 2021. Risk-of-bias VISualization (robvis): An R package and Shiny web app for visualizing risk-of-bias assessments. *Research Synthesis Methods* 12 (1): 55–61. doi: 10.1002/jrsm.1411.

Moher, D., A. Liberati, J. Tetzlaff, D. G. Altman, and PRISMA Group. 2009. Preferred reporting items for systematic reviews and meta-analyses: The PRISMA statement. *PLoS Medicine* 6 (7):e1000097. doi: 10.1371/journal.pmed.1000097.

Morales-Lazaro, S. L., and T. Rosenbaum. 2019. Cholesterol as a key molecule that regulates TRPV1 channel function. *Advances in*

Experimental Medicine and Biology 1135:105–17. doi: 10.1007/978-3-030-14265-0_6.

Nedergaard, J., and B. Cannon. 2018. Brown adipose tissue as a heat-producing thermoeffector. In *Handbook of clinical neurology*, eds Romanovsky A. A., Vol. 156, 137–52. Amsterdam: Elsevier. doi: 10.1016/b978-0-444-63912-7.00009-6.

Olah, E., L. Poto, P. Hegyi, I. Szabo, P. Hartmann, M. Solymar, E. Petervari, M. Balasko, T. Habon, Z. Rumbus, et al. 2018. Therapeutic whole-body hypothermia reduces death in severe traumatic brain injury if the cooling index is sufficiently high: Meta-analyses of the effect of single cooling parameters and their integrated measure. *Journal of Neurotrauma* 35 (20):2407–17. doi: 10.1089/neu.2018.5649.

Panchal, S. K., E. Bliss, and L. Brown. 2018. Capsaicin in metabolic syndrome. *Nutrients* 10 (5):630. doi: 10.3390/nu10050630.

Qin, Y., L. Ran, J. Wang, L. Yu, H. D. Lang, X. L. Wang, M. T. Mi, and J. D. Zhu. 2017. Capsaicin supplementation improved risk factors of coronary heart disease in individuals with low HDL-C levels. *Nutrients* 9 (9):1037. doi: 10.3390/nu9091037.

Ray, K. K., P. Corral, E. Morales, and S. J. Nicholls. 2019. Pharmacological lipid-modification therapies for prevention of ischaemic heart disease: Current and future options. *The Lancet* 394 (10199):697–708. doi: 10.1016/S0140-6736(19)31950-6.

Romanovsky, A. A., M. C. Almeida, A. Garami, A. A. Steiner, M. H. Norman, S. F. Morrison, K. Nakamura, J. J. Burmeister, and T. B. Nucci. 2009. The transient receptor potential vanilloid-1 channel in thermoregulation: A thermosensor it is not. *Pharmacological Reviews* 61 (3):228–61. doi: 10.1124/pr.109.001263.

Rosenson, R. S., H. B. Brewer, Jr., P. J. Barter, J. L. M. Bjorkegren, M. J. Chapman, D. Gaudet, D. S. Kim, E. Niesor, K. A. Rye, F. M. Sacks, et al. 2018. HDL and atherosclerotic cardiovascular disease: Genetic insights into complex biology. *Nature Reviews. Cardiology* 15 (1):9–19. doi: 10.1038/nrcardio.2017.115.

Roth, G. A., C. Johnson, A. Abajobir, F. Abd-Allah, S. F. Abera, G. Abyu, M. Ahmed, B. Aksut, T. Alam, K. Alam, et al. 2017. Global, regional, and national burden of cardiovascular diseases for 10 causes, 1990 to 2015. *Journal of the American College of Cardiology* 70 (1):1–25. doi: 10.1016/j.jacc.2017.04.052.

Sanati, S., B. M. Razavi, and H. Hosseinzadeh. 2018. A review of the effects of *Capsicum annuum* L. and its constituent, capsaicin, in metabolic syndrome. *Iranian Journal of Basic Medical Sciences* 21 (5):439–48. doi: 10.22038/ijbms.2018.25200.6238.

Sattar, N., D. Preiss, H. M. Murray, P. Welsh, B. M. Buckley, A. J. de Craen, S. R. Seshasai, J. J. McMurray, D. J. Freeman, J. W. Jukema, et al. 2010. Statins and risk of incident diabetes: A collaborative meta-analysis of randomised statin trials. *The Lancet* 375 (9716): 735–42. doi: 10.1016/S0140-6736(09)61965-6.

Shin, K. O., and T. Moritani. 2007. Alterations of autonomic nervous activity and energy metabolism by capsaicin ingestion during aerobic exercise in healthy men. *Journal of Nutritional Science and Vitaminology* 53 (2):124–32. doi: 10.3177/jnsv.53.124.

Skofitsch, G., J. Donnerer, and F. Lembeck. 1984. Comparison of nonivamide and capsaicin with regard to their pharmacokinetics and effects on sensory neurons. *Arzneimittel-Forschung* 34 (2):154–6.

Snitker, S., Y. Fujishima, H. Shen, S. Ott, X. Pi-Sunyer, Y. Furuhata, H. Sato, and M. Takahashi. 2009. Effects of novel capsinoid treatment on fatness and energy metabolism in humans: Possible pharmacogenetic implications. *The American Journal of Clinical Nutrition* 89 (1):45–50. doi: 10.3945/ajcn.2008.26561.

Sterne, J. A. C., J. Savovic, M. J. Page, R. G. Elbers, N. S. Blencowe, I. Boutron, C. J. Cates, H. Y. Cheng, M. S. Corbett, S. M. Eldridge, et al. 2019. RoB 2: A revised tool for assessing risk of bias in randomised trials. *BMJ* 366:l4898. doi: 10.1136/bmj.l4898.

Stone, N. J., and S. M. Grundy. 2019. The 2018 AHA/ACC/Multi-Society Cholesterol guidelines: Looking at past, present and future. *Progress in Cardiovascular Diseases* 62 (5):375–83. doi: 10.1016/j.pcad.2019.11.005.

Taghizadeh, M., N. Farzin, S. Taheri, M. Mahlouji, H. Akbari, F. Karamali, and Z. Asemi. 2017. The effect of dietary supplements containing green tea, capsaicin and ginger extracts on weight loss and metabolic profiles in overweight women: A randomized double-blind placebo-controlled clinical trial. *Annals of Nutrition and Metabolism* 70 (4):277–85. doi: 10.1159/000471889.

Thompson, P. D., P. Clarkson, and R. H. Karas. 2003. Statin-associated myopathy. *JAMA* 289 (13):1681–90. doi: 10.1001/jama.289.13.1681.

Townsend, N., M. Nichols, P. Scarborough, and M. Rayner. 2015. Cardiovascular disease in Europe-epidemiological update 2015. *European Heart Journal* 36 (40):2696–705. doi: 10.1093/eurheartj/ehv428.

Uchida, K., W. Sun, J. Yamazaki, and M. Tominaga. 2018. Role of thermo-sensitive transient receptor potential channels in brown adipose tissue. *Biological & Pharmaceutical Bulletin* 41 (8):1135–44. doi: 10.1248/bpb.b18-00063.

Urbina, S. L., M. D. Roberts, W. C. Kephart, K. B. Villa, E. N. Santos, A. M. Olivencia, H. M. Bennett, M. D. Lara, C. A. Foster, M. Purpura, et al. 2017. Effects of twelve weeks of capsaicinoid supplementation on body composition, appetite and self-reported caloric intake in overweight individuals. *Appetite* 113:264–73. doi: 10.1016/j.appet.2017.02.025.

Xu, Y., and M. Lopez. 2018. Central regulation of energy metabolism by estrogens. *Molecular Metabolism* 15:104–15. doi: 10.1016/j.molmet.2018.05.012.

Yuan, L. J., Y. Qin, L. Wang, Y. Zeng, H. Chang, J. Wang, B. Wang, J. Wan, S. H. Chen, Q. Y. Zhang, et al. 2016. Capsaicin-containing chili improved postprandial hyperglycemia, hyperinsulinemia, and fasting lipid disorders in women with gestational diabetes mellitus and lowered the incidence of large-for-gestational-age newborns. *Clinical Nutrition* 35 (2):388–93. doi: 10.1016/j.clnu.2015.02.011.

Zsiboras, C., R. Matics, P. Hegyi, M. Balasko, E. Petervari, I. Szabo, P. Sarlos, A. Miko, J. Tenk, I. Rostas, et al. 2018. Capsaicin and capsiate could be appropriate agents for treatment of obesity: A meta-analysis of human studies. *Critical Reviews in Food Science and Nutrition* 58 (9):1419–27. doi: 10.1080/10408398.2016.1262324.

Supplemental material

Table S1. PRISMA checklist.

Section/topic	#	Checklist item	Reported on page #
TITLE			
Title	1	Identify the report as a systematic review, meta-analysis, or both.	1
ABSTRACT			
Structured summary	2	Provide a structured summary including, as applicable: background; objectives; data sources; study eligibility criteria, participants, and interventions; study appraisal and synthesis methods; results; limitations; conclusions and implications of key findings; systematic review registration number.	1
INTRODUCTION			
Rationale	3	Describe the rationale for the review in the context of what is already known.	1-2
Objectives	4	Provide an explicit statement of questions being addressed with reference to participants, interventions, comparisons, outcomes, and study design (PICOS).	2
METHODS			
Protocol and registration	5	Indicate if a review protocol exists, if and where it can be accessed (e.g., Web address), and, if available, provide registration information including registration number.	2
Eligibility criteria	6	Specify study characteristics (e.g., PICOS, length of follow-up) and report characteristics (e.g., years considered, language, publication status) used as criteria for eligibility, giving rationale.	2
Information sources	7	Describe all information sources (e.g., databases with dates of coverage, contact with study authors to identify additional studies) in the search and date last searched.	2
Search	8	Present full electronic search strategy for at least one database, including any limits used, such that it could be repeated.	2
Study selection	9	State the process for selecting studies (i.e., screening, eligibility, included in systematic review, and, if applicable, included in the meta-analysis).	2
Data collection process	10	Describe method of data extraction from reports (e.g., piloted forms, independently, in duplicate) and any processes for obtaining and confirming data from investigators.	2
Data items	11	List and define all variables for which data were sought (e.g., PICOS, funding sources) and any assumptions and simplifications made.	2
Risk of bias in individual studies	12	Describe methods used for assessing risk of bias of individual studies (including specification of whether this was done at the study or outcome level), and how this information is to be used in any data synthesis.	2
Summary measures	13	State the principal summary measures (e.g., risk ratio, difference in means).	2
Synthesis of results	14	Describe the methods of handling data and combining results of studies, if done, including measures of consistency (e.g., I^2) for each meta-analysis.	2

Risk of bias across studies	15	Specify any assessment of risk of bias that may affect the cumulative evidence (e.g., publication bias, selective reporting within studies).	2-3
Additional analyses	16	Describe methods of additional analyses (e.g., sensitivity or subgroup analyses, meta-regression), if done, indicating which were pre-specified.	2-3
RESULTS			
Study selection	17	Give numbers of studies screened, assessed for eligibility, and included in the review, with reasons for exclusions at each stage, ideally with a flow diagram.	3-4, Figure 1
Study characteristics	18	For each study, present characteristics for which data were extracted (e.g., study size, PICOS, follow-up period) and provide the citations.	3-4; Table 1
Risk of bias within studies	19	Present data on risk of bias of each study and, if available, any outcome level assessment (see item 12).	4; Supplementary Tables S2-S6
Results of individual studies	20	For all outcomes considered (benefits or harms), present, for each study: (a) simple summary data for each intervention group (b) effect estimates and confidence intervals, ideally with a forest plot.	4-7; Figures 2-5, Supplementary Figures S1, S2
Synthesis of results	21	Present results of each meta-analysis done, including confidence intervals and measures of consistency.	4-6; Figures 2-5, Supplementary Figures S1, S2
Risk of bias across studies	22	Present results of any assessment of risk of bias across studies (see Item 15).	Supplementary Tables S2-S6, Figures S3-S8
Additional analysis	23	Give results of additional analyses, if done (e.g., sensitivity or subgroup analyses, meta-regression [see Item 16]).	4-7
DISCUSSION			
Summary of evidence	24	Summarize the main findings including the strength of evidence for each main outcome; consider their relevance to key groups (e.g., healthcare providers, users, and policy makers).	4, 7-9; Supplementary Tables S7, S8
Limitations	25	Discuss limitations at study and outcome level (e.g., risk of bias), and at review-level (e.g., incomplete retrieval of identified research, reporting bias).	9
Conclusions	26	Provide a general interpretation of the results in the context of other evidence, and implications for future research.	9
FUNDING			
Funding	27	Describe sources of funding for the systematic review and other support (e.g., supply of data); role of funders for the systematic review.	9

Table S2. Risk of bias assessment of randomized controlled trials included in the meta-analysis of serum total cholesterol and low-density lipoprotein levels using the revised tool for assessing risk of bias in randomized trials (Rob 2).

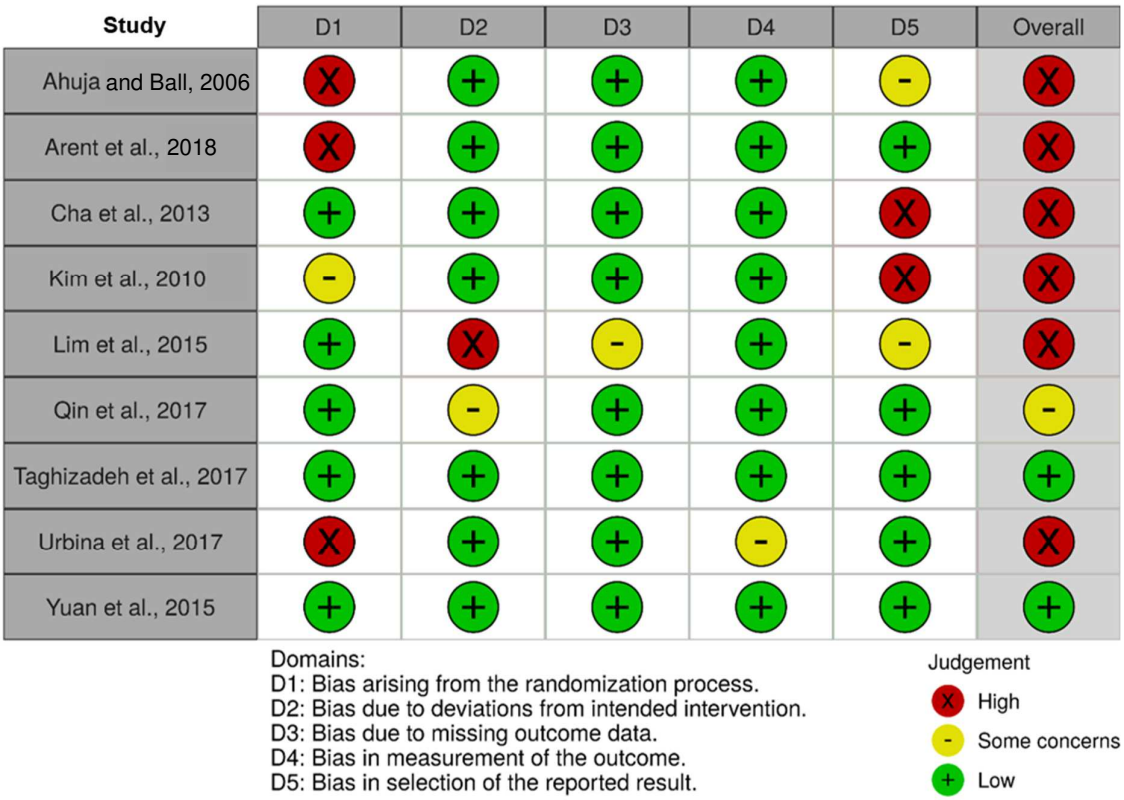

According to the Rob 2 tool in case of serum total cholesterol and low-density lipoprotein levels, 6 studies are considered overall as high risk (Ahuja and Ball 2006, Arent et al. 2018, Cha et al. 2013, Kim et al. 2010, Lim et al. 2015, Urbina et al. 2017), 1 study as raising some concerns (Qin et al. 2017), and 2 studies as low risk (Yuan et al. 2016, Taghizadeh et al. 2017).

Table S3. Risk of bias assessment of randomized controlled trials included in the meta-analysis of serum triglyceride and high-density lipoprotein levels using the revised tool for assessing risk of bias in randomized trials (Rob 2).

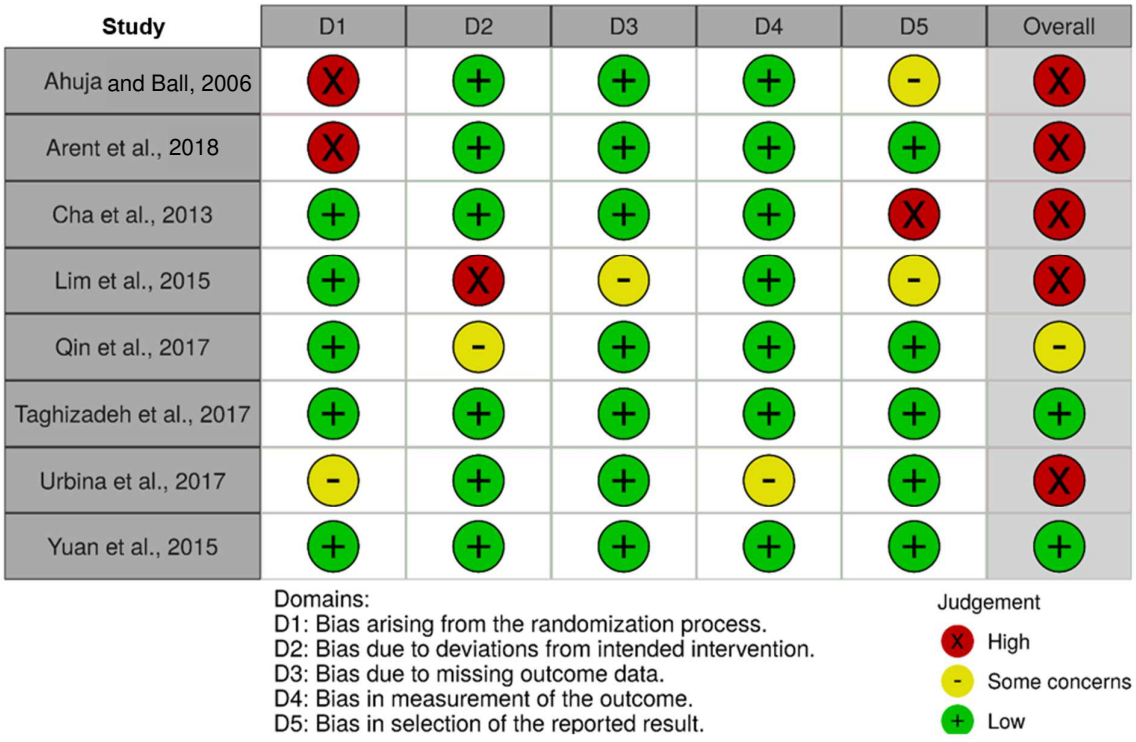

According to the Rob 2 tool in case of serum triglyceride and high-density lipoprotein levels, 5 studies are considered overall as high risk (Ahuja and Ball 2006, Arent et al. 2018, Cha et al. 2013, Lim et al. 2015, Urbina et al. 2017), 1 study as raising some concerns (Qin et al. 2017), and 2 studies as low risk (Yuan et al. 2016, Taghizadeh et al. 2017).

Table S4. Risk of bias assessment of randomized controlled trials included in the meta-analysis of fasting plasma glucose levels using the revised tool for assessing risk of bias in randomized trials (Rob 2).

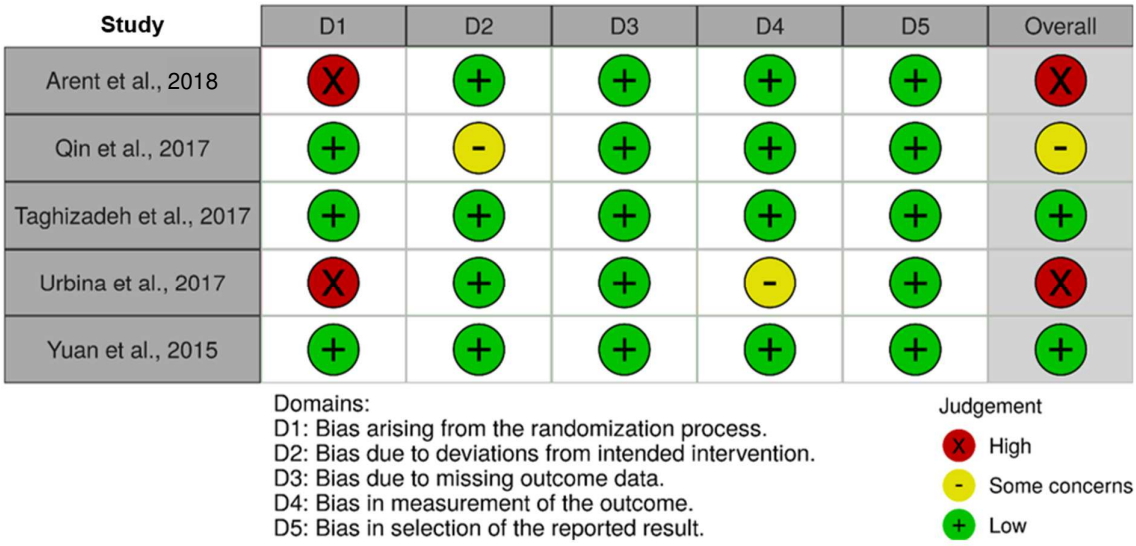

According to the Rob 2 tool in case of fasting plasma glucose levels, 2 studies are considered overall as high risk (Arent et al. 2018, Urbina et al. 2017), 1 study as raising some concerns (Qin et al. 2017), and 2 studies as low risk (Yuan et al. 2016, Taghizadeh et al. 2017).

Table S5. Risk of bias assessment of randomized controlled trials included in the meta-analysis of fasting plasma insulin levels using the revised tool for assessing risk of bias in randomized trials (Rob 2).

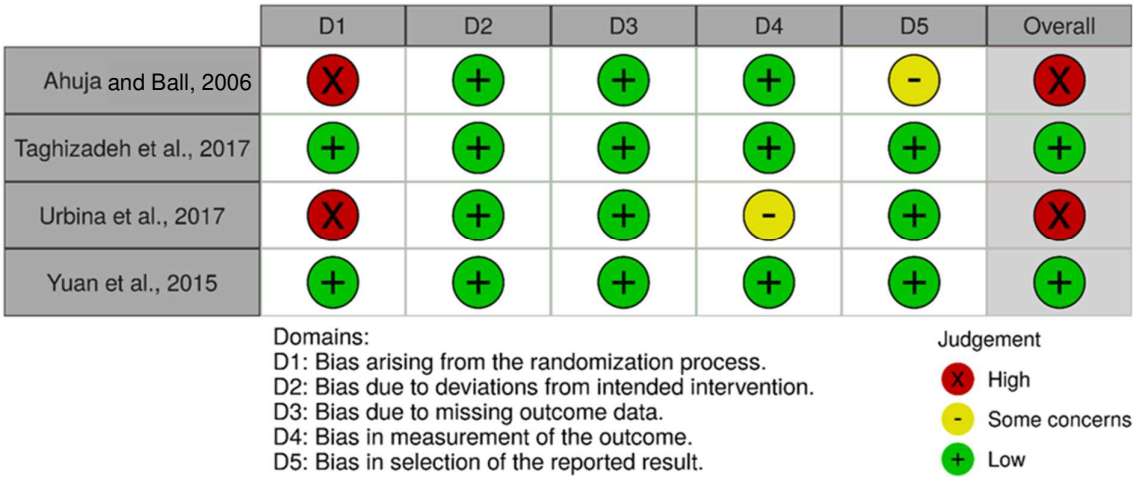

According to the Rob 2 tool in case of fasting plasma insulin levels, 2 studies are considered overall as high risk (Ahuja and Ball 2006, Urbina et al. 2017), and 2 studies as low risk (Yuan et al. 2016, Taghizadeh et al. 2017).

Table S6. Risk of bias assessment of a non-randomized crossover trial included in the meta-analysis using the ROBINS-I (Risk Of Bias In Non-randomized Studies of Interventions) tool.

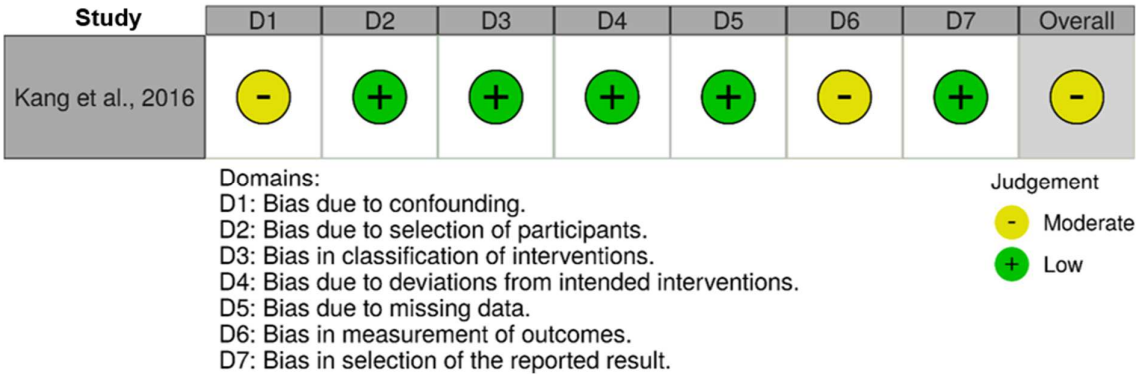

According to the ROBINS-I tool, the overall quality of the study by Kang et al. (2016) is considered as moderate.

Table S7. Summary of findings using the GRADE approach.

Analyzed blood parameter	Capsaicinoid - placebo SMD (95% CI)	Number of subjects (and studies)	Quality of the evidence
Total cholesterol	-0.52 (-0.83, -0.21)	398 (10)	⊕⊕**, Low** because of risk of bias and imprecision
LDL	-0.30 (-0.57, -0.02)	398 (10)	⊕⊕**, Low** because of risk of bias and imprecision
Triglyceride	-0.39 (-1.15, 0.37)	370 (9)	⊕⊕**, Low** because of inconsistency and imprecision
HDL	-0.03 (-0.37, 0.32)	370 (9)	⊕⊕**, Low** because of imprecision and inconsistency
Fasting glucose	0.41 (-0.26, 1.07)	213 (5)	⊕**, Very low** because of imprecision and inconsistency
Fasting insulin	0.28 (-0.25, 0.82)	166 (4)	⊕**, Very low** because of imprecision and inconsistency

CI, confidence interval; HDL, high-density lipoprotein; LDL, low-density lipoprotein; SMD, standardized mean difference.

Table S8. Quality of the evidence for all analyzed outcomes using the GRADE the approach.

Measured outcome	Study design	Risk of bias	Inconsistency	Indirectness	Imprecision	Publication bias	Other	Quality of evidence
Total cholesterol	Most studies were RCTs (starts as high quality)	High risk of bias in most analyzed studies (-1)	9 out of 10 studies involved healthy individuals; heterogeneity was moderate mainly due to one study (0)	The interventions contained capsaicinoids as defined in our PICO (0)	Wide CIs often crossing the null value (-1)	Some asymmetry in funnel plot (0)	None	**Low** ●●○○
LDL	Most studies were RCTs (starts as high quality)	High risk of bias in most analyzed studies (-1)	9 out of 10 studies involved healthy individuals; heterogeneity was moderate mainly due to one study (0)	The interventions contained capsaicinoids as defined in our PICO (0)	Wide CIs often crossing the null value (-1)	Some asymmetry in funnel plot (0)	None	**Low** ●●○○
Triglyceride	Most studies were RCTs (starts as high quality)	High risk of bias in most analyzed studies (-1)	8 out of 9 studies involved healthy individuals; heterogeneity was high mainly due to one study (0)	The interventions contained capsaicinoids as defined in our PICO (0)	Wide CIs often crossing the null value (-1)	Some asymmetry in funnel plot (0)	None	**Low** ●●○○
HDL	Most studies were RCTs (starts as high quality)	High risk of bias in most analyzed studies (-1)	8 out of 9 studies involved healthy individuals; heterogeneity was high mainly due to one study (0)	The interventions contained capsaicinoids as defined in our PICO (0)	Wide CIs often crossing the null value (-1)	Some asymmetry in funnel plot (0)	None	**Low** ●●○○
Fasting glucose	Most studies were RCTs (starts as high quality)	High risk of bias in most analyzed studies (-1)	1 out of 5 studies involved women with gestational diabetes; high heterogeneity (-1)	The interventions contained capsaicinoids as defined in our PICO (0)	Wide CIs often crossing the null value; low number of studies (-2)	Some asymmetry in funnel plot (0)	None	**Very low** ●○○○
Fasting insulin	Most studies were RCTs (starts as high quality)	High risk of bias in most analyzed studies (-1)	1 out of 4 studies involved women with gestational diabetes; high heterogeneity (-1)	The interventions contained capsaicinoids as defined in our PICO (0)	Wide CIs often crossing the null value; low number of studies (-2)	Some asymmetry in funnel plot (0)	None	**Very low** ●○○○

CI, confidence interval; HDL, high-density lipoprotein; LDL, low-density lipoprotein; PICO, Patients, Intervention, Comparison, Outcome model; RCT, randomized controlled trial.

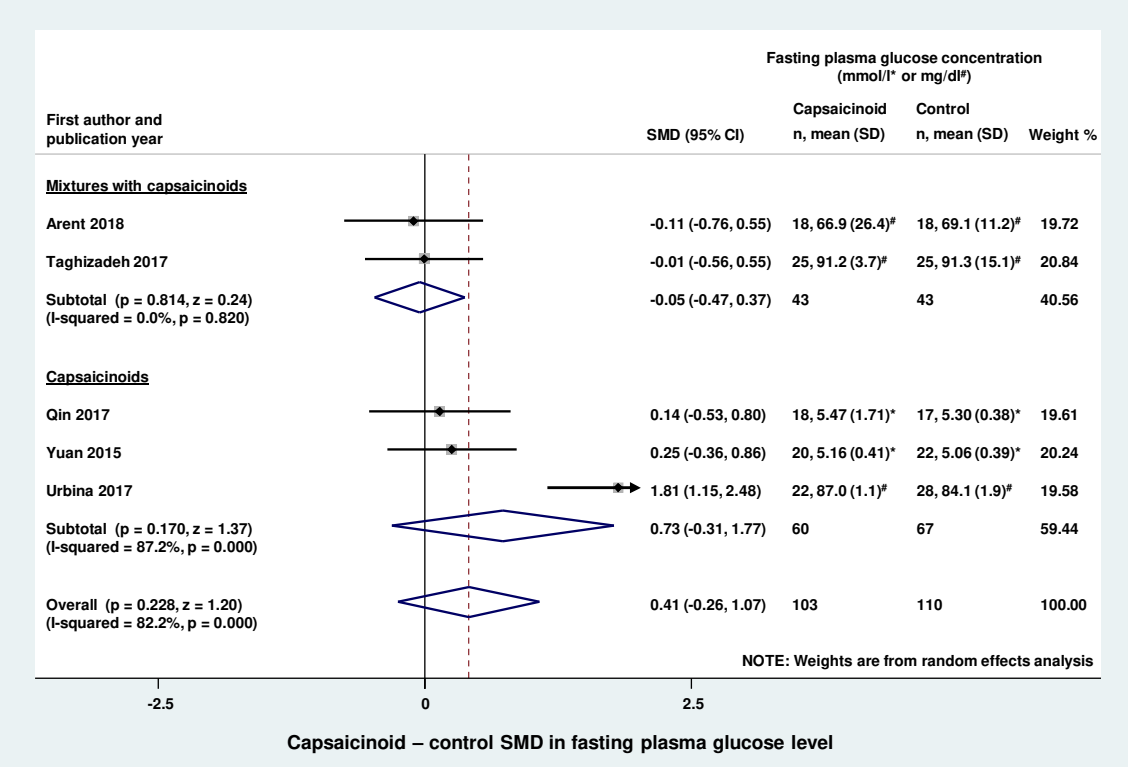

Figure S1. Forest plot of the effects of capsaicinoid-containing mixtures (top) and capsaicinoids (bottom) on fasting plasma glucose level. There was no significant difference between the two subgroups (Q = 1.846; p = 0.174). CI, confidence interval; SD, standard deviation; SMD, standardized mean difference.

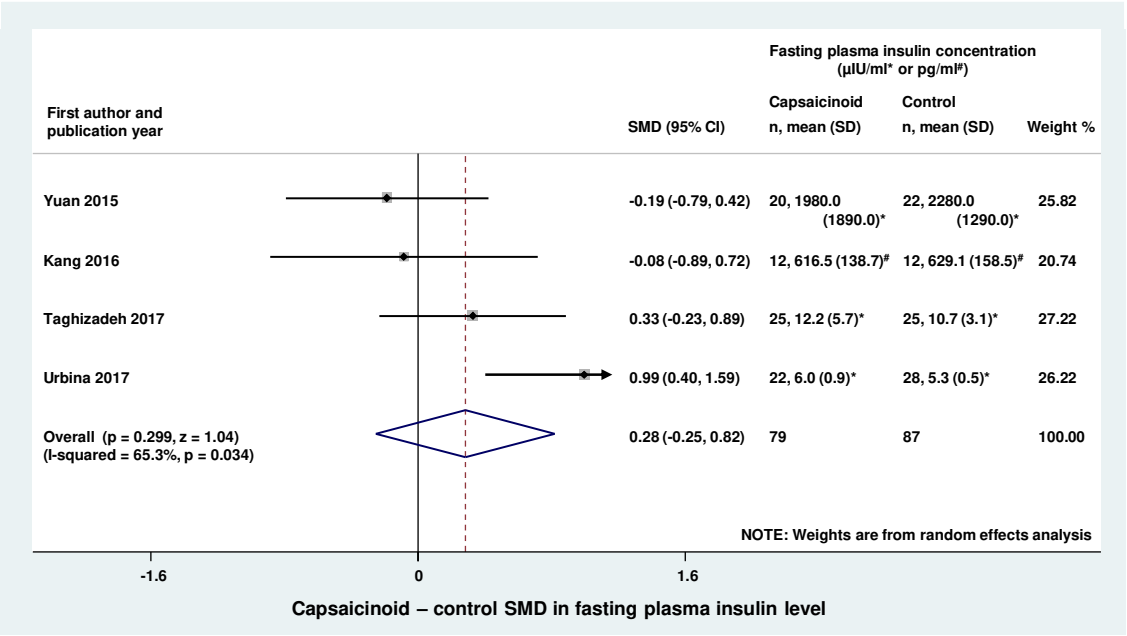

Figure S2. Forest plot of the effects of capsaicinoids (Kang et al. 2016, Urbina et al. 2017, Yuan et al. 2015) and capsaicinoid-containing mixtures (Taghizadeh et al. 2017) on fasting plasma insulin level. CI, confidence interval; IU, international unit; SD, standard deviation; SMD, standardized mean difference.

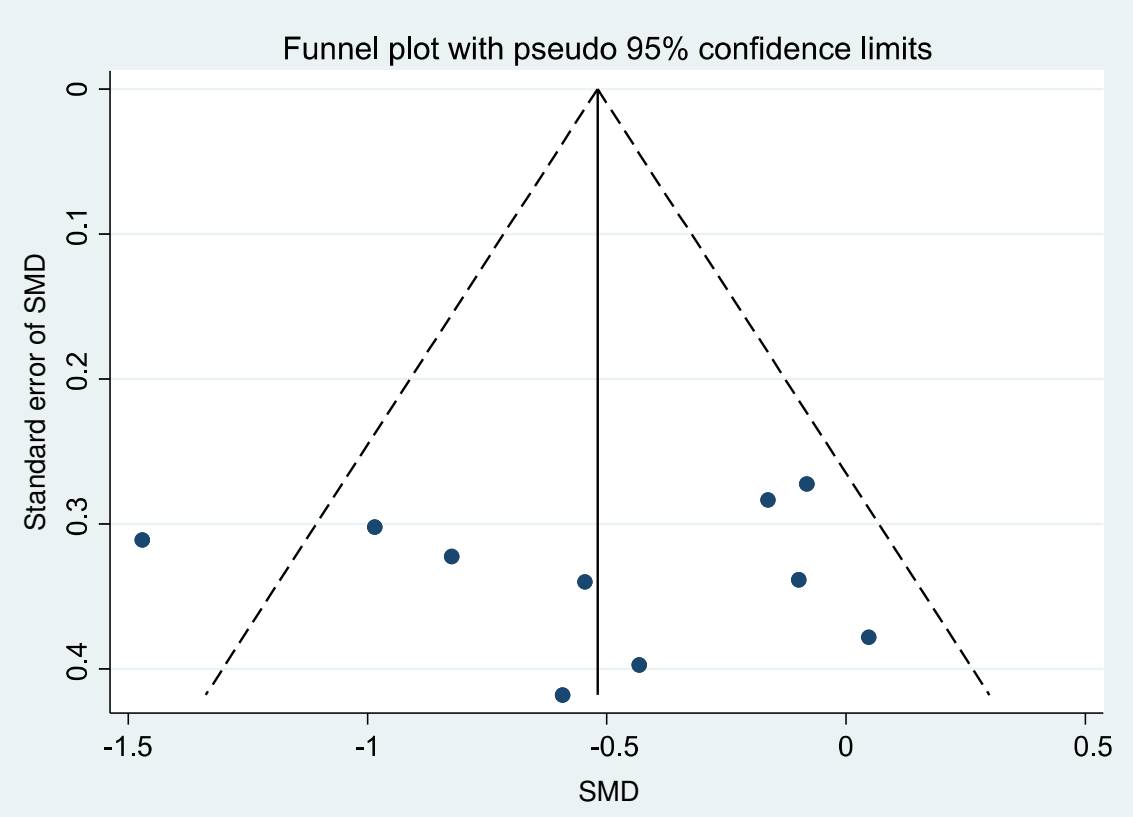

Figure S3. Funnel plot of the studies that were included in the forest plot of the standardized mean differences (SMDs) for serum total cholesterol level in the capsaicinoid-treated and the control groups (Figure 2) (Egger's test p = 0.973).

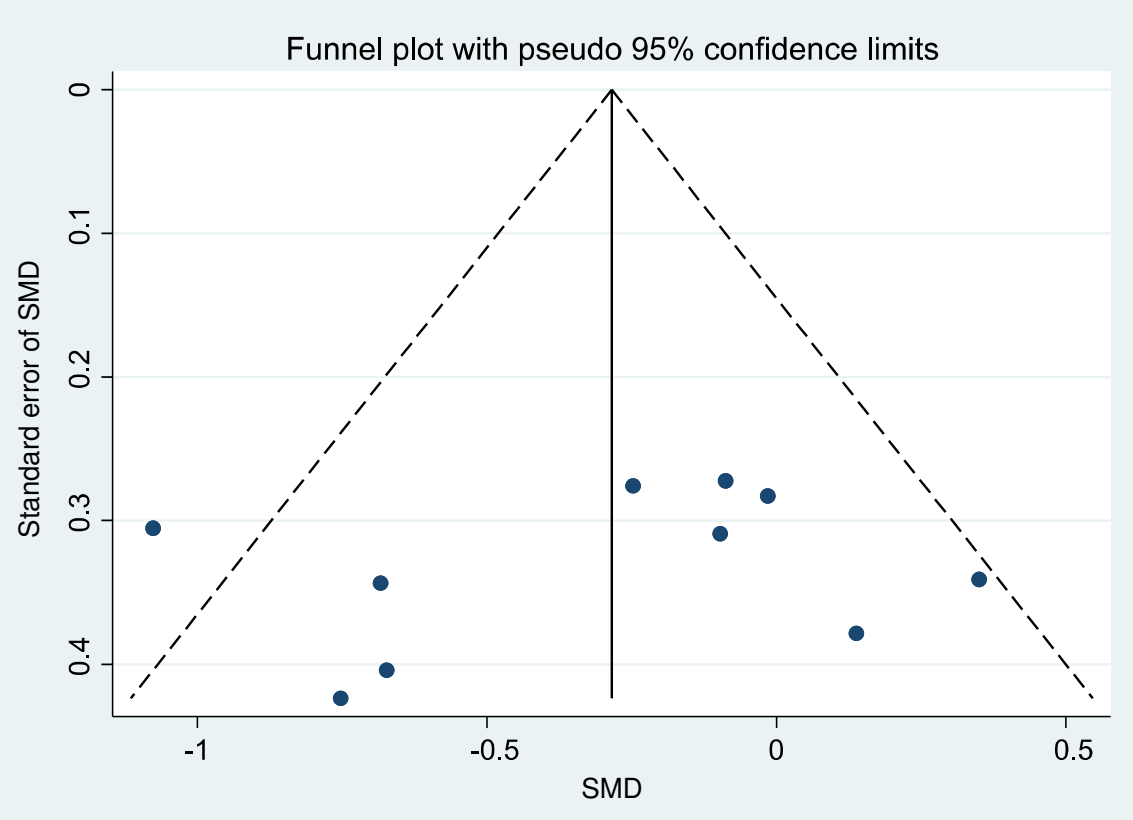

Figure S4. Funnel plot of the studies that were included in the forest plot of the standardized mean differences (SMDs) for serum low-density lipoprotein level in the capsaicinoid-treated and the control groups (Figure 3) (Egger's test p = 0.523).

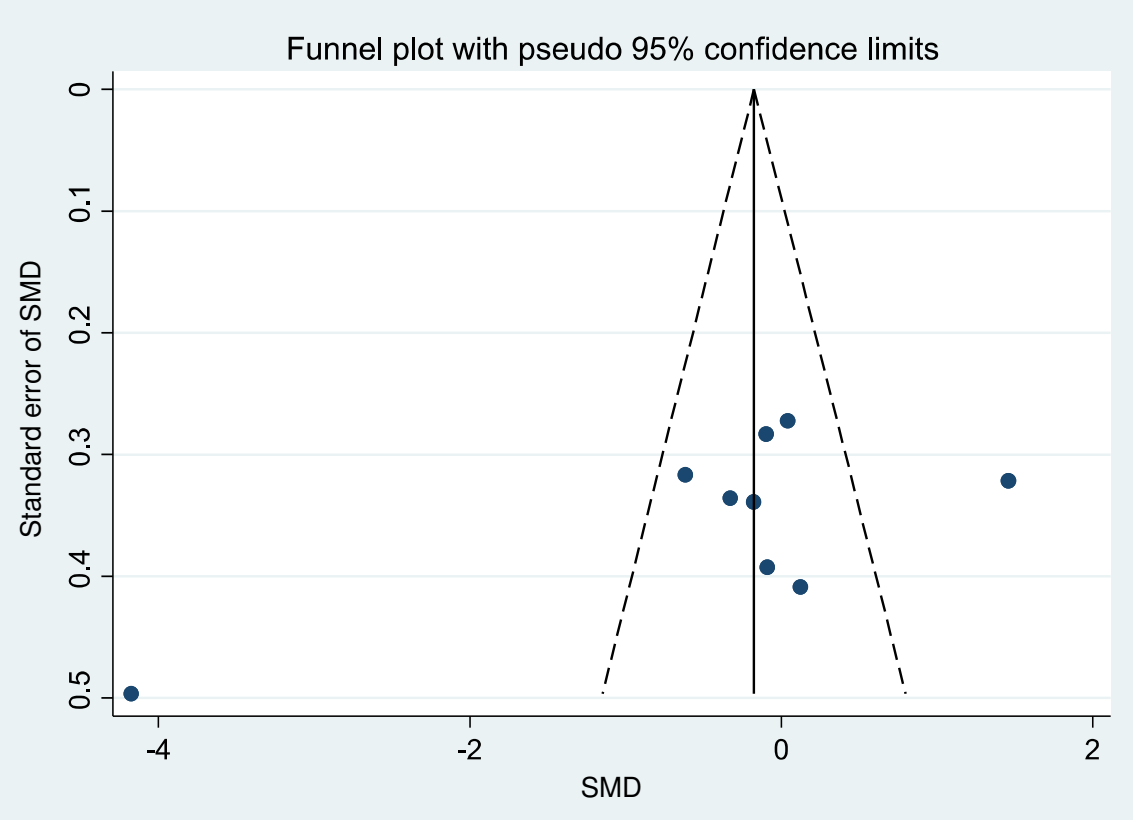

Figure S5. Funnel plot of the studies that were included in the forest plot of the standardized mean differences (SMDs) for serum triglyceride level in the capsaicinoid-treated and the control groups (Figure 4).

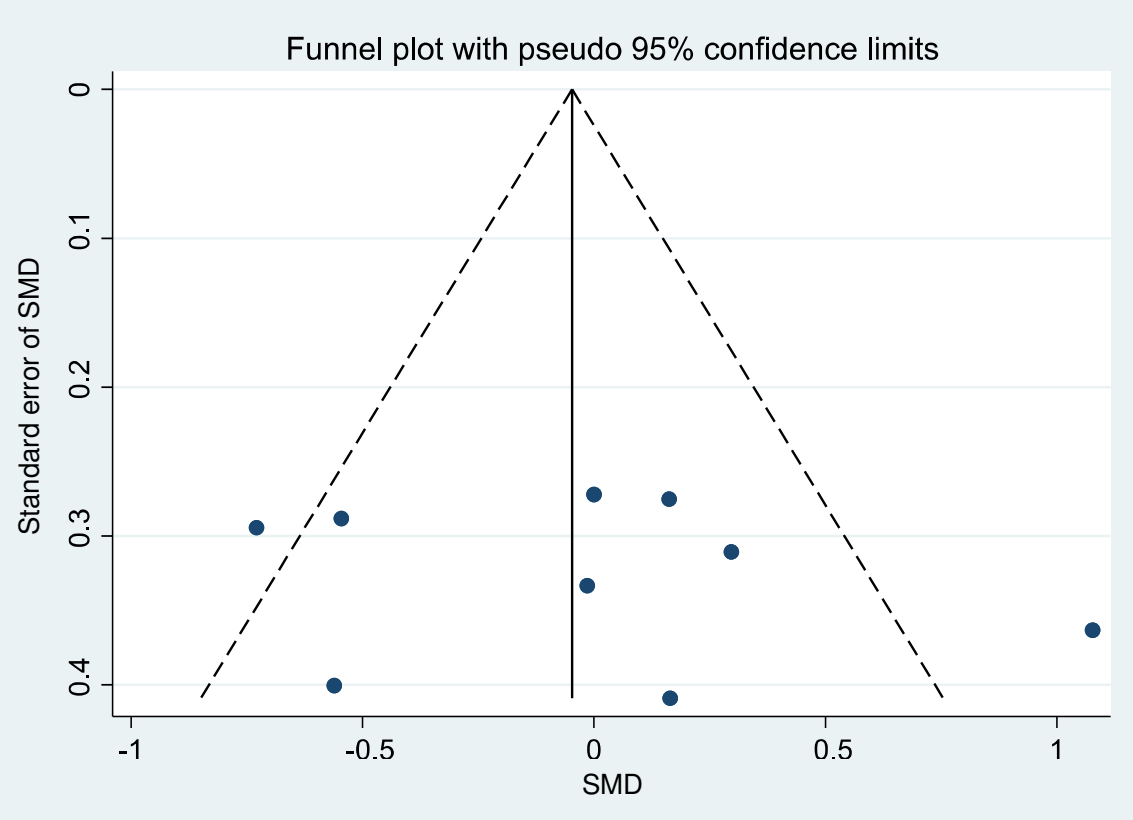

Figure S6. Funnel plot of the studies that were included in the forest plot of the standardized mean differences (SMDs) for serum high-density lipoprotein level in the capsaicinoid-treated and the control groups (Figure 5).

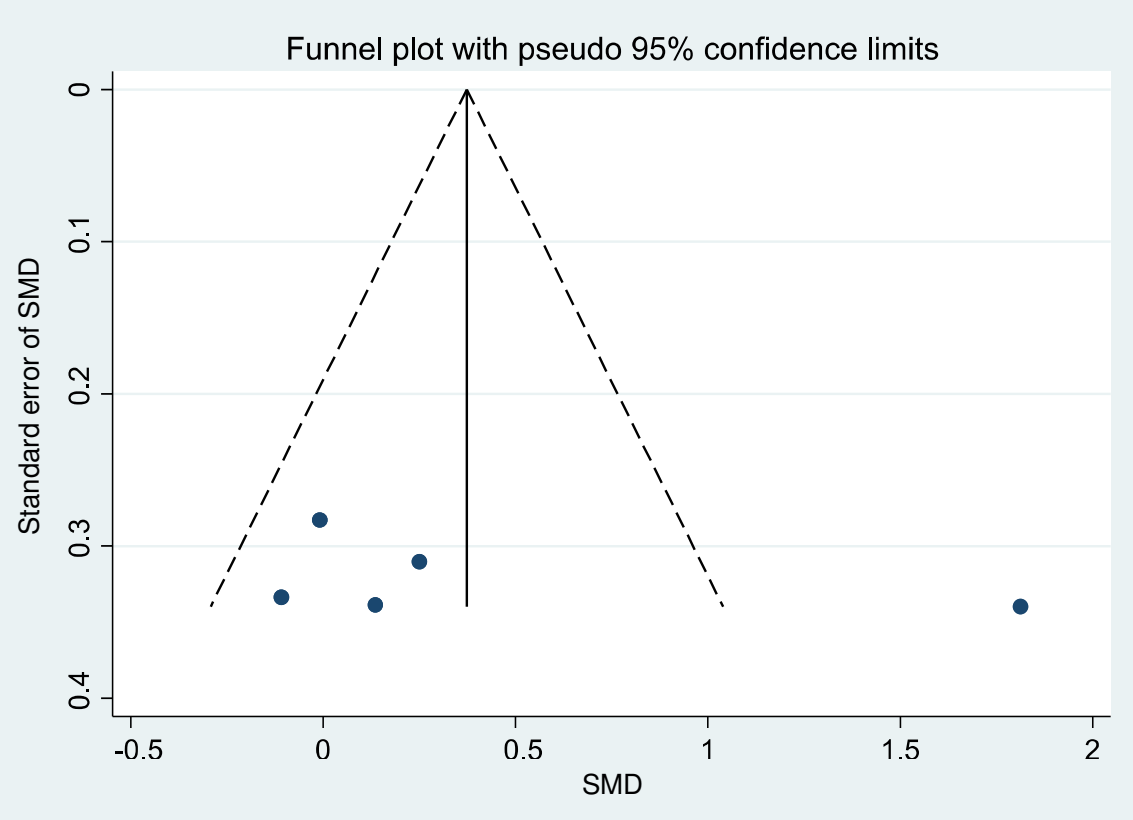

Figure S7. Funnel plot of the studies that were included in the forest plot of the standardized mean differences (SMDs) for fasting plasma glucose level in the capsaicinoid-treated and the control groups (Supplementary Figure S1).

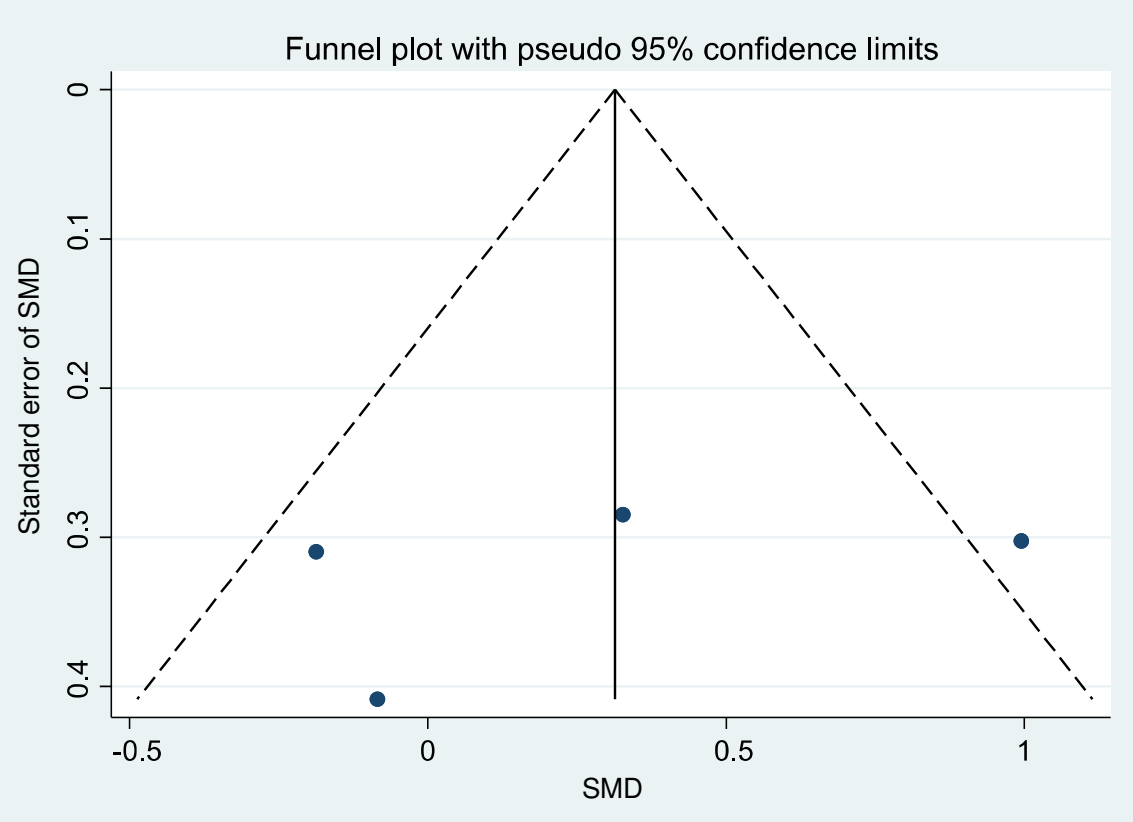

Figure S8. Funnel plot of the studies that were included in the forest plot of the standardized mean differences (SMDs) for fasting plasma insulin level in the capsaicinoid-treated and the control groups (Supplementary Figure S2).

polymers

MDPI

Article

Stereolithography 3D Printing of a Heat Exchanger for Advanced Temperature Control in Wire Myography

Leonardo Kelava [1], Ivan Ivić [1], Eszter Pakai [1], Kata Fekete [1], Peter Maroti [2,3], Roland Told [2,3], Zoltan Ujfalusi [4] and Andras Garami [1,*]

[1] Department of Thermophysiology, Institute for Translational Medicine, Medical School, University of Pecs, H-7624 Pecs, Hungary; leonardo.kelava@aok.pte.hu (L.K.); ivic.ivan@gmail.com (I.I.); eszter.pakai@aok.pte.hu (E.P.); kata.fekete@aok.pte.hu (K.F.)
[2] Medical Simulation Education Center, Medical School, University of Pecs, H-7624 Pecs, Hungary; marotipeter8@gmail.com (P.M.); told.roland@pte.hu (R.T.)
[3] 3D Printing and Visualization Center, University of Pecs, H-7624 Pecs, Hungary
[4] Department of Biophysics, Medical School, University of Pecs, H-7624 Pecs, Hungary; zoltan.ujfalusi@aok.pte.hu
* Correspondence: andras.garami@aok.pte.hu; Tel.: +36-(72)-503-647

Abstract: We report the additive manufacturing of a heat-exchange device that can be used as a cooling accessory in a wire myograph. Wire myography is used for measuring vasomotor responses in small resistance arteries; however, the commercially available devices are not capable of active cooling. Here, we critically evaluated a transparent resin material, in terms of mechanical, structural, and thermal behavior. Tensile strength tests (67.66 ± 1.31 MPa), Charpy impact strength test (20.70 ± 2.30 kJ/m^2), and Shore D hardness measurements (83.0 ± 0.47) underlined the mechanical stability of the material, supported by digital microscopy, which revealed a glass-like structure. Differential scanning calorimetry with thermogravimetry analysis and thermal conductivity measurements showed heat stability until ~250 °C and effective heat insulation. The 3D-printed heat exchanger was tested in thermophysiology experiments measuring the vasomotor responses of rat tail arteries at different temperatures (13, 16, and 36 °C). The heat-exchange device was successfully used as an accessory of the wire myograph system to cool down the experimental chambers and steadily maintain the targeted temperatures. We observed temperature-dependent differences in the vasoconstriction induced by phenylephrine and KCl. In conclusion, the transparent resin material can be used in additive manufacturing of heat-exchange devices for biomedical research, such as wire myography. Our animal experiments underline the importance of temperature-dependent physiological mechanisms, which should be further studied to understand the background of the thermal changes and their consequences.

Keywords: 3D printing; SLA; resin; mechanical characterization; thermal conduction; heat exchange; wire myograph; thermoregulation; thermophysiology

Citation: Kelava, L.; Ivić, I.; Pakai, E.; Fekete, K.; Maroti, P.; Told, R.; Ujfalusi, Z.; Garami, A. Stereolithography 3D Printing of a Heat Exchanger for Advanced Temperature Control in Wire Myography. *Polymers* **2022**, *14*, 471. https://doi.org/10.3390/polym14030471

Academic Editor: Chin-San Wu

Received: 30 December 2021
Accepted: 20 January 2022
Published: 25 January 2022

1. Introduction

Additive manufacturing is an increasingly applied technology in medicine and biomedical science [1,2], while it is also a cost-effective, reliable, and user-friendly tool for the creation of laboratory equipment [3]. Heat exchangers are widely used in thermal investigations both in engineering and in life sciences, and additive manufacturing has become an essential tool in the development and final production of these devices [4,5]. Besides metals and ceramics, which both have favorable thermal characteristics, polymers are also used to produce heat exchangers. In a previous study, Arie et al. used HDPE (high-density polyethylene) and PLA (polylactic acid) for additively manufacturing a polymer heat-exchanging device with excellent heat transfer performance [6]; however, the SLS (selective laser sintering) technology was also successfully applied to produce a polymer

heat exchanger with good thermal performance [7]. In a recent study, the use of a metal (aluminum) and polymer composite (ABS, acrylonitrile butadiene styrene) was highlighted [8], while another research group used resin-based composites for thermal investigation [9]. Furthermore, to increase stiffness and hardness, dos Santos et al. developed a composite of photocurable epoxy-acrylate resin and multiwalled carbon nanotubes [10]. Surprisingly, to our knowledge, there is no data available in the scientific literature about the use of resins and desktop stereolithography (SLA) technology for heat exchanger development and about fabrication of heat exchangers with standard, transparent, one-component resins, despite their broad availability and versatility. Previously, SLA 3D printing technology has been utilized only for the optimization of microchannel cooling configurations [11,12], but not for the development of a cooling device for biomedical research purposes, at which we aimed, for the first time to our knowledge, in the present study. Furthermore, the detailed thermal characteristics of the printouts of transparent resins, i.e., their differential scanning calorimetry with thermogravimetry analysis (DSC-TGA), have remained unknown, even though the DSC-TGA is an essential tool for efficiently and accurately mapping the thermal properties of heat-exchanging materials, thereby providing additional information about the thermal performance of the device to the users. Testing of the mechanical and thermal properties of 3D-printed parts is of high importance, because it can provide valuable information about the fusion of layers during printing, thus, about part quality and strength [13], as well as about the relations of the thermal and the fatigue parameters of the 3D-printed material under static and cyclic loading, including the self-heating phenomenon [14].

Efficient heat exchangers are particularly important for thermophysiology studies, in which body or organ responses at different temperatures are measured. In mammals, blood vessels are integral part of the thermoregulation system and are biologically responsive to changes in temperature. In the skin, upon cold exposure they promote heat conservation through vasoconstriction, whereas, upon exposure to warmth, they facilitate heat dissipation through vasodilation. Via their thermal responses, peripheral (e.g., cutaneous) blood vessels also affect systemic blood pressure, tissue blood flow, and the production of biologically active molecules [15]. Temperature fluctuations can be particularly pronounced in the skin, especially in small mammals (e.g., mice and rats). For example, when mice were exposed to severe cold (8 °C for 180 min), their skin and deep body temperatures dropped from 31 to 8 °C and from 37 to 13 °C, respectively [16]; still, they all recovered from the hypothermia after cessation of the cold exposure. Compared to small rodents, the larger body mass of humans ensures better heat conservation; nevertheless, in extreme situations, similarly low body temperatures as in the mouse experiments can also occur in humans. For example, a deep body temperature as low as 13.7 °C was recorded in a human subject in a skiing accident. It is notable that the patient survived with minimal consequences and no brain damage, which could be due to the rapid cooling of the brain leading to decreased metabolic rate, thereby to minimal ischemic damage [17]. Although it was shown that vasomotor responses to some substances differ at different temperatures [18], it is a challenge to perform the direct measurement of the vasomotor responses of isolated arteries in the cold, because of the lack of proper experimental methods possessing tight temperature control in cold environments. Wire myography was developed in the 1970s as a technique specifically designed to measure contractile forces of isolated vascular preparations [19]. At present, several manufacturers offer wire myographs with different technical specifications. It is a common feature that these instruments have integrated heaters, allowing to heat the baths containing the isolated vessels segment to temperatures that are above the room temperature, whereas none of them has the ability to actively cool the bath below the room temperature, thereby limiting their potential use for mimicking cold exposure, thus, to study vasomotor responses in the cold. Here, we present the development and the prototype of a unique heat exchanger as an accessory to the wire myograph, which is capable of tight temperature control of the bath in a wide range, also including its active cooling well below room temperature. Preliminary tests indicated that SLA 3D printing with a transparent resin could be used for additive manufacturing of the heat exchanger.

We aimed to evaluate and characterize a commercially available resin for desktop SLA and to critically investigate its potential use in the fabrication of heat-exchange devices for ex vivo thermophysiology studies.

2. Materials and Methods

2.1. 3D Printing and Mechanical Testing

In order to fabricate a watertight system, SLA additive manufacturing technology was applied. For 3D printing, a Formlabs Form 2 SLA desktop printer was used (Formlabs Inc., Somerville, MA, USA), and the selected material was the transparent Clear Resin V4 (Formlabs Inc., Somerville, MA, USA). To fabricate the test specimens for mechanical testing and thermal conductivity, the printer has been set to the parameters shown in Table 1. The parameters were chosen based on the material data sheet of the resin and based on our previous experience with the fabrication of microfluidic systems.

Table 1. Printing and post-processing parameters of SLA 3D printing.

SLA Printing Technology						Post Processing	
Material	**Color**	**Laser Beam Focus Width (μm)**	**Touchpoint Size (mm)**	**Raft Type**	**Layer Thickness (μm)**	**Washing Time in Isopropyl-Alcohol (min)**	**Time in 60 °C Ultraviolet Chamber (min)**
Clear resin	Clear	85	0.7	Full	100	10	15

2.1.1. 3-Point Flexural Test

The 3-point bending tests were carried out by a Zwick/Roell Z100THW universal material tester (ZwickRoell, Ulm, Germany). The tests were conducted according to ISO 178:2010 with the fabricated specimen. According to the standard, the size of specimen was 4 mm × 10 mm × 80 mm. The pre-load was 0.1 MPa and the speed was set at 2 mm/min during the entire test. The support distance was 64 mm and the maximum deformation was 4.7%. The tests were performed 5 times.

2.1.2. Tensile Test

The tensile tests were carried out with the same Zwick/Roell Z100THW tester (Zwick-Roell, Ulm, Germany), supplemented with and extensometer. The tests were conducted according to ISO 527-1:2019 with the fabricated specimen. The type of specimen was A1 from ISO 527-2:2012 and the pre-load was 0.1 MPa. The speed was set at 1 mm/min during the determination of Young's modulus, while it was 50 mm/min during the test. The number of test specimens was 5.

2.1.3. Charpy Test

The Charpy impact tests were performed by a Zwick/Roell Hit50P instrument with 5 J pendulum (ZwickRoell, Ulm, Germany) according to the 179-1:2010 standard: the size of specimen was 4 mm × 10 mm × 80 mm; the hit impacted the edge; and the tests were repeated 5 times.

2.1.4. Shore D Hardness

The Shore D hardness tester was a Zwick/Roell 3131/320154 device (ZwickRoell, Ulm, Germany). The tests were performed according to the 868:2003 standard. The instrument was on a stand and the specimen thickness was 5 mm. All measurements were carried out 5 times.

2.2. Thermal Conductivity

Thermal conductivity measurements were performed on 3 test samples. In order to perform the measurement, an apparatus was built with the following elements (see also Figure 1):

- Arduino Uno (Arduino, Somerville, MA, USA) with 2 thermistors;

- Rohde@Schwarz HMC8012 Digital Multimeter (Rohde & Schwarz, München, Germany);
- Ender 3 3D printer controller (Creality, Shenzhen, China) for control of the heated bed;
- 24 V, 160 W heated bed (Creality, Shenzhen, China);
- 8-cm thick Energosystem ES-EPS-80-8 polystyrene (Thermotrading Ltd., Cegléd, Hungary) for insulation of the measured system from the environment;
- Thermal grease (model: 51634; Qoltec, Gliwice, Poland) for thermal conductive adhesion.

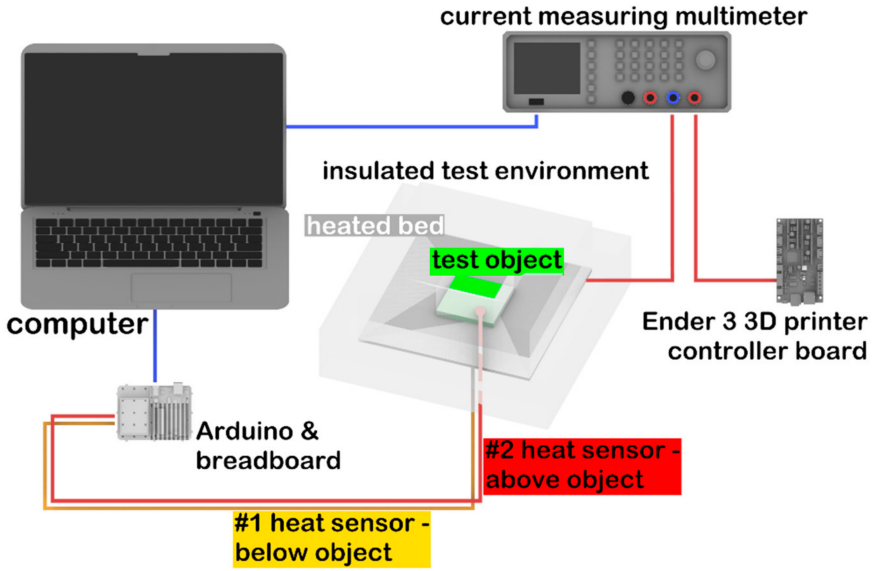

Figure 1. Schematic representation of the experimental setup used for thermal conductivity measurements.

The heating plate was surrounded by polystyrene foam (λ = 0.039 W/mK) as an insulation, except for a 7 cm × 7 cm wide opening, through which the test specimens were placed inside. The size of the 3D-printed test specimen was 5 mm × 70 mm × 70 mm. For the calibration of the device, a glass plate was used, which had the same size as the sample (λ_{ref} = 1 W/mK). Thermal sensors were positioned on the top and the bottom of the test specimen, and then the sample was placed on the heating bed. Measurements were recorded by the Arduino Uno with a frequency of 0.2/s. The heat flow was determined by the electric energy consumption of the heating bed. The multimeter was serially connected to the heating bed and the Ender 3 printer controller. Power consumption as a function of time was recorded on a personal computer (Figure 1).

The measurements were performed in five stages in the case of both glass and resin samples: (i) 35 °C for 45 min; (ii) 37 °C for 35 min; (iii) 44 °C for 30 min; (iv) 49 °C for 25 min; and (v) 58 °C for 20 min. The duration of a full heating cycle was 155 min. During the entire measurement cycle the heating bed was completely surrounded with polystyrene (except the 7 cm × 7 cm opening); thus, heat conductivity could be determined by measuring the loss of the current (for details, see below). Further data processing was performed in the Origin software (OriginLab Corporation, Northampton, MA, USA). In each phase, after reaching the thermodynamic equilibrium, the difference between the two thermosensors was determined by averaging the difference data obtained in three full heating cycles.

Heat flow was calculated on the basis of the ratio of the maximum usable current and the current related to the actual heating consumed over the three cycles, and then the amount of heat loss was deducted from this value. After that, the following equation was used:

$$\lambda = \left| \frac{\dot{Q}}{A \cdot \frac{T_2 - T_1}{\delta}} \right| \quad (1)$$

where $\dot{Q}$—heat flow (W), A—cross section of the test specimen (m^2), T_1, T_2—temperatures measured on both sides of the test specimen (°C), δ—thickness of the test specimen (m). The

measured and calculated values were fitted to an exponential curve that was determined by the following equation:

$$y = A \cdot e^{-\frac{x}{t}} + y_0 \quad (2)$$

where A, t, y_0 are constants and x marks the temperature.

The zero point correction factor of the device was determined by the following equation:

$$k = \frac{\lambda_{reference}}{\lambda_{measured}} \quad (3)$$

where k is the correction factor and $\lambda_{reference}$ and $\lambda_{measured}$ are the heat conductions for the reference material as determined by the manufacturer and as measured in our experiments at 23 °C, respectively. The correction was made at the ambient temperature at which the measurement was performed (23 °C).

2.3. DSC-TGA

LabSys Evo device (Setaram Ltd., Caluire-et-Cuire, France) was used to perform these experiments. The calibration of the instrument was recently performed by the manufacturer. The measurements were carried out under 100 mL/min nitrogen atmosphere and the mass of each sample was set between 5.2–5.5 mg. The applied temperature range for the measurements started at 30 °C, ended at 750 °C, and was increased at a rate of 10 °C/min. Because of the high temperatures, uncovered Al_2O_3 crucibles (Setaram Ltd., Caluire-et-Cuire, France) with a volume of 100 µL were used. The rate of the sample's spontaneous cooling was sufficient for the measurements; thus, the application of external cooler was not necessary. Data processing was performed using Origin 2021 software (OriginLab Corporation, Northampton, MA, USA).

2.4. Digital Microscopy

Images were taken of both the intact and broken surface of the specimens used in the Charpy test in order to evaluate the structure of the resin material with a König digital microscope (König Electronic GmbH, Reichelsheim, Germany) with 35× magnification.

2.5. Fabrication of the Heat-Exchange Device

The instrument was designed using Rhinoceros 6 CAD (computer-aided design) software (Robert McNeel & Associates, Seattle, WA, USA). The size of the final product was 75 mm × 120 mm × 7 mm, the cooling pipes were 10.5 mm long with a 5 mm inner and 7 mm outer diameter and were interspaced from each other by 1 mm (Figure 2). The slicing process was performed by the PreForm slicing software (Formlabs Inc., Somerville, MA, USA). The layer height was set to 50 µm, and the device was in "Y" printing orientation on the printing bed. The overall printing time was 13 h and 15 min and it required a total volume of 46 mL resin. The post processing included bathing in isopropyl alcohol for 10 min and UV curing at 60 °C for 15 min.

2.6. Thermophysiology Experiments

2.6.1. Animals

The thermophysiology experiments were performed in 22 Wistar rats. At the time of the experiments the rats aged 1–3 months and weighed 140–240 g. Animals were bred and kept at University of Pecs in standard plastic cages (model: 1290 D Eurostandard type III; Akronom Ltd. Budapest, Hungary) kept in a room with an ambient temperature maintained at 21–23 °C and humidity at 30–40%. The room was on a 12/12-h light/dark cycle (lights on at 5:00 a.m.). The rats had access to standard rodent chow and tap water ad libitum. All experiments were conducted under protocols approved by the Institutional Animal Use and Care Committee of the University of Pecs (registration no.: BA02/2000-6/2018, approved on 27 February 2018) and conformed to the guidelines from Directive 2010/63/EU of the European Parliament on the protection of animals used for scientific purposes.

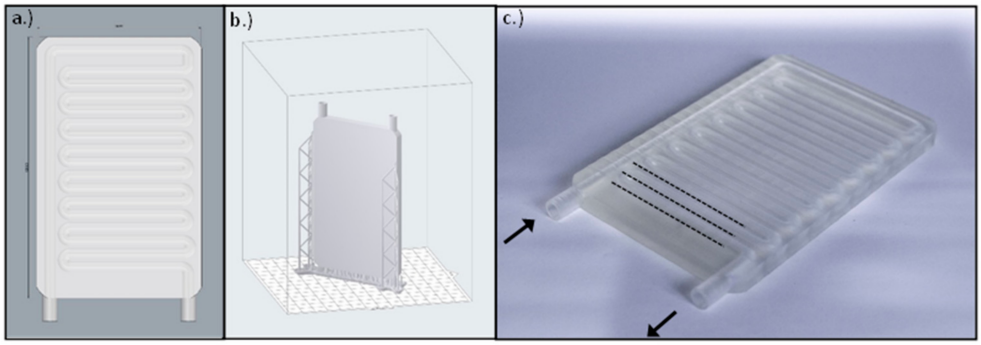

Figure 2. (**a**) The CAD model of the cooling plate created with Rhinoceros 6 CAD software. (**b**) The .stl model uploaded in the slicer software. (**c**) The manufactured cooling plate using a 3D printer. The arrows indicate the inflow and outflow pipes of the plate, and the dotted lines represent the parallel cooling pipes.

2.6.2. Experimental Procedures

The experiments were conducted in a multi wire myograph system (model DMT 610M; Danish Myo Technology A/S, Aarhus, Denmark). A heat-exchanger plate (developed in the present study) was placed on the top of the myo-interface unit underneath each of the four myograph chamber units. The heat-exchanger plates were connected to polyethylene peroxide-cured tubes, which were continuously perfused from a water tank. In the tank, the temperature of the water was tightly controlled with a heating and a cooling device (models GD120 and C1G, respectively; Grant Instruments Ltd., Cambridge, UK). Before each experiment, the calibration procedure of the myograph system was performed according to the manufacturer's instructions, while the temperature of the bath containing Krebs solution (NaCl: 119 mM, KCl: 4.7 mM, KH_2PO4: 1.2 mM, $NaHCO_3$: 25 mM, Mg_2SO_4: 1.2 mM, $CaCl_2 \times 2H_2O$: 1.6 mM, EDTA: 0.026 mM, and glucose: 11.1 mM) in the myograph chambers was maintained at 13, 16, or 37 °C. The ingredients of the Krebs solution were purchased from Sigma-Aldrich (St. Louis, MO, USA). The bath solution's temperature was recorded with a 12-channel scanning thermocouple thermometer (Cole-Parmer, Vernon Hills, IL, USA) throughout the calibration procedure and the experiment. The thermocouples (Omega Engineering, Stamford, CT, USA) were calibrated, and then inserted in the bath solution in a way that they did not touch the walls of the chamber.

The isolation of the tail artery was performed as in our earlier study [20]. In brief, the rats were anesthetized by the intraperitoneal injection of a ketamine-xylazine cocktail (81.7 and 9.3 mg/kg, respectively). A midline incision was made on the top of the tail; then, the tail artery was isolated and cleaned from its connective tissue. The proximal and distal ends of the isolated artery were ligated and the vessel segment between the ligations was excised. After the removal of the artery, the animal was euthanized with an intraperitoneal injection of pentobarbital (100 mg/kg; Cave Santa Animale, Libourna, France). The excised artery was dissected into four 2-mm long segments. The segments were mounted in the myograph chambers using tungsten wires with 40 nm diameter and allowed to rest for 60 min; then, normalization was performed according the manufacturer's instructions. After the normalization, the viability of the vessels was verified by the presence of vasoconstriction induced by 60 mM KCl. In the experiments, endothelium-dependent vasoconstriction was studied in response to increasing concentrations of phenylephrine (10^{-8} to 10^{-4} M; Sigma-Aldrich, St. Louis, MO, USA) added to the solution in 5 min intervals. After washout with Krebs solution, 60 mM KCl was used to evaluate the vessel's viability at the end of the experiment.

2.7. Statistical Analysis

The statistical analysis of the data obtained with mechanical testing, calorimetry, and thermal conductivity measurements was performed with OriginPro 2018 software (Origin-

Lab Corporation, Northampton, MA, USA). Results of the thermophysiology experiments were analyzed with the R software version 3.6.1 (R Development Core Team, Vienna, Austria). Since Levene's test revealed unequal variances, Welch's one-way ANOVA with post-hoc Games–Howell test was used to compare responses across different temperatures. Vasomotor responses to 60 and 90 mM KCl at 16 °C were compared with Student's *t*-test.

3. Results

3.1. Mechanical Characterization

The results of the mechanical characterization underlined that the selected resin is hard, durable, and can withstand the planned experiments after fabrication of the heat-exchange device (Table 2). The average value of tensile strength was 67.66 ± 1.31 MPa, the flexural stress at standard deflection was measured as 78.82 ± 1.17 MPa, while the Charpy impact test resulted in 20.70 ± 2.30 kJ/m^2. The shore D hardness was 83.00 ± 0.47.

Table 2. The results of the mechanical characterization of the fabricated heat exchanger.

		Mean	SD
Tensile Young's modulus	(MPa)	2304.80	42.90
Tensile strength	(MPa)	67.66	1.31
Flexural Young's modulus	(MPa)	2246.80	66.70
Flexural stress at standard deflection	(MPa)	78.82	1.17
Charpy impact	(kJ/m^2)	20.70	2.30
Shore D hardness		83.00	0.47

In an earlier study, Epon 828® resin, a commonly used epoxy polymer, exhibited tensile strength of 69 MPa and tensile Young's modulus of 2750 MPa [21], which are slightly higher values than what we found for the resin used in present study (Table 2). A recent summary of the tensile strength and modulus of fused filament fabrication 3D-printed PLA parts indicated that, if the design parameters were similar (i.e., XYZ build orientation; 0–45° raster angle; 0.15–0.20 mm layer thickness), then tensile strength varied between 41 and 59 MPa and the tensile modulus ranged from 3130 to 3520 MPa [22]. In the same study, the authors fabricated PLA specimen with the same technology and similar design parameters (XYZ build orientation, 0.14 mm layer thickness), which had tensile strength of 31–58 MPa and tensile modulus of 2900–3130 MPa depending from the raster angle (0–90°) [22]. The tensile strength of the investigated material in the present study was higher, but it was also more elastic (Table 2).

3.2. Thermal Conductivity of the Resin Material

The thermal conductivity measurements were performed on the transparent resin. Glass was used as a reference material. To the measured data points of resin, which were 0.314 W/mK at 35 °C, 0.311 W/mK at 37 °C, 0.361 W/mK at 44 °C, 0.351 W/mK at 49 °C, and 0.490 W/mK at 58 °C, a curve was fitted, and then the results were extrapolated based on the previously determined correction factor ($k = 0.931$). After the calibration of the setup, the heat conduction parameters were measured at 35, 37, 44, 49, and 58 °C, which resulted in heat conduction of 0.314, 0.311, 0.361, 0.351, and 0.490 W/mK, respectively (Figure 3).

The corrected average of heat conduction for the tested resin material was 0.280 W/mK, which was considered constant at all temperatures. To our knowledge, this is the first study that reports the thermal conductivity of SLA 3D-printed clear resin ($\lambda_{\text{clear resin}}$ = 0.280 W/mK), which is similar to the thermal conductivity of epoxy resin ($\lambda_{\text{epoxy resin}}$ = 0.202 W/mK) as determined earlier by other authors [23].

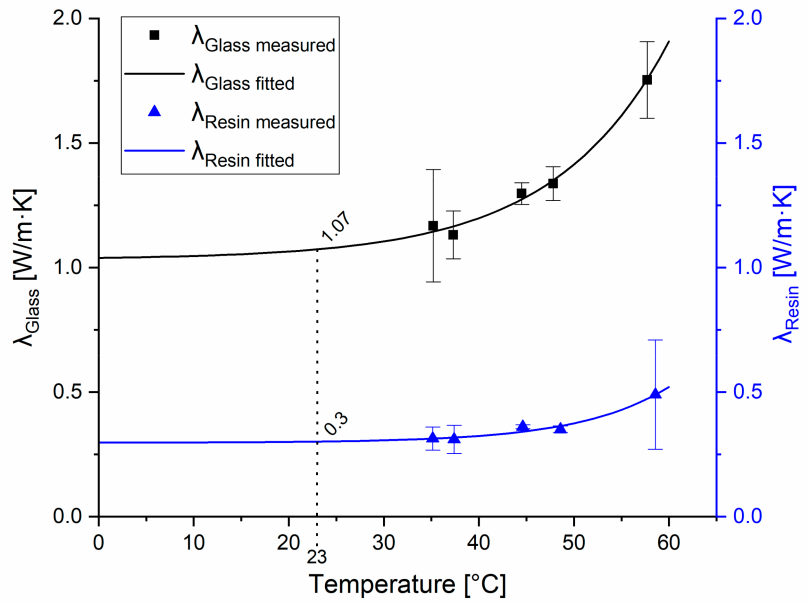

Figure 3. Measured and fitted heat conduction parameters of the tested materials. Heat conduction of the reference glass material is represented by the black curve; the squares show the average values with standard deviations measured at the indicated temperatures. Heat conduction parameters of the resin material are represented by the blue curve; triangles show the measured average values with standard deviations measured at the indicated temperatures.

3.3. Thermal Characterization of the Transparent Resin

The characterization of the thermal properties of the transparent resin samples revealed a relatively high heat stability of the printouts (Figure 4 and Table 3). According to the manufacturer, there is no significant change in the thermal properties of these samples until 250 °C, which has now also been confirmed with the results of our DSC-TGA (Figure 4). It should be noted, however, that a slight gradual loss of sample mass was present already from the beginning of the heating of the sample. The same tendency could be observed with ABS samples, though, in that case, the gradual decrease in sample mass started at higher temperatures [24]. Interestingly the TGA curve of the tested clear resin (Figure 4) is very similar to that of PLA shown in a previous study [24]. However, while PLA and other PLA-based composites usually have a melting temperature of approx. 150-170 °C [25], the clear resin stayed solid at that temperature and even far above (Table 3). Of note, other photopolymers, such as thermally cured structural self-adhesive tapes have much less thermal stability [26]. Such good thermal stability as the one observed in case of the SLA 3D-printed resin in the present study, can be achieved in case of several polymer materials only by the addition of nanoparticles or cellulose nanofibers to their structure, which can enhance various properties, including thermal stability [27,28]. Our research group has previously examined the thermal properties of 3D printouts from many composites, such as PLA, ABS, polyamide, high impact polystyrene, and polyethylene terephthalate glycol (data not shown) and none of these materials had the glass transition (Tg) and melting phases at such high temperatures as the transparent resin. However, the appearance of the fast phase of mass decrease at around 300 °C suggests that resin quickly destabilizes and loses its previous rigid structure above this temperature (Figure 4).

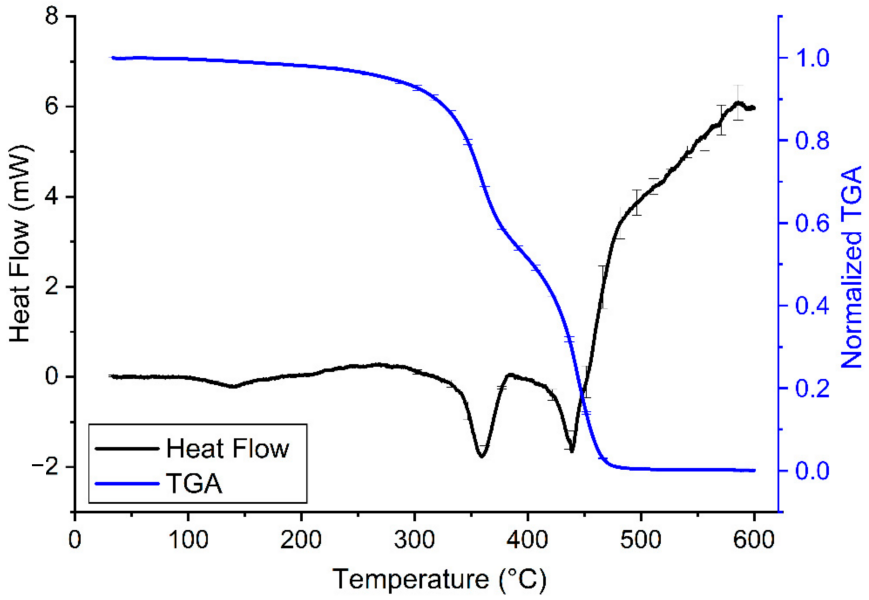

Figure 4. Heating curves of clear resin V4 (30–600 °C, black line) combined with TGA of the samples (30–600 °C, blue line) on a common temperature scale (i.e., abscissa) at a heating rate of 10 °C/min. On the heating curves, the endothermic process (i.e., when the sample melts) causes a drop in heat flow. A decrease in normalized TGA indicates loss of sample mass. The error bars show the standard error of means from at least 3 independent measurements.

Table 3. Corresponding temperature values of the characteristic DSC peaks in the heating cycle of the transparent resin samples (where T_{on} is the initial temperature, T_g is the glass transition temperature, and T_{end} is the final temperature of the phase). The data are shown in the mean ± standard error format.

T_{on} (°C)	T_g (°C)	T_{end} (°C)	Melting (°C)	Decomposition (°C)
100.82 ± 3.55	122.09 ± 4.15	138.96 ± 1.07	359.11 ± 0.27	438.93 ± 0.38

The quick phase-change is confirmed by the synchronicity of the prompt decrease in sample mass with the endothermic reaction (i.e., the melting of the sample). This indicates that pyrolysis and the melting of the sample are parallel. Based on our TGA, at around 500 °C, the majority of the sample was pyrolyzed (Figure 4).

3.4. Digital Microscopy

The images taken with the digital microscope revealed important information about the structure of the resin material. The fabricated material had an extremely smooth, glass-like surface, and a glassy breaking pattern. The layers were not clearly visible; they could not be separated visually with the used 35× magnification. The material was nearly transparent, therefore, ideal for the production of heat-exchange devices. On the intact surface, small bumps with 0.5 mm diameter could be observed. The raft, which is fundamental in this technology was connected on these protrusions, which must be considered during the 3D modeling and printing processes (Figure 5).

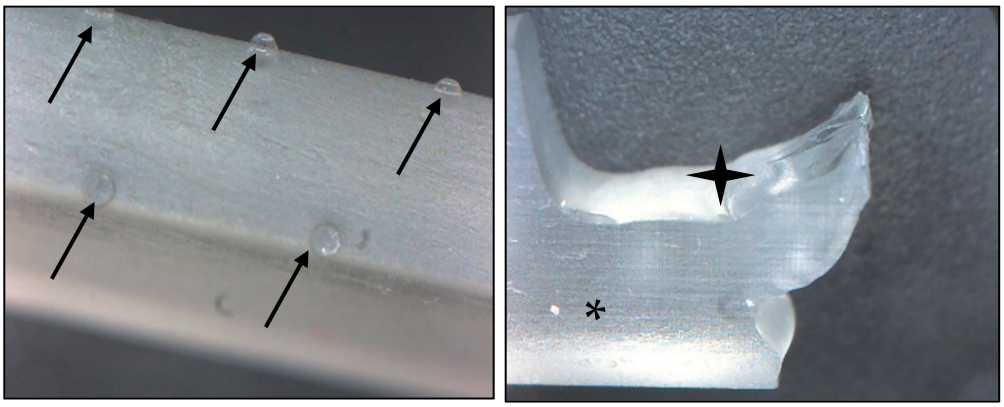

a **b**

Figure 5. Images of the fabricated resin material taken with a digital microscope. (**a**) Intact test specimen, surface on the edge. The black arrows point to the protrusions, which are the remains of the raft. (**b**) Broken test specimen. The black star indicates the broken, the asterisk marks the intact surface, where the glassy-like structure can be observed. Magnification: 35×.

3.5. Thermophysiology Experiments

The application of the heat-exchange device effectively reduced and maintained the temperature of the bath solution in all chambers of the wire myograph system at 13 and 16 °C. There was no meaningful difference in the temperature among the chambers as indicated by the relatively small standard deviations of the mean temperature of the four chambers: 0.72 °C at 13 °C and 16 °C, while 0.36 °C at 36 °C. There seemed to be a negative correlation between the target temperature and the standard deviation of the mean chamber temperature, but it did not reach the level of significance (corr = −0.50, $p = 0.08$).

As expected from earlier studies [20], we registered a significant increase in the isometric force in response to administration of 60 mM KCl, when the bath solution of the isolated rat tail arteries was maintained at 36 °C (Figure 6). However, when the temperature of the bath solution was reduced to 13 or 16 °C with the newly developed heat-exchange device, administration of the same concentration of KCl had no meaningful effect on the isometric force. In order to exclude the possibility that the wire myograph system or the arteries are not functional at 13 or 16 °C, we used phenylephrine, which causes vasoconstriction via distinct mechanisms from KCl. When we administered phenylephrine (10^{-8} to 10^{-4} M) under the same experimental conditions, it caused a marked increase in the isometric force at all tested temperatures (Figure 6), thereby indicating that the attenuation of the KCl-induced vasoconstriction is not due to methodological reasons, but instead it results from the cold-induced suppression of the vasomotor response to KCl.

In our thermophysiology experiments, the recorded increase in the isometric force in response to 60 mM KCl was 4.65 mN at 36 °C, whereas it was practically absent at 13 and 16 °C (Figure 7a). Welch ANOVA showed a significant effect of temperature on the KCl-induced vasomotor response ($p = 0.002$). With Games–Howell post hoc test, we found a significant difference in the KCl-induced change in isometric force between 13 and 36 °C ($p = 0.005$), as well as, between 16 and 36 °C ($p = 0.008$), while there was no significant difference between 13 and 16 °C. However, when the concentration of KCl was increased from 60 to 90 mM, we found a significant ($p = 0.041$) increase in the isometric force of the tail artery at 16 °C (Figure 7b). The latter finding further supports the capability of the used experimental setup to record vasomotor responses in the cold; furthermore it underlies the existence of temperature-dependent differences in vascular responses.

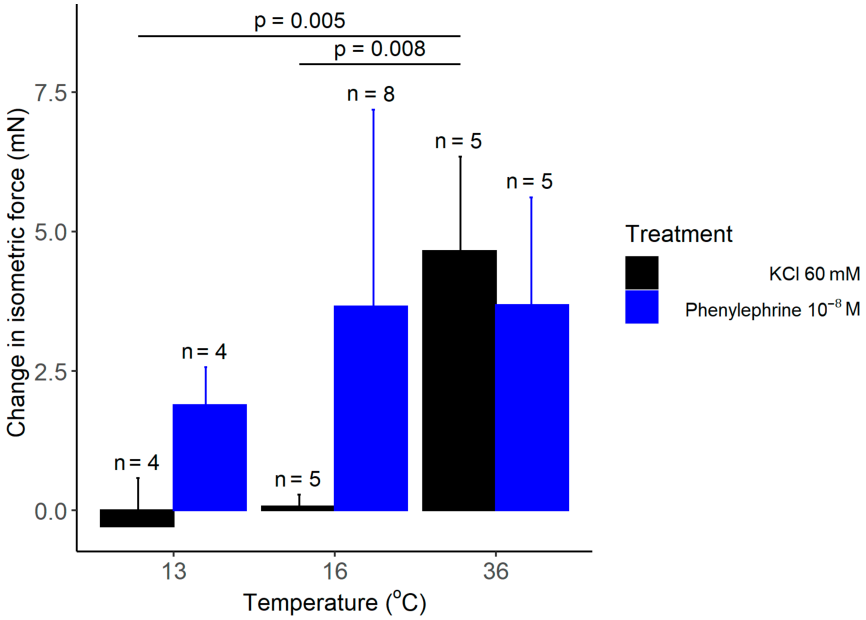

Figure 6. The change in the isometric force of isolated rat tail arteries after adding KCl or phenylephrine (doses indicated) to the bath solution maintained with the manufactured heat-exchanger plates at 13, 16, or 36 °C. Data are presented as mean ± standard deviation.

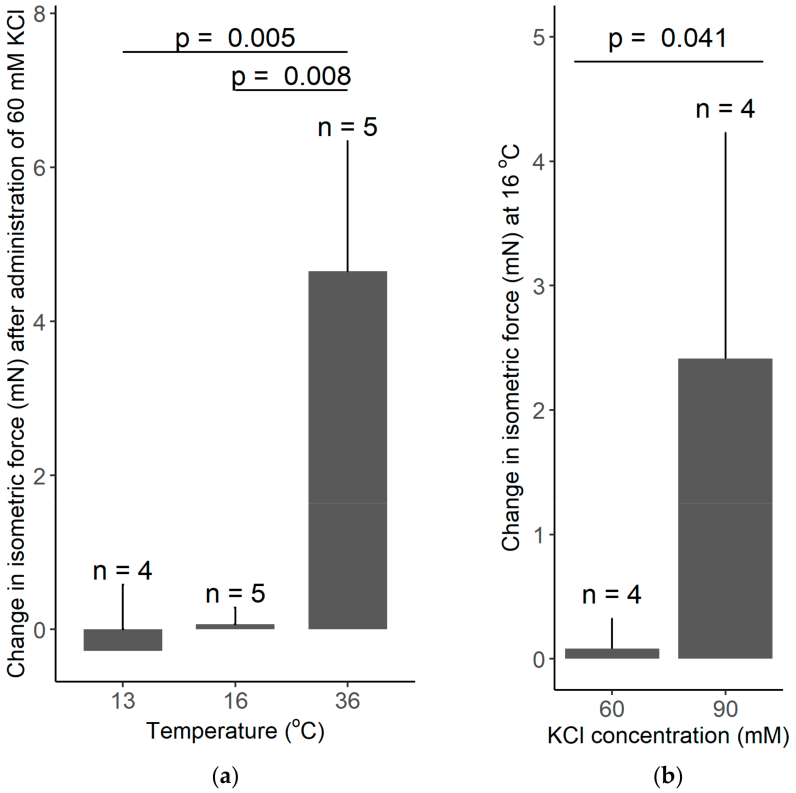

Figure 7. (**a**) The change in the isometric force of isolated rat tail arteries after adding 60 mM KCl to the bath solution maintained with the manufactured heat-exchanger plates at 13, 16, or 36 °C. Note that the KCl-induced vasoconstriction was abolished at low temperatures of 13 and 16 °C. (**b**) The change in the isometric force of isolated rat tail arteries after adding 60 or 90 mM KCl to the bath solution maintained at 16 °C. The higher concentration of KCl caused a significant vasoconstriction. Data are presented as mean ± standard deviation.

The vasomotor response to increasing doses of phenylephrine was also studied at the different temperatures. Phenylephrine caused an increase in the isometric force of the arteries at all temperatures (viz., 13, 16, and 36 °C) with similar dynamics (Figure 8). The maximal vasomotor response tended to be smaller in the cold (at 13 and 16 °C) than at 36 °C, but the effect of temperature did not reach the level of significance ($p = 0.11$).

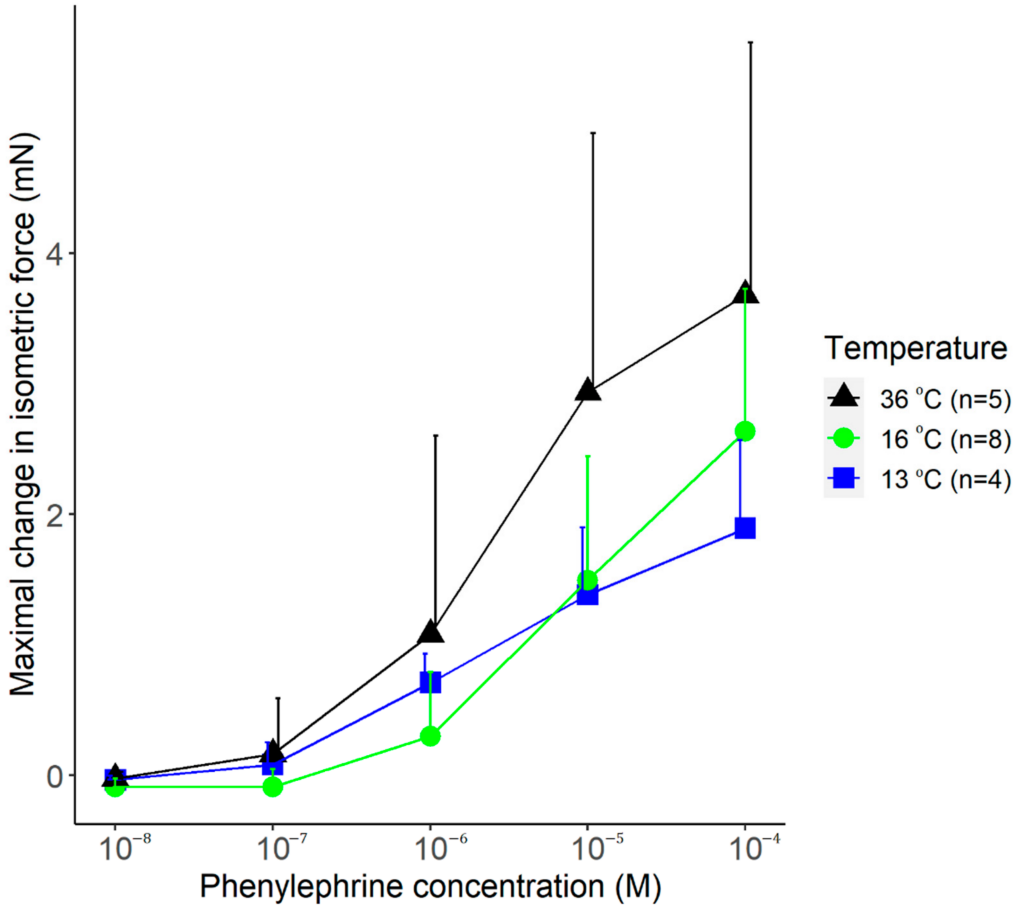

Figure 8. The maximal change in the isometric force of isolated rat tail arteries after adding phenylephrine (doses indicated) to the bath solution maintained with the manufactured heat-exchanger plates at 13, 16, or 36 °C. Data are presented as mean ± standard deviation.

4. Discussion

The mechanical and thermal experiments conducted in the present study underlined that resins with desktop SLA 3D printers can be potentially used for the fabrication of efficient and durable heat-exchange devices to be used in vascular physiology experiments. Our investigation is essential for basic science, because, to our knowledge, currently no studies are available about the characterization of clear resin material for such research purposes. Our mechanical tests revealed that the studied resin material is sufficiently hard and brite, with a Shore D hardness value of 83.0 ± 0.5. The flexural and tensile parameters of the used resin were relatively low compared to thermoplastics used in additive manufacturing, such as polyamide and PLA, which have significantly higher tensile strength based on a previous study [29]. The results of the mechanical testing were supported by images taken with digital microscopy: the structure of the resin sample showed a glass-like, smooth surface both on the intact and broken surfaces. Thermal conductivity measurements were also performed in order to evaluate if the resin material can be used for the development and fabrication of heat-exchange devices, which can be applied in thermophysiology measurements. According to the thermal analysis of the sample, the heat stability was shown up to slightly above 250 °C, although melting and

sample decomposition occurred relatively quickly above that temperature range. These findings confirm that the transparent resin material can be reliably used in biomedical applications. Furthermore, with thermal conductivity measurements, we aimed to examine how the material reacts to the changing temperature conditions. We found that a relatively effective heat insulation can be achieved by using the studied resin material. In addition, we also showed that the application of the fabricated heat-exchange device can maintain a nearly constant temperature in vascular physiology measurements. Based on our initial results, a heat-exchange device was designed and fabricated with SLA printing, and then a series of thermophysiology experiments in rat arteries was carried out by applying the newly developed heat exchanger as an accessory device in a wire myograph system.

By the additive manufacturing of heat-exchange plates, we developed a novel method for the measurement of vasomotor responses in the cold (at temperatures as low as 13 °C). With the cooling plates as accessories of the wire myograph system, our findings can contribute to the ex-vivo study of vasomotor responses of isolated vessels in the cold, which is currently an underrepresented field of research.

Body temperature variabilities influence all biological processes. Living organisms are exposed to different temperatures and dominant animal species on Earth (e.g., reptiles, birds and mammals) are euthermic and maintain their core body temperature in relatively narrow ranges by using behavioral and non-behavioral thermoregulation [30]. In contrast with the temperature of the core, temperatures of the body's shell (e.g., the skin) vary widely according to the actual environmental temperature [31]. When exposed to cold, the skin temperature of the cutaneous tissue can be close to that of the low ambient temperature due to the vasoconstriction of the cutaneous arteries. If the cold exposure is excessive, then temperature will not only decrease on the surface, but also in the core of the body. Similarly to cold, severe systemic inflammation (e.g., severe sepsis) can be also accompanied by decreased core body temperature (called as hypothermia), which is associated with higher mortality in human patients [32]. It should be also noted that, in contrast with the spontaneously developing hypothermia in the cold or in systemic inflammation, the induction of hypothermia can be used as a therapeutic intervention to improve the outcome of diseases, such as severe traumatic brain injury [33]. Regardless of its etiology, the decreased tissue temperature greatly influences biochemical processes, thereby also vascular reactions.

According to the van't Hoff law, all biochemical processes speed up 2–3 fold with each 10 °C increase, though this is just a simplification of the phenomenon [34]. The temperature-sensitivity of molecular functions can be expressed with the temperature coefficient Q_{10} that shows the change in the velocity of a chemical reaction caused by 10 °C rise in temperature. Changes in temperature influence the functions of all ion channels usually with Q_{10} of ~2–3; however, there are some channels that can be directly gated by temperature, which are, therefore, characterized by exceptionally high Q_{10} [35]. For example, in case of the heat-sensitive transient receptor potential vanilloid-1 channel, the Q_{10} value is 40 in the temperature range between 41 and 50 °C [35], while, for the cold-sensitive transient receptor potential melastatin-8, the calculated Q_{10} was 24 between 18 and 25 °C [36]. Importantly, both aforementioned temperature-sensitive channels were shown to play important roles in the mediation of vascular responses in the skin [20,37]. With in-silico methods, it is extremely difficult, if not impossible, to predict how temperature-dependent changes in molecular functions would affect physiological responses of different tissues or organs. Hence, it is essential to perform experiments in animal models at different temperatures and study how temperature influences different biological processes. Such studies can help the better understanding of pathological conditions involving temperature changes (e.g., sepsis) and can also help to pave the way towards the development of therapeutic options for safe and controlled modulation of temperature.

As the initial step of translational research with our newly developed heat-exchange device, we tested its application in biomedical research. For that reason, we performed a series of experiments in isolated tail arteries of rats at different temperatures. In our experi-

ments, we demonstrated that the fabricated heat-exchange device could be successfully used as an accessory of the wire myograph system to cool down the experimental chambers and to steadily maintain their temperatures at as low as 13 °C throughout the procedure. We were able to record the vasoconstriction of the arteries in the cold, thereby confirming the viability of the vessels as well as the capability of the system to study vasomotor responses at 13–16 °C. The sympathomimetic drug phenylephrine caused a concentration-dependent vasoconstriction at all studied temperatures (viz., 13, 16, and 36 °C). The extent of phenylephrine's effect seemed to depend on temperature, as the increase in the isometric force was smaller at all concentrations in the cold (13 or 16 °C) than at 36 °C; however, the difference did not reach the level of statistical significance ($p = 0.011$). We also studied the vasomotor response to KCl, which directly depolarizes smooth muscle cells, thereby leading to vasoconstriction. At the 60 mM concentration, KCl induced vasoconstriction at 36 °C, whereas at 13 and 16 °C, it had no effect. The absence of KCl-induced vasoconstriction was shown previously in arterioles isolated from bigger mammals, such as dogs and pigs; it was suggested to be associated with the temperature-dependence of calcium or potassium homeostasis [38–40]; however, the exact mechanisms have remained unknown. Alternatively, the reduced affinity of the Na^+/K^+ ATP pump for ATP was shown below 20 °C in cold-sensitive species [41], which could lead to accumulation of sodium within the cells and to a shift of the membrane potential to more positive values, thereby increasing the electromotive force needed for KCl to depolarize the cells. In support of a reduced activity of the Na^+/K^+ ATP pump in the cold, when the electrolyte levels were measured in canine arterioles after a 2-h long cold exposure, the intracellular concentrations of sodium and potassium were significantly increased and decreased, respectively [42]. In such a case, increased extracellular KCl concentrations might create enough electromotive force to depolarize the cells. In our experiments, we tested this hypothesis and found that, when we increased the concentration of KCl from 60 to 90 mM, we could observe the KCl-induced vasoconstriction in the cold. These findings demonstrate that our newly developed device is feasible for the investigation of the underlying mechanisms of cold-induced changes in vascular physiology.

As a limitation of using a heat exchanger in wire myography, it should be mentioned that during the experiment the chamber temperature should not be changed because the isometric force-measuring transducers are calibrated to a specific temperature value before the experiment. If the temperature deviates from its value used for calibration, then inaccurate readings and transducer drift (e.g., heat-induced expansion of the electronic parts in the transducer) may occur, introducing large errors into the experiment. Because of this limitation, the system should not be used to study the effects of dynamic temperature variations within the same experiment. It is also important to mention that standard photopolymers for additive manufacturing can have potential cytotoxic effects [43], and the investigated clear resin should not be considered as a non-toxic material. Experiments in cell cultures or living tissues which would require a direct contact with resin are not recommended [43]; however, if the resin is not in direct contact with the biological sample or its bathing solution but only with the experimental device—as was the case in the thermophysiological experiments in the present study—then it can be safely applied in biomedical research.

5. Conclusions

The examined transparent resin 3D-printed with desktop SLA device was found as a suitable material for the design, prototyping, and production of heat-exchange devices. The mechanical and thermal stability ensures its potential application in the biomedical field; however, it must be emphasized that further investigations are encouraged in order to find the optimal design and 3D printing parameters for this purpose. The findings of our study shed light on novel ways and methods to fabricate heat exchangers by using a widely available and cost-effective additive manufacturing technology.

When tested in thermophysiology experiments, the 3D-printed heat-exchanger plates as accessories in wire myography allowed us to cool the chambers below the room temperature and to demonstrate temperature-dependent differences in the vasoconstriction of rat tail arteries induced by different substances. To our knowledge, we are the first to report the inhibitory effects of cold on KCl-induced vasoconstriction in isolated rat tail arteries. The combined use of the newly developed cooling device and the rat species establishes a novel, widely accessible, and inexpensive experimental tool to study the effects of cooling on vasomotor responses of mammals. Our findings also suggest that temperature-dependent physiological mechanisms should be widely investigated and better understood in order to discover the background of the thermal changes and their consequences in pathological conditions, as well as in therapeutic implications.

Author Contributions: Conceptualization, A.G. and P.M.; methodology, L.K., I.I. and E.P.; software, L.K.; validation, A.G., L.K. and R.T.; formal analysis, L.K., K.F. and I.I.; investigation, L.K., K.F., I.I., E.P. and Z.U.; resources, P.M. and A.G.; data curation, Z.U.; writing—original draft preparation, L.K, A.G. and Z.U.; writing—review and editing, L.K., A.G., P.M., I.I., E.P., K.F., R.T. and Z.U.; visualization, L.K.; supervision, A.G.; project administration, A.G.; funding acquisition, A.G and P.M. All authors have read and agreed to the published version of the manuscript.

Funding: This work was supported by the National Research, Development and Innovation Office grant FK 138722 to A.G. and the Thematic Excellence Program 2020—National Excellence Subprogram; Biomedical Engineering Project ("2020-4.1.1-TKP2020") of the University of Pecs to P.M. and R.T. This research was supported by grants from EFOP-3.6.1-16-2016-00004 and GINOP-2.3.2.-15-2016-00022.

Institutional Review Board Statement: All experiments were conducted under protocols approved by the Institutional Animal Use and Care Committee of the University of Pecs (registration no.: BA02/2000-6/2018, approved on 27 February 2018) and conformed to the guide-lines from Directive 2010/63/EU of the European Parliament on the protection of animals used for scientific purposes.

Informed Consent Statement: Not applicable.

Data Availability Statement: Data is contained within the article.

Conflicts of Interest: The authors declare no conflict of interest.

References

1. Al-Dulimi, Z.; Wallis, M.; Tan, D.K.; Maniruzzaman, M.; Nokhodchi, A. 3D printing technology as innovative solutions for biomedical applications. *Drug Discov. Today* **2021**, *26*, 360–383. [CrossRef] [PubMed]
2. Culmone, C.; Smit, G.; Breedveld, P. Additive manufacturing of medical instruments: A state-of-the-art review. *Addit. Manuf.* **2019**, *27*, 461–473. [CrossRef]
3. Coakley, M.; Hurt, D.E. 3D printing in the laboratory: Maximize time and funds with customized and open-source labware. *J. Lab. Autom.* **2016**, *21*, 489–495. [CrossRef] [PubMed]
4. Niknam, S.A.; Mortazavi, M.; Li, D. Additively manufactured heat exchangers: A review on opportunities and challenges. *Int. J. Adv. Manuf. Technol.* **2020**, *112*, 601–618. [CrossRef]
5. Strobel, M.; Mortean, M.V.V. Pressure drop and fluid maldistribution analysis of a compact heat exchanger manufactured by 3D printing. *Int. J. Sci.* **2022**, *172*, 107331. [CrossRef]
6. Arie, M.A.; Shooshtari, A.H.; Tiwari, R.; Dessiatoun, S.V.; Ohadi, M.M.; Pearce, J.M. Experimental characterization of heat transfer in an additively manufactured polymer heat exchanger. *Appl. Eng.* **2017**, *113*, 575–584. [CrossRef]
7. Hein, L.L.; Mortean, M.V.V. Theoretical and experimental thermal performance analysis of an additively manufactured polymer compact heat exchanger. *Int. Commun. Heat Mass.* **2021**, *124*, 105237. [CrossRef]
8. Arie, M.A.; Hymas, D.M.; Singer, F.; Shooshtari, A.H.; Ohadi, M. An additively manufactured novel polymer composite heat exchanger for dry cooling applications. *Int. J. Heat Mass. Transf.* **2020**, *147*, 118889. [CrossRef]
9. Xing, Z.; Ke, H.; Wang, X.; Zheng, T.; Qiao, Y.; Chen, K.; Zhang, X.; Zhang, L.; Bai, C.; Li, A.Z. Investigation of the thermal conductivity of resin-based lightweight composites filled with hollow glass microspheres. *Polymers* **2020**, *12*, 518. [CrossRef]
10. dos Santos, M.N.; Opelt, C.V.; Lafratta, F.H.; Lepienski, C.M.; Pezzin, S.H.; Coelho, L.A.F. Thermal and mechanical properties of a nanocomposite of a photocurable epoxy-acrylate resin and multiwalled carbon nanotubes. *Mater. Sci. Eng. A* **2011**, *528*, 4318–4324. [CrossRef]
11. Kirsch, K.L.; Thole, K.A. Isolating the effects of surface roughness versus wall shape in numerically optimized, additively manufactured micro cooling channels. *Exp. Fluid Sci.* **2018**, *98*, 227–238. [CrossRef]
12. Liang, D.; Bai, W.; Chen, W.; Chyu, M.K. Investigating the effect of element shape of the face-centered cubic lattice structure on the flow and endwall heat transfer characteristics in a rectangular channel. *Int. J. Heat Mass. Transf.* **2020**, *153*, 119579. [CrossRef]

13. Vanaei, H.R.; Shirinbayan, M.; Deligant, M.; Khelladi, S.; Tcharkhtchi, A. In-process monitoring of temperature evolution during fused filament fabrication: A journey from numerical to experimental approaches. *Thermo* **2021**, *1*, 332–360. [CrossRef]
14. El Magri, A.; Vanaei, S.; Shirinbayan, M.; Vaudreuil, S.; Tcharkhtchi, A. An investigation to study the effect of process parameters on the strength and fatigue behavior of 3D-printed PLA-graphene. *Polymers* **2021**, *13*, 3218. [CrossRef]
15. Charkoudian, N. Skin blood flow in adult human thermoregulation: How it works, when it does not, and why. *Mayo Clin. Proc.* **2003**, *78*, 603–612. [CrossRef]
16. de Oliveira, C.; Garami, A.; Lehto, S.G.; Pakai, E.; Tekus, V.; Pohoczky, K.; Youngblood, B.D.; Wang, W.; Kort, M.E.; Kym, P.R.; et al. Transient receptor potential channel ankyrin-1 is not a cold sensor for autonomic thermoregulation in rodents. *J. Neurosci.* **2014**, *34*, 4445–4452. [CrossRef]
17. Gilbert, M.; Busund, R.; Skagseth, A.; Nilsen, P.A.; Solbo, J.P. Resuscitation from accidental hypothermia of 13.7 degrees C with circulatory arrest. *Lancet* **2000**, *355*, 375–376. [CrossRef]
18. Koo, A.; Liang, I.Y. Microvascular responses to norepinephrine in skeletal muscle of cold-acclimated rats. *J. Appl. Physiol. Respir. Environ. Exerc. Physiol.* **1978**, *44*, 190–194. [CrossRef]
19. Mulvany, M.J.; Halpern, W. Mechanical properties of vascular smooth muscle cells in situ. *Nature* **1976**, *260*, 617–619. [CrossRef]
20. Ivic, I.; Solymar, M.; Pakai, E.; Rumbus, Z.; Pinter, E.; Koller, A.; Garami, A. Transient receptor potential vanilloid-1 channels contribute to the regulation of acid- and base-induced vasomotor responses. *J. Vasc. Res.* **2016**, *53*, 279–290. [CrossRef]
21. Hong, S.Y.; Kim, Y.C.; Wang, M.; Kim, H.-I.; Byun, D.-Y.; Nam, J.-D.; Chou, T.-W.; Ajayan, P.M.; Ci, L.; Suhr, J. Experimental investigation of mechanical properties of UV-Curable 3D printing materials. *Polymer* **2018**, *145*, 88–94. [CrossRef]
22. Fayazbakhsh, K.; Movahedi, M.; Kalman, J. The impact of defects on tensile properties of 3D printed parts manufactured by fused filament fabrication. *Mater. Today Commun.* **2019**, *18*, 140–148. [CrossRef]
23. Gu, J.; Zhang, Q.; Dang, J.; Xie, C. Thermal conductivity epoxy resin composites filled with boron nitride. *Polym. Adv. Technol.* **2012**, *23*, 1025–1028. [CrossRef]
24. Ujfalusi, Z.; Pentek, A.; Told, R.; Schiffer, A.; Nyitrai, M.; Maroti, P. Detailed thermal characterization of acrylonitrile butadiene styrene and polylactic acid based carbon composites used in additive manufacturing. *Polymers* **2020**, *12*, 2960. [CrossRef]
25. Jia, S.; Yu, D.; Zhu, Y.; Wang, Z.; Chen, L.; Fu, L. Morphology, crystallization and thermal behaviors of PLA-based composites: Wonderful effects of hybrid GO/PEG via dynamic impregnating. *Polymers* **2017**, *9*, 528. [CrossRef] [PubMed]
26. Gziut, K.; Kowalczyk, A.; Schmidt, B. Free-radical bulk-photopolymerization process as a method of obtaining thermally curable structural self-adhesive tapes and effect of used type I photoinitiators. *Polymers* **2020**, *12*, 2191. [CrossRef]
27. Alexandre, M.; Dubois, P. Polymer-layered silicate nanocomposites: Preparation, properties and uses of a new class of materials. *Mater. Sci. Eng. R Rep.* **2000**, *28*, 1–63. [CrossRef]
28. Saba, N.; Safwan, A.; Sanyang, M.L.; Mohammad, F.; Pervaiz, M.; Jawaid, M.; Alothman, O.Y.; Sain, M. Thermal and dynamic mechanical properties of cellulose nanofibers reinforced epoxy composites. *Int. J. Biol. Macromol.* **2017**, *102*, 822–828. [CrossRef]
29. Rendeki, S.; Nagy, B.; Bene, M.; Pentek, A.; Toth, L.; Szanto, Z.; Told, R.; Maroti, P. An overview on personal protective equipment (PPE) fabricated with additive manufacturing technologies in the era of COVID-19 pandemic. *Polymers* **2020**, *12*, 2703. [CrossRef]
30. Romanovsky, A.A. The thermoregulation system and how it works. *Handb. Clin. Neurol.* **2018**, *156*, 3–43. [CrossRef]
31. Romanovsky, A.A. Skin temperature: Its role in thermoregulation. *Acta Physiol.* **2014**, *210*, 498–507. [CrossRef] [PubMed]
32. Rumbus, Z.; Matics, R.; Hegyi, P.; Zsiboras, C.; Szabo, I.; Illes, A.; Petervari, E.; Balasko, M.; Marta, K.; Miko, A.; et al. Fever is associated with reduced, hypothermia with increased mortality in septic patients: A meta-analysis of clinical trials. *PLoS ONE* **2017**, *12*, e0170152. [CrossRef] [PubMed]
33. Olah, E.; Poto, L.; Rumbus, Z.; Pakai, E.; Romanovsky, A.A.; Hegyi, P.; Garami, A. POLAR study revisited: Therapeutic hypothermia in severe brain trauma should not be abandoned. *J. Neurotrauma* **2021**, *38*, 2772–2776. [CrossRef] [PubMed]
34. Weihe, W.H. The effect of temperature on the action of drugs. *Annu. Rev. Pharm.* **1973**, *13*, 409–425. [CrossRef] [PubMed]
35. Liu, B.; Hui, K.; Qin, F. Thermodynamics of heat activation of single capsaicin ion channels VR1. *Biophys. J.* **2003**, *85*, 2988–3006. [CrossRef]
36. Brauchi, S.; Orio, P.; Latorre, R. Clues to understanding cold sensation: Thermodynamics and electrophysiological analysis of the cold receptor TRPM8. *Proc. Natl. Acad. Sci. USA* **2004**, *101*, 15494–15499. [CrossRef]
37. Thapa, D.; Valente, J.S.; Barrett, B.; Smith, M.J.; Argunhan, F.; Lee, S.Y.; Nikitochkina, S.; Kodji, X.; Brain, S.D. Dysfunctional TRPM8 signalling in the vascular response to environmental cold in ageing. *Elife* **2021**, *10*, e70153. [CrossRef]
38. Qin, G.; Chen, L.; Sjoberg, T.; Steen, S. How to avoid severe coronary vasoconstriction in potassium induced cardioplegia. *Scand. Cardiovasc. J.* **2018**, *52*, 344–347. [CrossRef]
39. Shepherd, J.T.; Rusch, N.J.; Vanhoutte, P.M. Effect of cold on the blood vessel wall. *Gen. Pharm.* **1983**, *14*, 61–64. [CrossRef]
40. Bruttig, S.P.; Roberts, D.E. Cold-Induced Changes in Arterial Sensitivity. Available online: https://apps.dtic.mil/sti/citations/ADA239493 (accessed on 29 December 2021).
41. Marjanovic, M.; Willis, J.S. ATP dependence of Na(+)-K+ pump of cold-sensitive and cold-tolerant mammalian red blood cells. *J. Physiol.* **1992**, *456*, 575–590. [CrossRef]
42. Murphy, J.C.; Carrier, O., Jr.; Sahadi, J. Effects of temperature on responses of fresh and refrigerated perfused blood vessels. *Am. J. Physiol.* **1973**, *225*, 1187–1191. [CrossRef]
43. Kress, S.; Schaller-Ammann, R.; Feiel, J.; Priedl, J.; Kasper, C.; Egger, D. 3D printing of cell culture devices: Assessment and prevention of the cytotoxicity of photopolymers for stereolithography. *Materials* **2020**, *13*, 3011. [CrossRef]